

Unclassified

SECURITY CLASSIFICATION OF THIS PAGE(When Data Entered)

Photoconductivity and photo-Hall studies have elucidated some of the optical transitions and showed evidence that much of the spectral shape is due to quenching effects. DLTS and thermally-stimulated current measurements were used to study oxygen doped and "undoped" semi-insulating GaAs, revealing a variety of deep and medium-deep levels. A combination of theory and experiment has proved valuable to the understanding of the photoionization cross sections, Fano anti-resonance, and local mode coupling of the deep impurity states.



Unclassified

SECURITY CLASSIFICATION OF THIS PAGE(When Data Entered)

Handwritten notes on the right margin, including the word "Class" and some illegible scribbles.

FINAL REPORT
to the
OFFICE OF NAVAL RESEARCH
on Contract
N00014-76-C-0890
DEEP IMPURITY STATES IN GALLIUM ARSENIDE

From the
UNIVERSITY OF MASSACHUSETTS

Principal Investigator
Claude M. Penchina

Amherst Mass. October 1981

TABLE OF CONTENTS

Abstract	11
I. Introduction	1
II. Summary of Results	2
III. Personnel	13
IV. Reprints of Publications Supported by ONR Contract	14

Accession For	
NTIS GRA&I	<input checked="" type="checkbox"/>
DTIC TAB	<input type="checkbox"/>
Unannounced	<input type="checkbox"/>
Justification	
By _____	
Distribution/	
Availability Codes	
Dist	Avail and/or Special
A	

ABSTRACT

We have studied opto-electronic properties of semi-insulating gallium arsenide, including oxygen doped, chromium doped, undoped, and ion-bombarded materials. We have found that the luminescence from chromium-doped samples has much fine structure which had not been previously seen; this led to a better understanding of chromium complexing and of local lattice vibration and Fano anti-resonance at a substitutional Cr site. We have identified two other luminescence bands as related to oxygen and native defects respectively. Photo-conductivity and photo-Hall studies have elucidated some of the optical transitions and showed evidence that much of the spectral shape is due to quenching effects. DLTS and thermally-stimulated current measurements were used to study oxygen doped and "undoped" semi-insulating Ga As, revealing a variety of deep and medium-deep levels. A combination of theory with experiment has proved valuable to the understanding of the photoionization cross sections, Fano anti-resonance, and local mode coupling of the deep impurity states.

I. Introduction

We have studied experimentally and theoretically, the effects of chromium and oxygen impurities and ion implantation on the optoelectronic properties of Gallium Arsenide.

Techniques which were used included photoconductivity, photo-Hall effect, optical absorption, cathodoluminescence, electroabsorption, electroreflection, and transient capacitance.

Most of the results are summarized briefly in the following section, and in more detail in the attached reprints of published works. Additional work on capacitance transients, photo-transport measurements, and ion implantation was begun on this contract and is still in progress. Reports on this research will be submitted when it is completed.

II. Summary of Results

1. ION IMPLANTATION IN GaAs

The apparent forbidden energy gap of GaAs as seen in electroabsorption was found to be somewhat reduced in the presence of impurities in the depletion region of a p-n junction (Penchina 1964). This property led us to use electroabsorption, electroreflectance, and optical transmission to study the effects of proton bombardment (hydrogen ion implantation) on the spectrum of Gallium Arsenide. The major effect was a broadening of intrinsic structure in the modulation spectra. No evidence was observed of specific sharp deep levels introduced by either the proton damage or the implanted hydrogen impurities [Oren, Quinton, and Penchina 1977]. The results were interpreted as due mainly to a gradual amorphization in islands with fairly well defined boundaries. These results are described more fully in an article by Oren, Quinton, and Penchina (Oren 1978).

A preliminary study of Cr implantation has shown that the 0.84 eV luminescence system is seen there also (Ushakov 1978). However, that study, although it claimed fairly good resolution in both the ion implanted and bulk GaAs:Cr, missed all the fine structure splitting which we have seen. The study did however note important problems which were interpreted as due to out-diffusion of Cr from the substrate into the implanted surface layer. This diffusion, if it is as interpreted, could have important implications for performance and degradation of GaAs epitaxial devices. We have implanted Cr and O into GaAs in order to study these impurities in a more controlled manner.

2. PHOTOCONDUCTIVITY, PHOTO-HALL EFFECT, AND LOW RESOLUTION OPTICAL ABSORPTION IN GaAs DOPED WITH OXYGEN AND/OR CHROMIUM.

The photoionization cross section of an oxygen related deep level in GaAs was determined from the measured spectrum of the photon flux needed to

maintain constant photocurrent. The results were interpreted as due to an axially symmetric center. This work is described in an article by Tyler, Jaros, and Penchina (Tyler 1977). A similar study was carried out on a Chromium doped sample, free of oxygen (NR #4-77L, kindly donated by Dr. E.M. Swiggard of the Naval Research Laboratory). This sample showed a broad optical absorption spectrum (Fig. 3), a remarkably similar Photo-Hall Mobility Spectrum (Fig 2) (qualitatively similar spectrum, but quantitatively an order of magnitude higher mobility), and a somewhat sharper room temperature photoionization cross section, which further sharpened considerably at lower temperatures (Fig 1). These results indicate that the sharp photoconductivity peak may be produced by hole excitation causing quenching of electron excitation rather than by a sharp resonance of a Cr^{2+} excited state as suggested earlier [Ippolitova 1975, Stocker and Schmidt 1976]. These new results have not yet been published, but were discussed in a paper [Penchina 1979] at the 2nd "Lund" International Conference on Deep Level Impurities in Semiconductors, St. Maxime, France, May 1979.

3. LUMINESCENCE AND HIGH RESOLUTION OPTICAL ABSORPTION IN GaAs DOPED WITH OXYGEN AND/OR CHROMIUM

Although Cr in GaAs had been the subject of several studies of optical and electrical properties for some time (see e.g. Allen 1968, Bois 1974, Lin 1976, Ippolitova 1975) it was not until 1976 that a zero-phonon line at about 0.84 eV (Stocker 1976) and one at about 0.56 eV (Koschell 1976) with associated lattice-phonon sidebands were first reported in the photoluminescence of GaAs:Cr. These zero-phonon lines were given several tentative explanations, such as band-to-level, resonance-to-level, or internal transition; various charge states of Cr were assumed. By 1978 these interpretations had more-or-less settled down to: internal transitions $5E$ to $5T_2$ of Cr^{2+} at 0.84 eV, and internal transitions of Cr^{3+} at 0.56 eV.

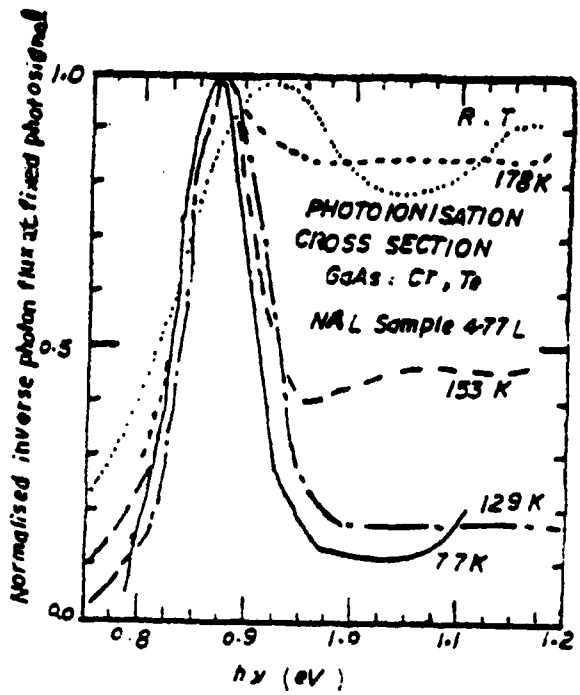


Fig. 1
 PENCHINA (1979)

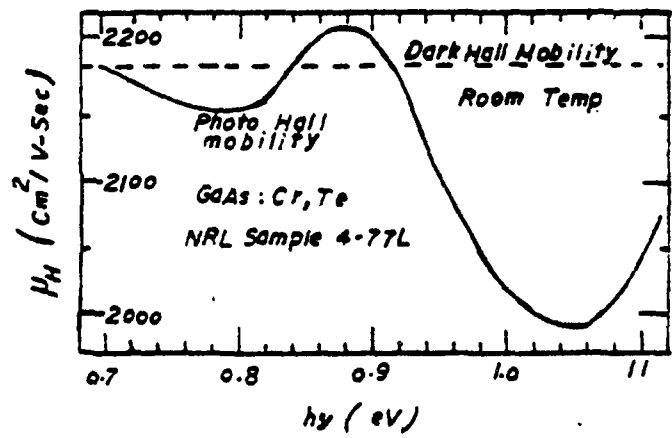


Fig. 2
 PENCHINA (1979)

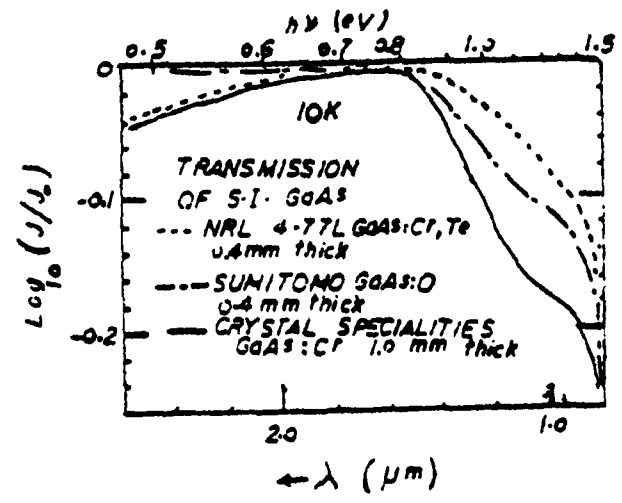


FIG. 3
 PENCHINA (1979)

Our experiments on cathodo-luminescence (Lightowers and PENCHINA 1978, PENCHINA and Lightowers 1978) quickly revealed a rich fine-structure of the zero-phonon lines which was not observed by previous investigators, and showed that the 0.56 eV system was present in LPE samples of Stocker and Schmidt (1976) where they had not been seen before and previously assumed absent. Further refinements of luminescence experiments, and high resolution optical absorption measurements (Lightowers, Henry, and PENCHINA 1978, 1979, PENCHINA et.al. 1979) both as functions of temperature, have led to a number of new findings which we plan to explore further.

- a. Cr 0.84 eV The 0.84 eV zero-phonon "line" consists in reality of at least 13 very sharp (width less than kT at 4.2K) closely spaced lines. Thermalization of the intensities of these lines led to a tentative energy level scheme for internal transitions (Lightowers and PENCHINA 1978); it does not seem to be fully compatible with the ground state splitting of Cr^{2+} reported from ESR (Krebs 1977A,B), and may be due to Cr complexed with a nearest neighbor donor (White 1979).

The absorption band observed by Bois and Pinard (1974) is a background absorption added to the 0.84 eV system, rather than the phonon sidebands of the 0.84 eV zero-phonon absorption lines, further indicating the possibility of something other than Cr^{2+} involved in the luminescence transitions.

The wavelengths of many of the zero-phonon lines which we observed in cathodoluminescence and optical absorption were confirmed on different samples, using photoluminescence (Koschel 1978), further showing that the fine structure is not a property of a few particular samples or of artifacts of the experiment (their resolution was insufficient to confirm all our 13 lines).

A preliminary study of the spectral shape of the phonon sidebands in cathodoluminescence indicated a Franck-Condon shift (due to lattice relaxation) of about 0.06 eV, independent of temperature. The positions of zero phonon lines shifted by less than 0.1 nm over the full temperature range where they were observable.

b. Cr 0.56 eV The 0.56 eV zero-phonon luminescence "line" was found to be three fairly closely spaced broad (broader than kT at liquid He temperature) zero-phonon lines. Thermalization measurements led to a tentative energy level diagram [Lightowers & Penchina 1978, Lightowers Henry & Penchina 1979].

The broadness of the zero-phonon luminescence lines, and an interference dip preceding them, combined with some recent optical measurements, leads to the conclusion [Penchina et.al.1979,1980] that there is a Fano Anti-Resonance with transitions involving a level degenerate with a band.

An additional phonon replica, due to a local-mode phonon of 40.7 meV was found [Lightowers, Henry and Penchina 1978] to accompany these zero-phonon lines, but not those around 0.84 eV, leading to the conclusion that the 0.56 eV transitions involve different charge states and thus different local phonon coupling than the 0.84 eV transitions.

We have observed these three 0.56 eV zero-phonon lines in all our samples which show both the 0.84 eV lines, and a luminescence background due to oxygen sufficiently weak to prevent hiding of the signal in the noise. Neither the fine structure of the zero-phonon lines nor the local-mode phonon replica has been reported by other experimenters to date.

c. Oxygen We have observed a broad luminescence emission band [Lightowers, Henry, and Penchina 1978] which peaks at about $2 \mu\text{m}$ in almost all samples, scales with the oxygen concentration. When this band is present, even weakly, it makes the 0.56 eV Cr spectrum difficult to observe. When it is stronger, it buries the 0.56 eV Cr spectrum in the noise, and distorts the shape of the 0.84 eV Cr spectrum. We have found two samples which contain oxygen which do not show this band: one shows other bands, and one shows no bands obviously characteristic of oxygen. These two exceptions indicate that oxygen may enter GaAs in different configurations, charge states, or complexes, but that in the majority of samples it does take one preferred state which leads to a well characterized luminescence band.

d. Native Defect We have observed a weak band peaked around $1.6 \mu\text{m}$ in nearly all samples studied, independent of oxygen or chromium concentration. We observed this same band in an undoped sample of semi-insulating GaAs from NRL similar to one in which a similar band was previously reported [Swiggard 1977]. We attribute this band to a native defect present in all samples, and must take it into account carefully since it contributes to the background of the Cr 0.84 eV luminescence system and the broad oxygen luminescence band.

4. UNDOPED SEMI-INSULATING GaAs

We studied thermally stimulated current (TSC) from several samples of GaAs with Oxygen and Chromium. In order to better understand these data, we needed a control sample. For this, we chose semi-insulating undoped GaAs grown by LEC (liquid encapsulated Czochralski) method at NRL (kindly donated by Dr. Swiggard) which had very little deep level luminescence (see 3d above). However, it was found that this undoped GaAs has in fact a large number of medium-deep levels which are easily observed in TSC and prevent it from being a good control.

These results indicate that the undoped GaAs, although semi-insulating, is not extremely pure. Since the impurity content is not controlled, but inadvertent, and since these types of materials are becoming popular for use as substrates for semiconductor devices, it would be advisable to conduct additional research to determine the nature and behavior of these impurities.

5. THEORY

We have carried out several theoretical studies concerning the properties of deep defects in semiconductors, with particular emphasis on problems associated with high resistivity GaAs. The chief objective was, first of all, to establish a simple link between theoretical considerations (e.g. a priori calculations of electronic energies and wave functions) and the observed spectra. Hence, attempts have been made both to interpret fresh experimental results (obtained at Amherst and elsewhere), and to improve the theoretical framework itself.

Analytical impurity wave functions associated with deep levels in semiconductors (e.g. GaAs:O, GaP:O) were calculated, using a pseudopotential scheme [Jaros 1977] in which a realistic and convergent model was employed to represent the host crystal band structure and the impurity potentials. The effects determining the form of the wave function were studied with a view to establishing a relationship between the position of a deep level in the gap and the localization of the wave function.

The optical impurity-to-band cross sections involving deep levels were computed as a function of photon energy and temperature [Jaros 1977, Tyler 1977]. The electron-phonon interaction was taken into account within the strong coupling model of Huang and Rhys. A relatively simple formula was derived which can be used to interpret optical cross sections associated with deep centers dominated by a short range potential. Numerical results were obtained for GaP:O, GaAs:O and Si:Au and the threshold energies, the magnitude of the Franck-Condon effect and the temperature dependence

of the binding energies determined. It was possible to relate the optical spectra to the recombination processes in the material.

A theoretical estimate of Auger recombination cross sections from full-scale calculations of electron-electron and electron-lattice interactions was also made and related to numerous observations in III-V materials. [Jaros 1978]

The most important conclusions can be summarized as follows:

- a. Given the band structure of the host crystal and a localized potential dominated by a medium or short range term, we can compute the energy spectrum almost as accurately as necessary. This excludes atoms with open d-shells.
- b. Both the conduction and valence bands play a significant part in the formation of the impurity energy and wave function. The final position of the level depends on a delicate cancellation process.
- c. In the past the localization of the wave function has been assessed by relating the argument of the exponential tail of the function to the impurity energy defined with respect to the nearest relevant band edge. As a result, the localization becomes a sensitive function of the impurity energy. This view is inadequate in the case of deep levels.
- d. The localization of the wave functions has been shown sufficient to cause a substantial Franck-Condon effect.
- e. During displacements of a certain symmetry, the localization of the wave function does not deteriorate substantially even if the level approaches the band edge. Thus, it becomes a highly localized shallow impurity. [Brand 1977] Accordingly, the multiphonon transition probability can be large, as indicated by observed thermal broadening.
- f. Many (most?) deep centers can bind more than one particle. The electron-electron interaction is about 0.1 - 0.2 eV/electron and the Auger-type recombination cross section can be large ($10^{-13} - 10^{-6} \text{ cm}^2$).

Theoretical analysis of the Fano-anti resonance and local mode sidebands in luminescence [Penchina et al 1979, Penchina 1980] has shown that Cr on an As site slightly increases the local force constants, and has optical transitions to resonant state degenerate with the continuum.

6. WORK STILL IN PROGRESS

A study of capacitance transients in O doped GaAs, studies of photo-Hall effect and Photoconductivity in O and Cr doped GaAs, and studies of GaAs selectively implanted with isotopes of Cr and O were begun under this contract. Some of this work is still in progress. A report on these studies will be submitted as an Appendix when the work is completed.

6. REFERENCES

1. Allen, G.A., J. Phys. D 1, 593 (1968).
2. Bois, D., and Pinard, P., Phys. Rev. 39, 4171 (1974).
3. Ippolitova, G.K., Omelaynovskii, EM., and Pervova, L. Ya., Physics and Technics of Semiconductors 9, 1308 (1975); Engl. Transl.: Sov. Phys. Semicond. 9 364 (1975).
4. Koschel, W.H., Bishop, S.G. and McCombe, B.D., Solid St. Commun. 19, 521, (1976).
5. Koschel, W. H., Private Communication (1978).
6. Krebs, J.J., and Stauss, G.H., Phys. Rev. B15, 47 (1977A)
7. Krebs, J.J., and Stauss, G.H., Phys. Rev. B16, 971 (1977B)
8. Lightowers, E.C. and Penchina, C.M., J. Phys. C 11, L405 (1978)
9. Lightowers, E.C., Henry, M.O., and Penchina, C.M., Int. Conf. on Recombination in Semiconductors (unpublished) (1978B).
10. Lightowers, E.C., Henry, M.O., and Penchina, C.M., Inst. Phys. Conf. Ser. 43; 307-310 (1979).
11. Lin, A.L. and Bube, R.H., J. Appl. Phys. 47, 1859 (1976).
12. Oren, M., Quinton, A.R. and Penchina, C.M., in Radiation Effects in Semiconductors 1976 Ed: N.B. Urli & J.W. Corbett, Inst. of Physics Conf. Ser No 31 p.512 (1977).
13. Oren, M., Quinton, A.R., and Penchina, C.M., J. Electrochem Soc. 125, 776 (1978).
14. Penchina, C.M., Frova, A. and Handler, P., Bull.Am.Phys.Soc. 9, 714 (1964).
15. Penchina, C.M. and Lightowers, E.C., Bull.Am. Phys.Soc. 23, 200 (1978).
16. Penchina, C.M., Masut, R., Lightowers, E.C., Henry, M., Zavetova, M., and Velicky, B., 2nd "Lund" Int. Conf. on Deep Level Impurities in Semiconductors, Sainte Maxime (1979) unpublished

17. Penchina, C.M., Lightowers, E.C., Henry, M.O., Zavetova, M., and Velicky, B., in Radiative Recombination and Related Phenomena in III-V Compound Semiconductors, RECON '79, p.181-186, Prague, Sept.4-7, (1979)
18. Penchina, C.M., in "New Developments in Semiconductor Physics" Eds F. Beleznay, G. Ferenczi and J. Giber, Springer-Verlag Lecture Notes in Physics No. 122. P.97 (1980).
19. Stocker, H.J. and Schmidt, M., J. Appl. Phys. 47, 2450 (1976).
20. Swiggard, E.M., Lee, S.H., and Von Batchelder, F.W., in L.F. Eastman, Ed., "Gallium Arsenide Symposium", Inst. Phys. Conf. Ser. No. 33B, p.23 (1977).
21. Tyler, E.H., Jaros, M., and Penchina, C.M., Appl.Phys. Letters 31, 208 (1977).
22. Ushakov, V.V., Gripius, A.A. and Kernilav, B.V., Phys. and Technics of Semicond. (Russian) 12, 358-363 (1978).
23. White, A.M., Solid State Comm. 32, 399 (1979)

III. PERSONNEL

The following were the major research personnel who worked on this
ONR contract:

Senior Personnel:

Principal Investigator: Dr. Claude M. Pechina

Other Investigator: Dr. Arthur R. Quinton

Visiting Professor/Consultant: Dr. Milan Jaros
Dr. Hans J. Stocker
Dr. P.S. Nayar

Postdoctoral Research Associate: Dr. Ernest H. Tyler

Graduate Students: Bruce Black
Remo Masut
Dale Syphers

Undergraduate Honors Students: Benjamin Crooker
Karta Khalsa
Michael Plum
Dale Syphers

IV. Reprints of Publications Supported by ONR Contract

(Page) Listed alphabetically by first author.

- 16 1. S. Brand and M. Jaros, "Pseudopotential calculations of the effect of displacement upon the impurity levels introduced by deep donor oxygen in GaAs, GaP, Si and nitrogen in diamond", Solid St. Commun. 21, 875-877, 1977.
- 19 2. M. Jaros, "Wave functions and optical cross sections associated with deep centers in semiconductors", Phys. Rev. B16, 3694-3706 (1977).
- 32 3. M. Jaros, "A case for large auger recombination cross sections associated with deep centers in semiconductors", Solid State Comm. 25, 1071-4 (1978).
- 36 4. D.V. Lang, R.A. Logan, and M. Jaros, "Trapping characteristics and a persistent donor-complex (DX) model for photoconductivity trapping DX center in Te-doped $Al_xGa_{1-x}As$ ".
- 52 5. E.C. Lightowers and C.M. Penchina "Fine structure in the cathodoluminescence spectrum from chromium-doped gallium arsenide", J.Phys. C. 11, L405 (1978).
- 57 6. E.C. Lightowers, M.O. Henry and C.M. Penchina, "Temperature Dependence of the Fine Structure in the Cathodoluminescence and Absorption Spectra of Chromium-doped Gallium Arsenide", Inst. Phys. Conf. Ser. 43, 307-310 (1979).
- 61 7. A. Mircea , A. Mitonneau, J. Hallais, and M. Jaros, "Study of the main electron trap in $Ga_{1-x}In_xAs$ alloys", Phys. Rev. B16, 3665-3675 (1977).
- 72 8. M. Oren, A.R. Quinton and C.M. Penchina, "Optical modulation study of proton-bombarded GaAs" in Radiation Effects in Semiconductors 1976, Ed: N.B. Urli & J.W. Corbett, Inst. Phys. Conf. Ser. No. 31, p.512-513 (1977).
- 73 9. M. Oren, A.R. Quinton and C.M. Penchina, "Effect of proton damage on optical modulation spectra of gallium arsenide", J. Electrochem. Soc. 125, 776-781 (1978).

(page)

- 79 10. C. M. Penchina, E.C. Lightowers, M.O. Henry, M. Zavetova, and B. Velicky, "Luminescence in GaAs:Cr Fano Resonances and Local Modes" in Proceedings of the International Conference Radiative Recombination and Related Phenomena in III-V Compound Semiconductors RECON '79, Prague, Czechoslovakia, Sept. 4-7(1979) Czech. Academy of Sciences.
- 83 11. C.M. Penchina, "Luminescence of Chromium in Gallium Arsenide" in F. Belezny, G. Ferenczi, and J. Giver Eds. "New Developments in Semiconductor Physics" Proceedings, Szeged 1979, Springer-Verlag, Lecture Notes in Physics No. 122, p97-106 (1980).
- 92 12. H.J. Stocker, "A study of deep impurity levels in GaAs due to Cr and O by ac photoconductivity", J. Appl. Phys. 48, 4583-4586 (1977).
- 96 13. E.H. Tyler, M. Jaros, and C.M. Penchina, "Extrinsic photoconductivity in high-resistivity GaAs doped with oxygen", Appl. Phys. Letters 31, 208-210 (1977).

PSEUDOPOTENTIAL CALCULATIONS OF THE EFFECT OF DISPLACEMENT UPON THE IMPURITY LEVELS INTRODUCED BY DEEP DONOR OXYGEN IN GaAs, GaP, Si AND NITROGEN IN DIAMOND

S. Brand

Department of Theoretical Physics, The University, Newcastle Upon Tyne, U.K.

and

M. Jaros*

Department of Physics and Astronomy, University of Massachusetts, Amherst, MA. 01003 USA

(Received 29 October 1976 by A.O. Chynoweth)

Calculations of the effect of displacement upon deep donor levels suggest significant differences between groups IV and III-V semiconductors. We conclude that oxygen in GaAs and GaP should possess tetrahedral symmetry and predict a large trigonal distortion for substitutional nitrogen in diamond. Our results indicate that the level due to N in diamond occurs in the upper half of the band gap.

We have calculated the effect of displacement on the position of deep, oxygen-like donor levels in the forbidden band gap of GaAs, GaP, Si and diamond. Our results indicate substantial differences between group IV and III-V materials. In particular, we show that a static trigonal (outward) displacement of the substitutional donor nitrogen in diamond leads to an increase in the impurity ionization energy. Although our results for N in diamond suffer from a large uncertainty due to the choice of the impurity potential and lack of self-consistency at large displacements, these results suggest that the donor level occurs in the upper half of the band gap.

Oxygen is a very common impurity in most semiconductors. In GaP it is known to be a deep substitutional donor. The depth of the level (0.9 eV) in the band gap is governed by the short range part of the potential which is basically derived from the difference of the atomic cores of oxygen and the host atom (i.e. P), screened with an appropriate dielectric function. Under such circumstances one might expect oxygen in, say, GaAs to behave in a similar fashion. Here we are not referring to the ground state energy (which is known to be very sensitive to the depth and range of the impurity potential) but rather to the nature of the state, i.e. its symmetry and most likely paths of recombination, and the form of the lattice distortion in the vicinity of the impurity. Accordingly, in this study, we take the potential characteristic of oxygen in GaP and set out to study the role of the host lattice in determining the properties of deep donor levels due to this potential in GaAs, GaP, Si and diamond. In all cases, this potential produces a deep donor level in the upper half of the forbidden gap.

Recently, we have attempted to model non-

radiative (multiphonon) recombination via the two-electron level of oxygen in GaP and Zn-O pair in GaP by displacing the impurity pseudo-atoms from their substitutional (perfect crystal) positions and evaluating the impurity energies as

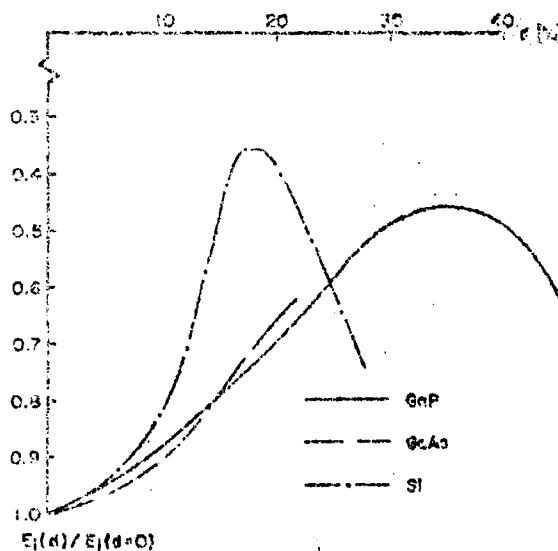


Fig. 1: The impurity energy $E_i(d)$ (measured from the conduction band of the host material), as a function of displacement d which is expressed as a percentage of the relevant perfect crystal nearest neighbour distance.

* on leave of absence from the Department of Theoretical Physics, The University, Newcastle Upon Tyne, U.K.

Supported in part by NSF, under contract #K00014-76-0220

a function of the lattice coordinate[1]. The method required for such a calculation and its convergence properties have been described in some detail [2,3]. The essence of the method consists in expressing the impurity wave function in terms of the unperturbed host crystal eigenfunctions and solving the one-electron Schrödinger equation numerically. Typically, ten bands and several thousand points in the reduced zone are required to achieve satisfactory results. The impurity is represented by a screened atomic pseudopotential [4]. This may be a severe approximation since the concept of a neutral pseudatom presupposes an atom in a strictly periodic lattice. Therefore, our model cannot yield a truly quantitative description of the problem. However, it is hoped that calculations such as ours may well supplement the existing often merely phenomenological considerations in this field.

In Fig. 1 we present the results of our calculations of the change in the impurity energy E_i , as a function of the displacement d . The energy E_i of the impurity with respect to the conduction band of the vibrating lattice is

impurity ground state is insensitive to the trigonal mode of displacement, the diamond lattice seems unstable and the impurity energy drops deeper into the forbidden gap. The results for silicon are also different from those for GaP and GaAs. It is worth emphasizing that the

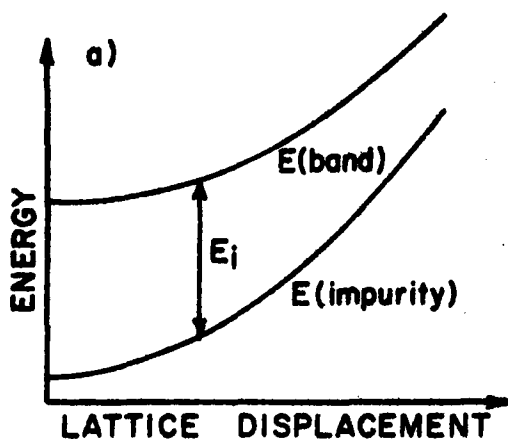


Fig. 2a: The impurity energy E_i , shown in Fig. 1, and in Fig. 3, represents the energy with respect to the conduction band in a vibrating lattice. Thus E_i can be pictured as a separation of the potential curves in a standard configuration coordinate diagram shown above.

calculated as in ref. [1]. E_i and d are illustrated in Fig. 2a and b, resp. In Figs 1, 3 and 4 the displacement is expressed as a percentage of the corresponding perfect crystal nearest neighbour distance. Fig. 3 shows the results for diamond.

As expected, very little difference is found as far as GaP and GaAs are concerned. Although we present our results for displacements as large as 40%, it must be emphasized that our model becomes quite unrealistic for large d . However, in spite of their rather academic character, the results for $d \approx 10-30\%$ do help us to understand the overall trend. In contrast with the case of GaAs and GaP, where the

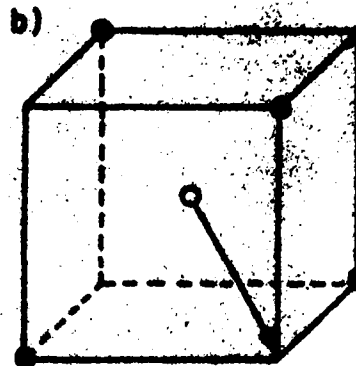


Fig. 2b: The displacement considered in the present study is indicated. The open circle represents the impurity atom.

results in Figs. 1, 3 are not sensitive to the precise position of the deep level in the band gap and may be regarded as typical for this class.

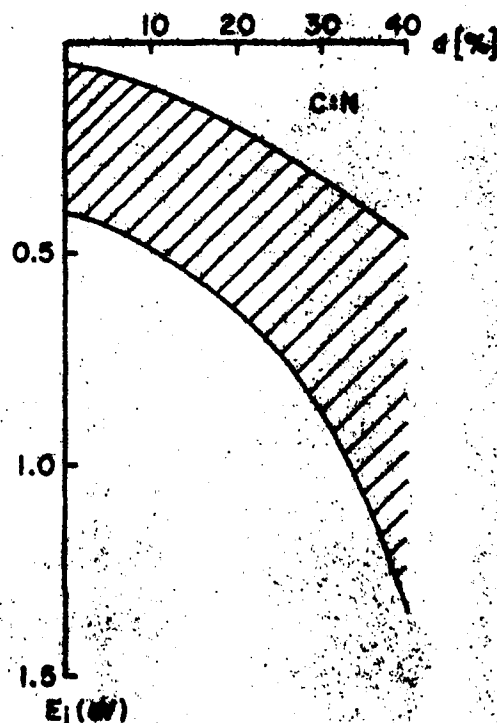


Fig. 3: The impurity energy E_i , calculated with oxygen potential used in Fig. 1, as a function of displacement d in diamond. E_i and d are defined as in Fig. 1 and 2.

of impurity (i.e. a deep donor). The potential we use in our calculations for GaP and GaAs is quite realistic and a good estimate was obtained [2] of the depth of the corresponding single donor levels in these materials. The potentials for GaP:O and GaAs:O are of almost identical shape and similar strength. Therefore the results shown in Fig. 1 of the displacement calculations on these materials, at least for small d , are amenable to experimental verification. However when we come to use this potential in Si and diamond we are merely examining the effect of the host crystal properties upon the change in the position of a state associated with such a potential. Hence the results in Figs. 1 and 3 concerning Si and diamond do not correspond to any observable process.

It would appear that the covalent lattice is less stable in the presence of a deep donor and may favour lower symmetry configuration for the impurity. The existing experimental data does point in the same direction. Luminescence spectra associated with oxygen in GaP [5] are consistent with a model based on T_d symmetry for the centre. Our numerical efforts [3,6] to assess the effect of a static distortion upon this impurity are in agreement with this experimental evidence. On the other hand both oxygen in silicon and nitrogen in diamond are known to possess lower symmetry [7,8].

N in diamond is of particular interest since it is a "simple" donor. Therefore we decided to attempt a calculation of the binding energy of a substitutional nitrogen donor in diamond. A calculation of the effect of static displacement upon a deep level has been described in ref. 3 and will not be repeated here. As before, no correction is made to account for changes in the valence band due to the displacement. Therefore, we cannot predict a minimum energy displacement and our model becomes unrealistic for large d . Another difficulty arises in connection with the choice of the potential since several somewhat different pseudopotentials are available [9,10]. Also some error is introduced by processing the potential for the calculation. To avoid the difficulties involved in choosing "the best" potential, we performed our computations with all likely candidates and show the results for the weakest and strongest potentials in Fig. 4. The gap between the two curves is large but it is obvious that the outward trigonal (static) displacement always increases the binding energy

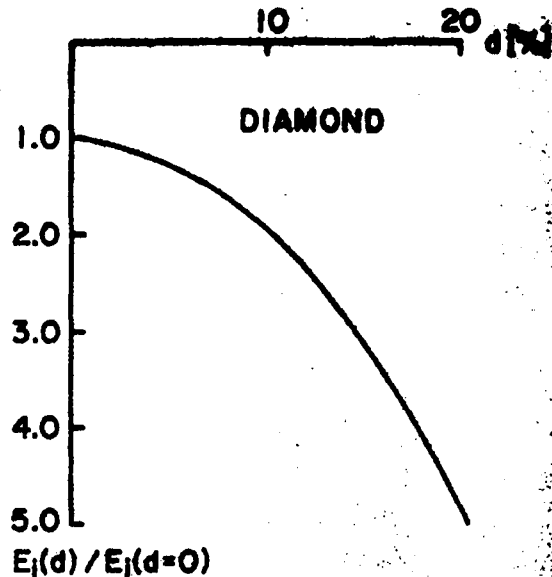


Fig. 4: The effect of a static displacement upon the ionization energy, e_i , associated with a substitutional nitrogen donor in diamond. d is defined as in Fig. 1. e_i is measured from the bottom of the conduction band in eV. The gap between the lower and upper curves indicates the uncertainty due to the choice of the impurity potential.

of the donor. The results in Fig. 4 suggest that the level due to paramagnetic nitrogen in Ib diamonds should be found in the upper half of the forbidden band gap, in contrast with the predictions of Messmer and Watkins [11]. Indeed the optical and thermal excitation experiments of Farrer [12] showed that the nitrogen level may lie at ~ 1.7 eV from the bottom of the conduction band. This view is supported by an up-to-date analysis of the existing experimental data [8].

Acknowledgement—We are grateful to Dr. G. Davies for making his review article available to us prior to publication.

REFERENCES

- JAROS, M. and BRAND, S., Proc. Int. Conf. Phys. Semiconductors, Roma 1976 (in press).
- JAROS, M., J. Phys. C **8**, 2455 (1975).
- JAROS, M. and BRAND, S., Phys. Rev. **B14**, 4496 (1976).
- JAROS, M. and ROSS, S.F., J. Phys. C **6**, 3451 (1973).
- DEAN, P.J., J. Luminescence **1/2**, 398 (1970).
- JAROS, M. and ROSS, S.F., Proc. Int. Conf. Phys. Semiconductors, Stuttgart 1974, p. 401.
- NEWMAN, H.C., Adv. Phys. **18**, 545 (1969).
- DAVIES, G., Chemistry and Physics of Carbon, Vol 12, Ed. P.L. Walker, Jr. and P.A. Throver (in press).
- JONES, D. and LETTINGTON, A.H., Sol. St. Comm. **11**, 701 (1972).
- APPAPILLAI, M. and HEINE, V., Technical Report No. 5, 1972, Cavendish Lab., Cambridge, U.K. (Unpublished).
- MESSMER, R.P. and WATKINS, G.D., Phys. Rev. **B1**, 256A (1973).
- FARRER, R.G., Sol. St. Comm. **1**, 685 (1969).

Wave functions and optical cross sections associated with deep centers in semiconductors

M. Jaros*

Department of Physics and Astronomy, University of Massachusetts, Amherst, Massachusetts 01003

(Received 7 February 1977)

Analytical impurity wave functions associated with deep levels in semiconductors (e.g., GaAs:O, GaP:O) are calculated, using a pseudopotential scheme in which a realistic and convergent model is employed to represent the host-crystal band structure and the impurity potentials. The effects determining the form of the wave function are studied with a view to establishing a relationship between the position of a deep level in the gap and the localization of the wave function. It was found that the localization is not a sensitive function of the impurity energy measured from the nearest band edge. The optical impurity-to-band cross sections involving deep levels are computed as a function of photon energy and temperature. The electron-phonon interaction is taken into account within the strong-coupling model of Huang and Rhys. A relatively simple formula is derived which can be applied to interpret optical cross sections associated with deep centers dominated by a short-range potential. Numerical results are presented for state one and two of GaP:O, and the threshold energies, the magnitude of the Franck-Condon effect, and the temperature dependence are determined. A brief discussion is given of optical cross sections associated with deep centers in GaAs and Si.

I. INTRODUCTION

Photoexcitation has been widely used with success to study shallow and deep impurities in semiconductors. The main features responsible for this success are the speed, sensitivity, and the spectroscopic character of the technique. In contrast with standard conductivity measurements of the thermal-activation energy of the Hall constant, the optical method provides data for the relevant transition-matrix elements. The spectral distribution of the optical cross section can be determined at a number of photon energies and in a wide range of temperatures. Thanks to the great sensitivity of the technique, the spectral distribution can be accurately assessed over several orders of magnitude. Hence it is possible to study the broadening of the signal due to the electron-phonon interaction in some detail. In brief, the information provided by a well-planned experiment of this kind may yield the position of the impurity level in the forbidden gap, the character and magnitude of the coupling between the impurity and lattice, the properties of the impurity wave function, and the temperature dependence of the impurity level. Accordingly, the method has recently been refined in several directions. For example, the technique of photocapacitance spectroscopy has been developed which allows the deep levels within the space-charge layer of a p - n junction or Schottky barrier to be studied directly.^{1,2} This technique has been demonstrated by Henry and collaborators^{3,4} to be a fine tool for the study of deep levels. A quasi-equilibrium spectroscopic method which uses two light sources and a differentiated photocapacitance signal has been developed by White *et al.*⁵ Grimmeiss *et al.*⁷ have pioneered a method which is

based on the fact that the occupancy of an impurity level is not changed during illumination with photons of different energy if the photocurrent is kept constant. As a result of this lively development a great deal of experimental data has been made available. The strong overlap of this information with that provided by related methods, e.g., luminescence, optical absorption, etc., further enhances the value of the above-mentioned efforts. Unfortunately, the interpretation of the experimental data concerning the optical cross section is not always straightforward and a theoretical model is an essential ingredient in any event. Although the processes associated with shallow impurities seem well understood, this is not the case for deep chemical impurities and defects. Indeed, a truly quantitative analysis cannot be hoped for at the present time because our general understanding of the deep level problem is still poor. Yet it may seem desirable to make use of the existing insight and aim at producing a general prescription which would enable us to extract as much information as possible from a given experimental data.

Recently, we have performed calculations of impurity energies associated with chemical impurities⁸ and lattice defects⁹ in III-V semiconductors. In some cases we also computed the wave functions associated with deep states. In Sec. II we extend this calculation with a view to establishing a relationship between the position of the level in the forbidden gap and the localization of the wave function. In the past the localization of the impurity wave function has been assessed by relating the argument of the exponential "tail" of the wave function to the impurity energy defined with respect to the nearest relevant band edge. As a result the localization becomes a sensitive function of the position of the

impurity level in the gap. This approach has been shown correct in the case of "shallow" impurities, i.e., those impurities whose nature is determined by a prevailing role of the long-range Coulomb potential. Our calculations indicate that the position of a *deep* state in the gap may not necessarily be a good indication of the degree of localization. This result can be understood if we study the formation of the impurity energy and wave function in terms of the individual contributions associated with various parts of the wave-vector space. In general, numerically significant contributions can be found even from bands lying farther from the principal gap. The position of the impurity level in the gap is a result of a delicate cancellation process in which all these contributions play a part. Consequently, the "depth" of the level is not simply linked to the degree of localization of the corresponding wave function. Since the impurity energy defined in this way is really a difference between large terms of opposite signs, it is not surprising that it is a sensitive function of the strength and symmetry of the impurity potential. The impurity wave function appears to be highly localized and the degree of localization is not so sensitive to the strength of the potential. Both these observations seem useful. In particular, they allow us to simplify calculations of the optical matrix elements. In Sec. III we deal with photoionization cross section $\sigma_p(h\nu)$ as a function of photon energy $h\nu$ and temperature T . The electron-phonon interaction is accounted for within the strong coupling model, in the quasiclassical approximation.^{10,11} We arrive there at a simple prescription which allows us to deduce from a set of experimental data the position of the level in the gap, the magnitude of the Franck-Condon effect, the temperature dependence of the impurity level, and to a large degree, also the symmetry of the impurity wave function. In Sec. IV we apply our model to a set of data concerning GaP:O. We also comment on optical properties of similar states in GaAs and Si. We emphasize there the need for studies of temperature dependence of the optical cross sections, without which any data would seem to be incomplete and its interpretation at least to some extent ambiguous.

II. IMPURITY WAVE FUNCTIONS ASSOCIATED WITH DEEP LEVELS IN SEMICONDUCTORS

Recently, we have reported detailed calculations concerning energy levels associated with "deep" chemical impurities and lattice defects in GaAs and GaP.^{8,9} The most obvious aim of such calculations is to predict the positions of the impurity levels in the forbidden gap. Indeed, the impurity energy is often the only observable that is available from experiment. However, with the advance of

various techniques of optical and capacitance spectroscopy some additional data, e.g., carrier capture or photoionization cross sections, is becoming available. In most cases, such an information cannot be processed and made use of in the absence of a reliable description of the impurity wave function. It is, perhaps, characteristic of the state of art in this field that very little is known about the wave functions associated with levels lying further within the band gap. One might expect, as usual in quantum theory, the wave function to be a more sensitive indicator of any inadequacies of a model.

It has been shown in the early days of solid-state theory that the wave functions of the so-called shallow impurities can be thought of as a product of an envelope slowly varying smooth function, and a periodic function derived from the lowest-lying band minima.¹² It was also shown that such an approximation must break down if the dominant part of the impurity potential becomes more localized. If we then expand the impurity wave function ψ in terms of the complete set of eigenfunctions $\phi_{n,\vec{k}}$ of the perfect crystal Hamiltonian H_0 ,^{13,14}

$$\psi(\vec{r}) = \sum A_{n,\vec{k}} \phi_{n,\vec{k}}(\vec{r}), \quad (1)$$

the coefficients $A_{n,\vec{k}}$ associated with bands and wave vectors farther from the absolute band minima or maxima may still be numerically significant. [In (1), n, \vec{k} label bands and reduced wave vectors, respectively.] The simple separation of the impurity wave function into the envelope and periodic parts is no longer possible and the wave function ψ must be calculated numerically. We can, for instance, compute the impurity energy and coefficients $A_{n,\vec{k}}$ following the methods of Refs. 8 and 9 and output $\psi(\vec{r})$ of Eq. (1) at some real space points \vec{r}_0 . As we shall see later, such a procedure reveals some interesting properties of the wave function. However, it might be more convenient to generate ψ directly in an analytic form as a solution of the Schrödinger equation with the proper Hamiltonian and impurity energy.

It is borne in mind that a small angular variation, and a nodal structure extending far beyond the nearest-neighbor distance may not be relevant if we choose to deal with a deep state of $A_1(T_4$ group) symmetry.^{8,13} Indeed, one expects a carrier with an energy near the middle of the gap to be well localized within the volume comprising the impurity and its nearest neighbors. In such a case only a few parameters may be sufficient to capture the most important features of ψ and provide a useful analytic function which is well behaved for large values of \vec{r} and has a correct normalization.

Let us begin by choosing a trial function

$$\psi^0 = a_1 f_1 + a_2 f_2, \quad (2)$$

where

$$f_1 = (N_1)^{-1/2} e^{-\alpha r}, \quad f_2 = (N_2)^{-1/2} (1 + \beta r) e^{-\alpha r}, \quad (3)$$

and define β , N_1 , and N_2 so as to ensure

$$\int_0^\infty f_i f_j r^2 dr = \delta_{ij}. \quad (4)$$

The function ψ^0 must satisfy the Schrödinger equation

$$(H_0 + h)\psi = \epsilon\psi, \quad (5)$$

where h , ϵ represent the impurity potential and energy, respectively, and are assumed to be known from our earlier calculations of ϵ .^{8,9} We may write

$$(H_0 - \epsilon)\sum A_{n,\bar{k}} \phi_{n,\bar{k}} + h\psi^0 = 0, \quad (6)$$

and substitute for ψ^0 from (2), multiply by $\phi_{n',\bar{k}'}$ and integrate to obtain

$$A_{n',\bar{k}'} + \sum_{i=1}^2 a_i \frac{\langle \phi_{n',\bar{k}'} | h | f_i \rangle}{E_{n',\bar{k}'} - \epsilon} = 0. \quad (7)$$

Multiply by $\langle f_j | \phi_{n,\bar{k}} \rangle$, and $\sum_{n,\bar{k}}$ gives

$$\sum_{n,\bar{k}} A_{n,\bar{k}} \langle f_j | \phi_{n,\bar{k}} \rangle + \sum_{i=1}^2 a_i \times \sum_{n,\bar{k}} \frac{\langle \phi_{n,\bar{k}} | h | f_i \rangle \langle f_j | \phi_{n,\bar{k}} \rangle}{E_{n,\bar{k}} - \epsilon} = 0; \quad (8)$$

the sums can be readily computed following the procedures in Refs. 8 and 9, and the parameter α can be determined from the condition $\text{Det} = 0$.¹⁴ Finally, the coefficients a_1 , a_2 can be calculated and ψ^0 of Eq. (2) rewritten

$$\psi^0 = N^{-1/2} (1 + \gamma r) e^{-\alpha r}. \quad (9)$$

To test the reliability of the wave function ψ^0 defined in (9) we can invoke a consistency condition based on Eq. (6). If we compute a coefficient $A_{n,\bar{k}}^0$ from

$$A_{n,\bar{k}}^0 = -\langle \phi_{n,\bar{k}} | h | \psi^0 \rangle / (E_{n,\bar{k}} - \epsilon), \quad (10)$$

then

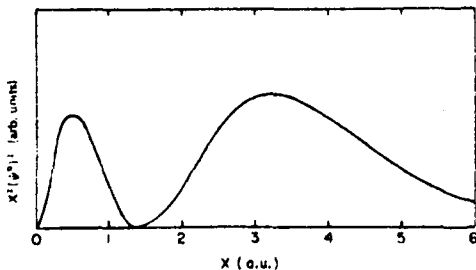


FIG. 1. Sketch of $x^2(1-0.68x)^2 \exp(-1.72x)$.

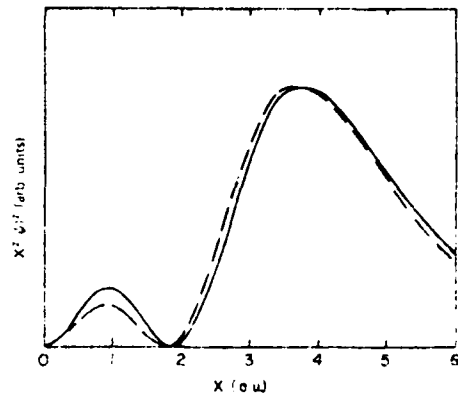


FIG. 2. $x^2\chi(x)\chi^*(x)$ of Eq. (11) for the trial-function parameters $\alpha=0.86$, $\gamma=-0.68$ (solid line) and $\alpha=0.50$, $\gamma=-0.55$ (interrupted line).

$$\chi = \sum A_{n,\bar{k}}^0 \phi_{n,\bar{k}} \quad (11)$$

should be indistinguishable from ψ^0 .

As we indicated earlier our procedure might have the best chance of success if applied to what is basically an s -like state. Calculations of the impurity energies concerning a substitutional donor oxygen in GaP and GaAs have been performed⁸ and deep levels obtained. Therefore the above procedure was applied to compute ψ^0 and χ for GaAs:O ground state. We find $\gamma=-0.68$ and $\alpha=0.86$, in atomic units (the energy $\epsilon=0.78$ eV was used in this calculation). $r^2\psi^0(r)^2$ is sketched in Fig. 1. In Fig. 2 we plot $x^2\psi^0(x)^2$. We also show the values obtained with $\gamma'=-0.55$ and $\alpha'=0.50$ for comparison.

In Fig. 3 we show $\chi\chi^*$ for both sets of γ, α to reveal the form near $|\bar{k}| \rightarrow 0$. Since the details of $\chi(x)$ are relatively insensitive to the choice of the parameters γ, α , we might ask whether the form of χ is at all similar to the form of ψ introduced via Eq. (1) (i.e., the function obtained via $A_{n,\bar{k}}$ without the help of a trial function ψ^0). When the calculation of ψ is carried out, it turns out that $x^2|\psi(x)|^2$ lies in between the two curves shown in Fig. 2 and can be well reproduced from (9)-(11) with a trial function (9) if $\gamma'=-0.56$ and $\alpha'=0.69$ a.u.

The difference between $\alpha'(=0.69)$ and $\alpha(=0.86)$ may indicate the degree of accuracy of determining the localization of the wave function. In this regard the pessimism of our introductory remark seems well justified. It might be argued that a higher-order polynomial in (9) could improve the situation. Alternatively, we may feel that it is sufficient to determine the wave packet of Eq. (1) at a grid of points in space and fit a polynomial function which describes these points. Naturally, such options



FIG. 3. $\chi(x)$ $\chi^2(x)$ of Eq. (11) for the two sets of parameters α, γ . Notation as in Fig. 2.

cannot be ruled out since, in principle, they are perfectly straightforward—although tedious prescriptions to follow. However, even for a state of A symmetry which is being considered here, the angular properties of the wave packet in the region of the second and higher nodes pose problems. Furthermore, the amplitudes of $|\psi|^2$ in the region of, say, $r \approx 10$ a.u. are typically by two or three orders of magnitude smaller than $|\psi(0)|^2$. The technical requirements which are set by these circumstances seem unreasonable. For example, we would have to aim at *less* than 1% error in ψ in order that the small amplitudes at larger r be meaningful at all!

There are several reasons which seem to diminish the importance of the discrepancy brought about by the large difference between α and α' . The parametrization chosen in Eqs. (2) and (3) links the parameter α which appears in the exponential, to the parameter β and consequently to the position of the node. Although this form is computationally convenient, it may impose a constraint upon α . It can be seen from Figs. 1–3 that the position of the node is always enforced, no doubt at the expense of an increased error in α .

We can show that the same difference between α and α' is found for the two-electron state O in GaP. In Ref. 8 we presented the first-principles wave function [derived via Eq. (1)] for the ground

state of this center. If we apply the procedure of Eqs. (2)–(9) to this case we arrive at $\alpha = 0.83$, $\gamma = -0.68$. A glance at Fig. 1 of Ref. 8 will confirm that the same relationship between the primed and unprimed parameters is found.

Since our early efforts¹³ in this field we have repeatedly observed that the localization of the wave function did not change as expected from the change in the position of the level in the gap. The data presented in Ref. 15 are also an eloquent example. The simplest way to demonstrate this effect is to scale the impurity potential, i.e., to multiply it by a suitable constant (the impurity energy of an s -like state changes quite substantially with scaling^{8,9}) and subsequently compute a new wave function. If, for instance, we bring the energy per electron in the above-mentioned two-electron state of GaP:O down from 1.15 to 0.75 eV, the parameters α, γ become 0.79 and -0.61 , respectively.

In the above paragraphs we have emphasized that both the conduction and valence band must be included in the expansion (1) in order that a convergence result for ϵ and ψ be ensured. The convergence properties of the calculation as far as the impurity energy ϵ is concerned have been shown in detail.^{8,9} It might be of interest to point out that an analogical comparison is possible as far as the wave function is concerned. We can recall our earlier calculation in which the wave functions for¹⁸ GaAs:O and¹⁹ GaP:O were computed with an expansion in Eq. (1) truncated to include effectively only the lowest two conduction bands. In those calculations the technique of solving the Schrödinger equation was somewhat different but the general form of both expansion (1) and the pseudopotential exactly the same. The first node of the wave function $\psi(x)$ appeared at a larger value ($\approx \frac{1}{2} a_{\text{lattice}} \sqrt{3}$) of x than that shown in Fig. 2. Also the results from the truncated expansion appear to be less localized. However, the overall character of the wave function is *not* much changed which emphasizes the prevailing role of the conduction bands in the formation of these states.

This important observation can be extended to include states dominated by contributions from valence bands. Our calculations concerning energies and wave functions introduced by lattice defects in GaAs,⁹ and also in¹⁷ GaP certainly support this view.

It is borne in mind that if the above conclusions are correct then we can hardly expect the difference in localization of the impurity wave function to help us greatly in distinguishing one impurity from another when we come to relate the localization to the observed spectra. Also there seems to be no substantial change in the nodal character of ψ as a

function of impurity energy provided that the symmetry is preserved. It is worth emphasizing that so far we have concentrated our attention on defects or deep impurities possessing the high symmetry of a substitutional site in the zinc-blende lattice. Our conclusions cannot be of course automatically extended to interstitials or defects of very low symmetry.

In the past the localization of wave functions associated with levels lying deeper in the gap than the so called shallow donors or acceptors has been estimated from the quantum-defect theory.¹⁸ For example, in their interesting study of the isotope shift for zero-phonon optical transition at traps in semiconductors,¹⁹ Heine and Henry evaluate the probability P of a carrier being on an atom. To compute P for deep donor oxygen in GaP, they introduce an envelope function

$$R(r) \sim r^{\nu-1} e^{-r/a}, \quad (12)$$

where $a = (2m^* E_i)^{-1/2}$ (a.u.). The parameter ν is determined by relating the effective mass (hydrogenic¹²) value E_H for a donor in GaP to the actual value of the impurity energy E_i ,

$$\nu^2 = E_H / E_i. \quad (13)$$

For a deep donor like GaP:O, $\nu \approx (0.05/0.9)^{1/2} \ll 1$ and the envelope function in (12) becomes very similar to the solution of the Schrödinger equation with a δ -function impurity potential.^{20,21} Our calculations on this subject show quite clearly that a substantial area in the wave-vector space is involved in the formation of the donor ground state and the effective-mass parameter is not applicable in the circumstances. Therefore the localization of the wave function cannot be well represented with the function of Eq. (12). However, the nodal character of the wave function is dominated by the standing waves of the lowest parts of the conduction band as conceived in the quantum defect model. Perhaps as a simple approximation we can still formally write the impurity wave function as a product of a periodic part determined rather well by the nodal properties of the dominating band states and a decaying (localized) function. The precise nature of the latter may be immaterial because it probably does not change strongly enough from defect to defect to be helpful in our analysis of most spectroscopic data.

III. OPTICAL CROSS SECTIONS

The experimental results of a photoconductivity or optical-absorption study can normally be reduced to a normalized cross section σ per photon, and it is our prime interest to relate this observation to a particular defect or impurity. In practice,

we really want to *distinguish* one curve from another, i.e., the real task is to predict the temperature dependence and the shape of the function $\sigma_T(h\nu)$ (where $h\nu$ is the photon energy and T stands for temperature) in relation to the nature of the impurity concerned. We propose to characterize a deep level by a set of parameters E_i , E_m , d_{FC} , and ΔE_T . E_i is the binding energy and is defined as the true energy of the state taking part in the transition with respect to the edge of a specified band of the host crystal. The maximum of the normalized cross section occurs at a photon energy E_m . d_{FC} is the magnitude of the Franck-Condon effect. ΔE_T is the shift of the impurity level at E_i in the gap, caused by a change in temperature. We also desire to determine symmetry properties of the impurity wave function.

Let us first choose to consider the optical cross section associated with an impurity-to-band transition assuming that the electron-phonon interaction is weak and can be left out. Then it is a standard approximation to write

$$\sigma(h\nu) = \frac{\text{const}}{h\nu} \sum_{n,\vec{k}} |\langle \psi | \exp(-i\vec{k}_1 \cdot \vec{r}) \vec{\epsilon}_1 \cdot \vec{\beta} | \Phi_{n,\vec{k}} \rangle|^2 \times \delta(E_i + E_{n,\vec{k}} - h\nu). \quad (14)$$

\vec{k} is the wave vector of the radiation field and λ is the polarization direction. In the usual dipole approximation we have $\exp(-i\vec{k}_1 \cdot \vec{r}) \sim 1$. The momentum matrix element in (14) really indicates an average over all degenerate initial and final states. The band wave functions and energies indicated by $\Phi_{n,\vec{k}}$ and $E_{n,\vec{k}}$ must be generated at a large number of points in the Brillouin zone and the expression in (1) evaluated numerically if a truly quantitative answer is required. Also the impurity wave function ψ is needed as an input in such an exercise. In this application it is convenient to express ψ as in (1), i.e., via the coefficients $A_{n,\vec{k}}$. A calculation along these lines has been performed⁸ for a transition from the two-electron state of oxygen in GaP to the conduction band at low temperatures. However, a proposition that such calculations be performed for all cases of interest, is unrealistic. Indeed, as soon as the temperature rises and strong electron-phonon interaction allowed for, the prospect of accomplishing this task disappears from our horizon. On the other hand, the impact of any simplification we make must be carefully assessed. The detailed calculation showed that the sum in (14)—when performed with a highly localized function ψ —is not a sensitive function of the form of ψ . The powerful averaging process implied in (14) always leads to a smooth curve for $\sigma(h\nu)$ and its shape reflects mainly the nodal mismatch between ψ and $\Phi_{n,\vec{k}}$, as well as the variation

in the density of states of the continuum.

In Sec. II we indicated the localization of the impurity wave function associated with a deep state and pointed out that it does not change considerably with impurity energy. This will help to simplify (14). The momentum matrix element in (14) is, with ψ from (1),

$$\langle \psi | p_x | \Phi_{n,\vec{r}} \rangle = \sum A_{n,\vec{r}}^* \langle \Phi_{n,\vec{r}} | p_x | \Phi_{n,\vec{r}} \rangle. \quad (15)$$

We can rewrite (5) with ψ from (1), multiply from the left by $\Phi_{n,\vec{r}}^*$ and integrate over all coordinates to obtain $A_{n,\vec{r}}$,

$$-A_{n,\vec{r}} = \langle \Phi_{n,\vec{r}} | h | \psi \rangle / (E_{n,\vec{r}} - E_I). \quad (16)$$

Since we generate h , $E_{n,\vec{r}}$, and $\Phi_{n,\vec{r}}$ within a pseudopotential scheme, the crystal wave functions are represented by linear combinations of plane waves, i.e.,

$$\Phi_{n,\vec{r}} = \sum_{\vec{G}_j} b_{n,\vec{r}}(\vec{G}_j) \exp[i(\vec{k} + \vec{G}_j) \cdot \vec{r}], \quad (17)$$

where \vec{G} stands for a reciprocal-lattice vector. The bands n and the reduced wave vectors \vec{k} which contribute to the transition probability at a particular photon energy $h\nu$ are selected by the δ function and the optical integral which appear in (14). Because of our declared intention not to get involved in the lengthy business of computing the sum in (14) by a sampling procedure, we must now enter upon the dangerous path of simplifications. Let us choose to represent the band wave functions by those of an isotropic semiconductor.^{22,23} Accordingly, the band functions take a form

$$F_{\pm}^{\pm} = (e^{i\vec{k}\vec{r}}/\sqrt{2})(C_1 e^{i\vec{k}\vec{r}} \pm C_2 e^{-i\vec{k}\vec{r}}), \quad (18)$$

with $C_1 = C_2 = 1$, and with + and - referring to the valence and conduction bands, respectively. At the band edge, the band functions are just $(1/\sqrt{2})(C_1 e^{i\vec{k}\vec{r}} \pm C_2 e^{-i\vec{k}\vec{r}})$. $\frac{1}{2}k_F^2$ is the free-electron Fermi energy in a.u.

It is easy to show that the Fourier transform indicated by the matrix element in (16) is constant over the range of energies $E_{n,\vec{r}}$, over which the mismatch between the nodal character of $\Phi_{n,\vec{r}}$ and ψ remains (on average) the same. In Sec. II we concluded that ψ may be formally written as a product of two terms, one representing the nodal properties of ψ and the other being a strongly localized function. We may, for instance, write

$$\psi = (e^{-\alpha r}/r) F_0^{\pm}. \quad (19)$$

The analogy with the quantum-defect effective-mass theory is merely in the form since we do not propose to choose α according to Eq. (12). The nodal part is chosen as a standing wave associated with the relevant band edge. We will return to comment upon this assumption later.

In the case of most deep states, the impurity potential is dominated by its short-range part. The impurity pseudopotential generally derives its strength from the area near the optimized-model potential radius which is typically of the order of the tetrahedral covalent radius r_c , or less. Therefore, we are not likely to overestimate the localization of h if we choose $h \sim r e^{-r/r_c}$. Then the leading term in the expression for the matrix element in (16) is

$$I(E_{n,\vec{r}}) = \langle \Phi_{n,\vec{r}} | h | \psi \rangle \sim \frac{C_1^2 \pm C_2^2}{k} \times \int_0^{\infty} \sin(kr) r e^{-ur} dr, \quad (20)$$

where $u = \alpha + 1/r_c$. Hence

$$I(E_{n,\vec{r}}) \sim I_k \sim [u/(k^2 + u^2)^2] (C_1^2 \pm C_2^2). \quad (21)$$

In Sec. II, we presented some results concerning the localization of the impurity wave functions associated with deep states. We found that $\alpha \sim 0.5$ (a.u.). The typical value for r_c is 2 a.u. so that $u \sim 1$ a.u. Since the range of photon energies is restricted to $h\nu \leq E(\text{gap})$ (and in fact the ionization energy E_I constitutes a substantial portion of that energy), the values of k^2 entering (21) appear to be small compared to u , i.e., I is for any practical purposes a constant. It is now easy to see that this result does not really depend upon the choice of a particular analytic form of ψ , $\Phi_{n,\vec{r}}$ since for a somewhat different choice the result would be the same. However, we do need the simplified form of $\Phi_{n,\vec{r}}$ shown in (18) since it will enable us to eliminate the sampling procedure. Then we can introduce the band density of states $\rho(E)$ and write (14) as

$$\sigma(h\nu) = \text{const } I \frac{\rho(E)}{h\nu} \left| \frac{\langle F_1^{\pm} | p | F_2^{\pm} \rangle (C_1^2 \pm C_2^2)}{E - E_I} \right|^2. \quad (22)$$

Only a transition to a band with nodal properties "matching" those of ψ is allowed and since $h\nu = E + |E_I|$, we arrive at

$$\sigma_L(h\nu) \sim [(h\nu - |E_I|)/h\nu]^2 \rho(h\nu - |E_I|). \quad (23)$$

With $\rho \sim (h\nu - |E_I|)^{1/2}$, the normalized cross section of (23) has the same form as that of the well-known Lucovsky formula.²⁰ Had we assumed, as did Lucovsky, that the potential h in (20) is a δ function we would have arrived at $I = \text{const}$ and consequently Eq. (23) as well. Here we obtain Eq. (23) without having sacrificed much of the realistic form of h and ψ . Note that (23) predicts the maximum of $\sigma(h\nu)$ to occur at $h\nu = 2|E_I|$. As we pointed out earlier, our choice to represent the nodal part of ψ , F_0^{\pm} , in terms of the band-edge standing waves, is merely a convenient vehicle for modeling (at a later stage) the change in the nodal mismatch of the impurity and band wave functions. It means

that we can also observe the "forbidden" transition since in most cases of practical interest $C_1^2 - C_2^2 \neq 0$. Hence we arrive at another limiting case, analogous to the Lucovsky formula for our "allowed" transition, i.e., $\sigma(h\nu) = \rho(h\nu - |E_i|)/h\nu^3$ postulated by Kopylov and Pikhin.²¹

On our way from Eq. (19) to (22), we kept the mismatch between the nodal structure of ψ and the band wave function unchanged. Even in the most favorable of circumstances such an assumption becomes invalid when we excite the carrier into states lying farther from the band edge. This is particularly so in the case of the conduction band in direct-gap materials where the importance of the multivalley character of the band structure is manifest. The changes concerning the density of states can be, at least at low temperatures, well accounted for via ρ . The change in the nodal mismatch, alas, presents an unsurmountable difficulty since its precise rate can only be established by a very detailed calculation. To demonstrate the essence of the problem let us suppose that $\psi = e^{-\alpha r} \times \phi_{n_0, \vec{k}_0}/r$. Then at each sampling point n_i, \vec{k}_i [chosen in order to evaluate numerically the sum in (14)] the leading contribution to $I = I(E_{n_i, \vec{k}_i}) = M_{n_i, \vec{k}_i}$ where

$$M_{n_i, \vec{k}_i} = \sum_j b_{n_i, \vec{k}_i}^*(\vec{G}_i) b_{n_0, \vec{k}_0}(\vec{G}_i). \quad (24)$$

In evaluating (20) we chose ϕ_{n_0, \vec{k}_0} and ϕ_{n_i, \vec{k}_i} in such a way that M happened to be one or zero. However, the value of M will fluctuate as we proceed to sample states farther from the band edge. So in general, we must expect a detailed calculation to *reduce the average value of I as we increase E_{n_i, \vec{k}_i}* . In the language of our simplified formalism for the evaluation of I , the average value of $I_h \sim C_1^2 \pm C_2^2$ where

$$1 \leq C_1^2 + C_2^2 \leq 2 \quad (25)$$

and, for the minus sign,

$$0 \leq C_1^2 - C_2^2 \leq 1. \quad (26)$$

This can be taken into account if we introduce a function $\eta = \eta(E)$ such that near the band edge $\eta = 1$ but $\eta \rightarrow 0$ as $(h\nu - |E_i|) \rightarrow \infty$. The cross section then becomes

$$\sigma(h\nu) = \frac{\rho(E)}{h\nu} \left| \frac{1 \pm \eta}{|E + |E_i||} (E)^{1/2} + \frac{1 \mp \eta}{|E_i| - E_f - E} (E_f)^{1/2} \right|^2. \quad (27)$$

The appearance of the (negative) second term on the right-hand side represents the fact that the wave function ψ of a deep impurity can now couple to both the conduction and valence band. Formula (27) obviously oversimplifies this relationship. For example the results presented in Ref. 8 show

that only the lowest two valence bands contribute significantly to the totally symmetric ground state of GaP:O. This observation is easy to understand if we recall that the top of the valence band is basically p -like, whereas the lowest parts of the conduction band are predominantly s -like. Only the s -like part of the valence band contributes significantly. Hence, in the language of our isotropic semiconductor model, only the valence states outside the optical gap contribute. We may then change the denominator of the second term to $|E_i| - \frac{1}{2}E_f - \frac{1}{2}E_g - E$, where E_g is the average (Penn)^{22,23} gap. It is borne in mind that the degree of cancellation brought about by the appearance of the second term on the right-hand side of (27) depends on the symmetry of the impurity center. By analogy with the states of oxygen in GaP we expect a deep state which is being dominated by the valence bands to have small coefficients A_{n_i, \vec{k}_i} associated with the bottom of the conduction band. Only farther from the edge would the p character of the band states give rise to a region where A_{n_i, \vec{k}_i} be numerically significant.

In (27) we also assumed that $k^2/2m^* = E = h\nu - |E_i|$ instead of trying to achieve a better balance between $E^{1/2}$ and $(E_f)^{1/2}$ by employing some additional corrective parameter. Since this is only relevant for small E where the second term should not apply in any case, such an addition would not be much of an improvement. However, whatever the precise quantitative form of $\eta(E)$ and other parameters in (27), the effect upon the shape of $\sigma(h\nu)$ can only be that the maximum of $\sigma(h\nu)$ shifts towards lower photon energies. We can now understand why the "Lucovsky" form of Eq. (23) so well fits photoionization curves associated with "medium" deep impurities like In in Si [$E_i \approx 3E_f$ (hydrogenic)] but not those of "shallow" and "deep" impurities. In the case of the shallow impurities the impurity potential is dominated by its long-range Coulomb part and the wave function is very extended. The Fourier transform implied by the matrix element I is then a sensitive function of k and its shape depends on the degree of localization of the impurity wave function. As a result the maximum σ occurs at $h\nu < 2|E_i|$.¹⁸ For deep levels dominated by a short-range potential, $2|E_i|$ is a large number, and before $h\nu$ reaches $2|E_i|$ the excitations occur from the deep level into the band states lying farther from the band edge. The change in the nodal mismatch leads to a shift of the maximum to $h\nu < 2|E_i|$. Although there can hardly be much doubt about the nature of this trend, its quantitative appreciation is difficult to establish. There are obviously many ways of representing η which will in turn affect the precise form of $\sigma(h\nu)$.

There is some hope, however, that the actual

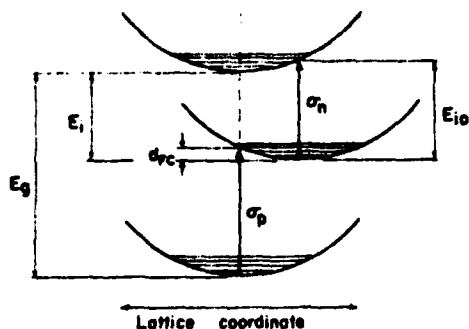


FIG. 4. Configuration-coordinate diagram involving a deep level with binding energy E_1 and the conduction and valence bands separated by a band gap E_2 . d_{FC} indicates the magnitude of the Franck-Condon effect. The transitions from the level to the conduction band (σ_n) and from the valence band to the level (σ_p) are indicated. E_{10} is the optical-ionization energy.

form of $\eta = \eta(E)$ may not be of great significance. We must remember that the sole purpose of introducing this parameter is to take account of the change in the average value of the matrix element I with E due to the change in the nodal mismatch of ψ and the band wave function. Hence $\eta(E)$ must be a slowly varying function of E . It should also change very little with temperature. Indeed η must change with E slowly enough so that the cross sections of medium deep levels are unaffected. Now the minimum gap is always small compared to the average (Penn)^{22,23} optical gap E_p , and since E_p is a good measure of the strength of the crystal potential, the rate of change in $\eta(E)$ should go as $\sim(E_p/2)^{-1}$. Thus we may choose for $\eta(E) = \exp(-2E/E_p)$ which interpolates smoothly between its apparent values at $E=0$ and $E=\infty$. Should this prove inadequate E_p can be used as a free parameter to achieve a better agreement with experiment.

In our discussion of the impurity wave functions associated with deep levels in semiconductors we noted that these functions are highly localized. It is therefore to be expected that when such a state is occupied with an electron, some additional lattice relaxation may take place which significantly changes the position of the level in the gap. It is customary to picture such an effect in a configuration coordinate diagram shown in Fig. 4. The electronic transitions from and into the impurity level, indicated in this figure, reflect the magnitude of this effect (which is connected with the name of Franck and Condon). In the event of strong coupling between the impurity and lattice, the transition probability can be expressed following the model of Huang and Rhys.²⁴ In this model, the equations for the electronic and phonon functions separate. Only

the electron-phonon interaction which is linear in the lattice coordinates is included. The cross section σ becomes

$$\sigma_T(h\nu) = \frac{1}{h\nu} \sum_{n,i} |\langle \psi | \exp(-i\vec{k}_\lambda \cdot \vec{r}) \vec{\epsilon}_\lambda \cdot \vec{p} | \Phi_{n,i} \rangle|^2 J_{n,i}, \quad (28)$$

where the function $J_{n,i}$ carries the information about the vibrational states and for the model in question can be evaluated exactly.¹¹ At high temperatures and for strong electron-phonon coupling, the expression for $J_{n,i}$ simplifies to

$$J_{n,i} \sim (4\pi k_B T S \hbar \omega)^{-1/2} \exp\left(-\frac{(h\nu - [E_{10}^T + E_{n,i}])^2}{4k_B T S \hbar \omega}\right) \quad (29)$$

Here $\hbar\omega$ refers to the phonon energy and the term $S\hbar\omega = d_{FC}$ is shown in Fig. 4. k_B is the Boltzmann constant. E_{10} is the optical-ionization energy of the impurity at T . The preexponential term obviously does not affect the shape of the optical cross section and for our purposes can be omitted. We may now recall the simplifications which lead us from (14) to (22). Including the expression (29), we rewrite Eq. (28) as follows:

$$\sigma_T(h\nu) = \frac{1}{h\nu} \int_0^\infty dE \rho_T(E) \left\{ \frac{(1 \pm \eta)E^{1/2}}{|E_{10}^T| + E} + \frac{(1 \mp \eta)(E_p)^{1/2}}{|E_{10}^T| - E - (E_p + E_p)/2} \right\}^2 \times \exp\left(-\frac{(h\nu - [E_{10}^T + E])^2}{4k_B T d_{FC}}\right). \quad (30)$$

IV. NUMERICAL RESULTS AND DISCUSSION

A glance at Eq. (30) may assure us that had we decided to keep the true band structure in the expression for $\sigma_T(h\nu)$ [Eq. (14)] we would now have to face an unenviable task of computing the optical sums as many times as necessary in order to accomplish the numerical integration implied in (30). In the light of this observation, we may feel fully justified in having introduced the simplification outlined in Sec. III. Instead of relying on a detailed computer sum evaluation, our simple model describes the changes in the matrix element I due to the nodal mismatch (between the impurity wave function and the band states of a particular energy) in terms of the parameter $\eta = \eta(E_p, E)$. In this study we regard this as the sole purpose of introducing η . E_p may be, if necessary, treated as a free parameter, together with E_{10}^T and d_{FC} . The computations implied by (30) are minimal and the smallest computer allows them to be repeated as often as required. Hence, a given set of experimental data, i.e., the normalized cross-section

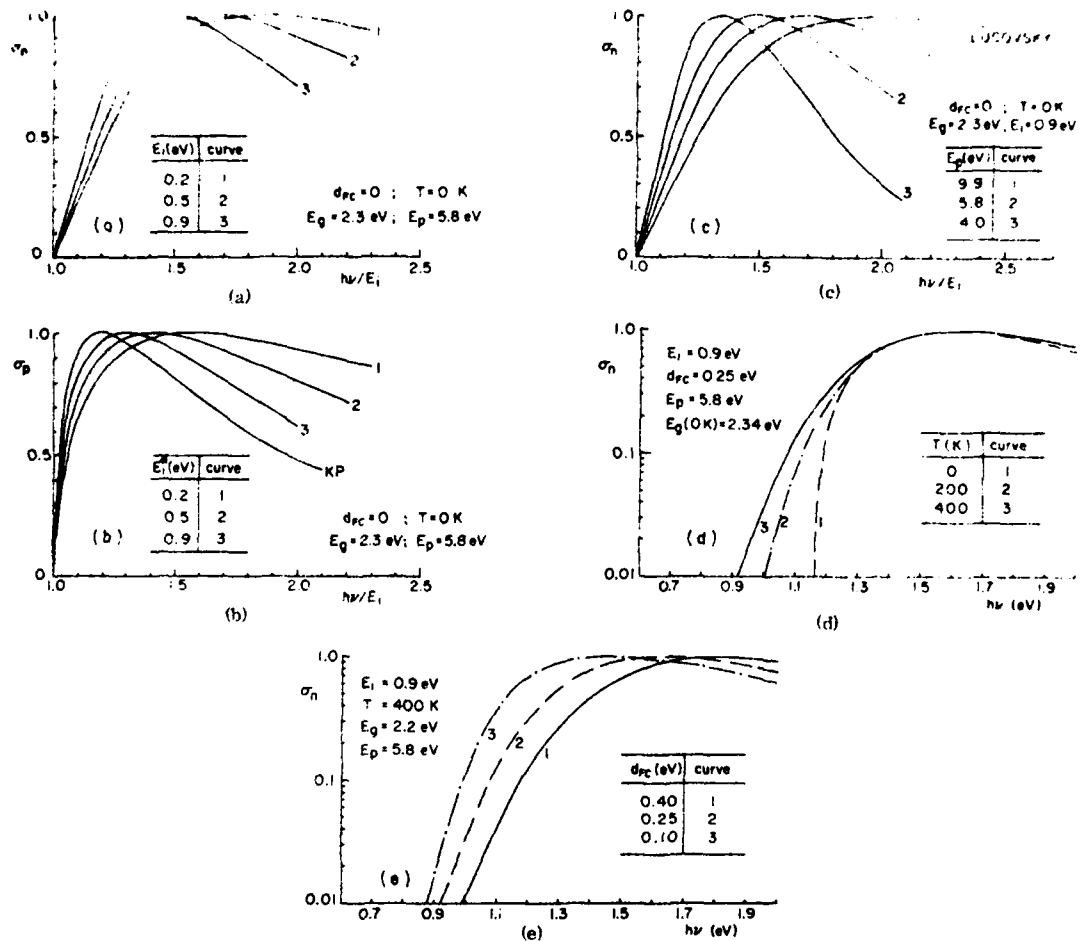


FIG. 5. Normalized cross sections σ_n, σ_p for several values of the parameters E_i, d_{FC}, E_p and temperature T , from Eq. (28). The nodal properties of the impurity wave function are determined by F_0^+ [Eqs. (18) and (19)]. The relevant values of the parameters are indicated throughout (see also Fig. 4). In (b) the binding energy E_i^* is measured from the top of the valence band. Note that σ_L (c) and σ_{KP} (b) are the special cases discussed in the text following Eq. (23). The parameter E_p is introduced and discussed in Sec. III, between Eqs. (23) and (24). Note that $E_p=5.8\text{ eV}$ is the average optical gap of GaP. In (d) it is assumed that E_i is independent of temperature.

curves $\sigma = \sigma_r(h\nu)$, at several values of temperature T , can be interpreted in terms of the optical-ionization energy E_{i0}^* and the Franck-Condon shift d_{FC} , fitted to reproduce the data. By selecting F_0^+ or F_0^- in (18) and (19) which indicates the origin of the nodal character of ψ and employing (30) we may arrive at a sensitive tool capable of distinguishing cross sections of centers possessing different symmetry properties. In Fig. 5, we summarize some general predictions based on the formula (30). We can see there the shape of the cross sections σ_n and σ_p , associated with transitions from a level to the conduction band and from the valence band to the deep level in the gap, respectively. The notation is consistent

with that in Fig. 4 which shows the transitions in a simple diagram including the Franck-Condon effect parameter d_{FC} . The effect of temperature upon σ is also demonstrated and it is assumed that the level does not have any temperature dependence (i.e., the binding energy E_i does not change with temperature). Note that the ambiguity introduced by our somewhat arbitrary choice of the parameter E_p is not very significant unless E_p is taken to be much smaller than the average optical gap.

One of the important conditions for a successful interpretation of the experimental data is that the cross-section measurements are taken at several temperatures. It is also essential that the range

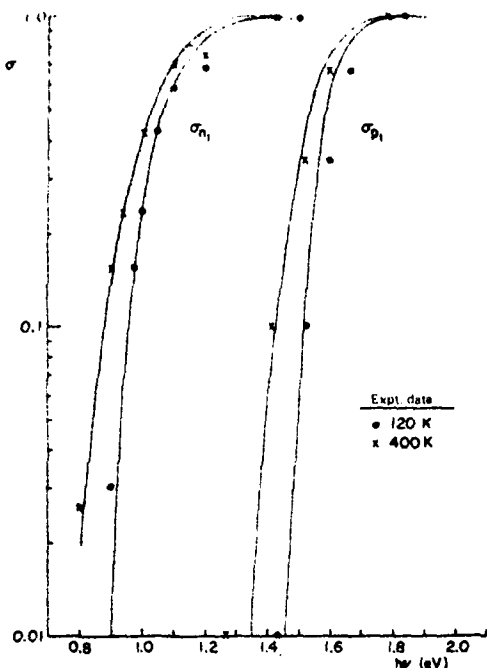


FIG. 6. σ_{n_1} and σ_{p_1} are the transitions from and to the oxygen donor (state 1) ground state [$E_1(4\text{ K}) = 896$ meV from the conduction band] indicated schematically in Fig. 4. The curves refer to the present calculation with $d_{FC} = 80$ meV, $E_1(120\text{ K}) = 0.87$ and $E_1(400\text{ K}) = 0.82$ eV. The points are the experimental results (Refs. 3 and 26) shown for comparison.

of photon energies covered in the experiment is sufficient to reach both the exponential low-energy tail and the point where $\sigma(h\nu)$ appears to have a maximum. Should experimental results for $\sigma_T(h\nu)$ at one temperature only be used for the fit to the formula (30), the result is bound to be ambiguous since in the presence of large Franck-Condon effect there are too many free parameters. With data at different values of T we might be able to diminish the uncertainty introduced via η .

In Sec. III we proposed that transitions from the valence band to the impurity level be treated in an analogical fashion to those from the level to the conduction band which take place in the area near the X point. This point is in the center of the Jones-zone flat-surface area.²³ At and near that point our attempt to imitate the "multiband" character of the observed transition by a simple formula in (27) or (30) might be well justified. However, the transitions from the valence band (Fig. 4) occur near the Γ point where the direct (optical) gap is much smaller and the Bragg reflections at higher reciprocal-lattice vectors affect the band wave functions. Our formulas of (27) and (30), if

simply inverted and used to interpret the above-mentioned transitions, must of necessity give a poorer representation of the experimental data.

It is outside the scope of this paper to comment upon the precautions an experimentalist must take in order to generate a trustworthy set of data. Often the photoconductivity data are not supported by any control data (e.g., photo-Hall mobility.) Then, in the absence of other arrangements, it is not clear whether the observed signal is just a "convolution" representing a number of transitions or whether it corresponds to only one type of transition from one deep level in the gap. In brief, of the vast literature on deep levels only a very small fraction is amenable to theoretical treatment. It goes without saying that the very threshold observed in an experiment is in many cases difficult to establish from data taken at one temperature only. This is particularly apparent in the case of deep levels exhibiting strong coupling to the lattice.

Oxygen in GaP is perhaps the only "deep" impurity as far as III-V semi-conductors are concerned which has been studied extensively enough so that the data required seems available. We will, therefore, concentrate our attention on GaP:O. We will also discuss the applicability of (30) to deep levels in GaAs. Finally, we will discuss some important dopants in silicon, e.g., gold.

A. GaP:O—State 1 (one-electron donor state)

The transitions from the donor ground state to the conduction band (σ_{n_1}) and also the transitions from the valence band to the state in the gap (σ_{p_1}) have been measured as a function of photon energy and temperature.^{3,4,25-28} The experimental points are shown, for $T = 120\text{ K}$ and $T = 400\text{ K}$, in Figs. 6 and 7. The band gap of GaP changes from ~ 2.32 to ~ 2.22 eV in this range of temperatures.²⁹

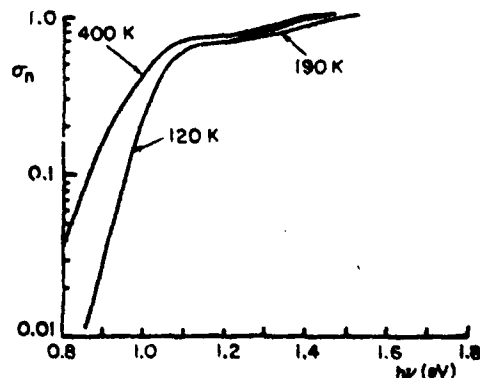


FIG. 7. Plot of the experimental results for $\sigma_{n_1}(\text{GaP:O})$ at 120, 190, and 400 K (Refs. 3 and 26).

The temperature broadening of σ_{n_1} is relatively small. Taking $d_{FC} = 0.08$ eV and recalling that the low-temperature binding energy of GaP:O is 0.896 eV (Ref. 30) we arrive at curves shown in Fig. 6 which seem in reasonable agreement with the experimental values. Note that consistent results are obtained for both σ_{n_1} and σ_{p_1} . It transpires that with $d_{FC} = 80$ meV between 120 and 400 K the oxygen binding energy with respect to the conduction band decreases by 50 meV. The assessment of the temperature dependence is confirmed by the shift of $\sigma(\text{max})$ as well. The numerical estimate of both figures (80 and 50 meV) is, of course, subject to a large error and these numbers are probably correct only to within ± 10 meV. The result is in principal agreement with the assessment of Braun and Grimmeiss.²⁸

The difference between the observed and calculated cross sections σ_{p_1} is not difficult to accept because of the approximate nature of (30). Also for small d_{FC} (and/or low temperatures), formula (30) cannot be expected to reproduce faithfully the details of σ . The difference between the calculated and observed σ_{n_1} is more important. To illustrate the effect with greater precision we reproduce the data separately in Fig. 7. The dip in $\sigma_{n_1}(h\nu)$ starting at $h\nu \sim 1.15$ eV persists up to high temperatures without any significant change. Therefore, it is not entirely clear whether it can be attributed to a change in the band density of states only. It may be that some other transition is responsible for this odd effect. The point is certainly worth investigating since our understanding of the levels introduced by O in GaP is more advanced than in other cases, where it may serve as a useful (and rare) guide.

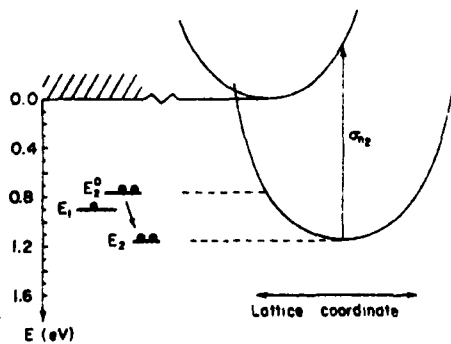


FIG. 8. Summary of computer calculations concerning the two-electron state (state two) of GaP:O (Ref. 8). E_1 is the ground state of the state one. The second electron is captured at E_2^0 and the following lattice relaxation brings the energy per electron down from E_2^0 to E_2^1 . The transition of an electron to the conduction band (σ_{n_2}) is also shown.

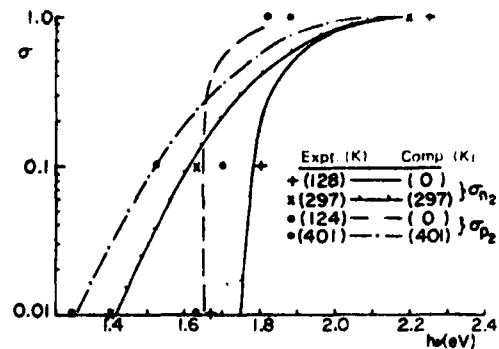


FIG. 9. The computed and experimental (Ref. 3) results for the electron transitions from the two-electron state of GaP:O (σ_{n_2}) to the conduction band, and from the valence band to the level (σ_{p_2}). The curves correspond to a Franck-Condon shift of 0.55 eV. The first-principles calculation (Ref. 8) gave 0.4 eV (see Fig. 8).

B. GaP:O - State 2 (two-electron state)

The oxygen potential is strong enough to bind two electrons.^{8,14,31} The photocapacitance measurements^{3,4} were used to extract the optical cross sections $\sigma_{n_2}(h\nu)$ and $\sigma_{p_2}(h\nu)$ involving an electron transition from the two electron state to the conduction band and from the valence band to the level in the gap, respectively. The temperature dependence of σ points to a strong coupling to the lattice. A calculation was performed⁸ to estimate the magnitude of the change in the electron energy due to lattice relaxation which follows the capture of the second electron and electron charge polarization. That result is pictured in Fig. 8, in terms of a simple configuration coordinate diagram. The shape of σ_{n_2} was also calculated. However, the threshold energy at which this transition should be observed is not easy to deduce from such a calculation, although we know the energy per electron in both, the one and two electron states (and before and after the lattice relaxation takes place), measured with respect to the binding energy of the single donor (i.e., ~ 0.9 eV). In order to excite one electron from the two-electron state to the conduction band, the energy required to reaccommodate the other electrons in the system must be accounted for. Hopefully this term is small so that E_{i0} is approximately given by the line shown in Fig. 8. In the present study we can treat E_{i0} as a function of temperature. A comparison of the present calculation with experiment is shown in Fig. 9. It would appear that the parameter d_{FC} should be less than 0.55 eV. The above-mentioned computer calculation gave 0.4 eV. The results of our calculations as $T=0$ and $T=400$ K, presented in Fig. 9, are compared with the experimental data of Kukimoto

*et al.*¹ The computed curves for $T=0$ nicely illustrate the dramatic changes brought about by an increase in temperature. An overall agreement in Fig. 9 is good but the shape of σ_p near its maximum is difficult to understand. However, it must be remembered that these cross sections cannot be easily extracted from the experimental data and the relevant rate equations.^{3,4} In a difficult multi-level problem some error is inevitable. Also, our formalism is based on a linear-coupling model which employs only one phonon mode. Nonlinear effects may bring about some additional changes in the shape of σ_n and σ_p , and may affect them differently. It would then seem as if the two transitions were effectively associated with a different d_{FC} , an impression one might get from the comparison in Fig. 9. It is indeed impossible to fit the high-temperature curves well with d_{FC} being the same for both, σ_n and σ_p .

C. GaAs

A single donor substituting for arsenic is expected near the middle of the gap.⁸ Experimental data, although in one way or another referring to oxygen, has so far produced no clear confirmation of the prediction. Perhaps because of this uncertainty, and also because of a large number of deep levels present in this material, it is to the best of our knowledge impossible at this stage to gather a set of data equivalent to those for GaP:O. The confusing state of affairs is well documented in recent papers by Lang and Logan³² or Lin *et al.*³³ A similar situation is characteristic of another important dopant Cr.³⁴ We will, therefore, make only general comments on the differences we should expect when comparing GaP and GaAs. As we pointed out earlier,^{6,35} some effect upon the shape of the cross section σ_n might be expected due to the low density of states area near Γ . We have also indicated that the nearly-free-electron-like model we introduced to allow for a better fit of σ may be

a poor approximation at Γ where the concept of an isotropic semiconductor breaks down. As a result somewhat sharper spectra might be expected compared to GaP. However, as in GaP, the data available at present does indicate a number of deep levels in GaAs strongly coupled to the lattice.

D. Si

The optical cross sections of several important deep dopants in Si have been measured. The data on deep levels introduced for instance, by Zn,³⁶ S,³⁷ Au,³⁸ and Co (Ref. 39) is customarily interpreted⁴⁰ as indicating that none of these impurities exhibits strong coupling to the lattice. This is most remarkable since it might support the old belief that all these may be simple substitutional donors or acceptors. The proposal that gold and cobalt impurities are somewhat related to a complex with vacancy⁴¹ would lead us to anticipate a great deal of lattice relaxation and the temperature dependence of the optical cross sections should show broadening.

Unfortunately, a careful inspection of published material on levels in Si indicates that there are substantial differences between results available in the literature (gold donor being a good example). The complications brought about by the presence of several optically active levels in the material under investigation, and in most cases a restricted range of temperature considered increase the degree of uncertainty. Also the band gap of Si is smaller than that of GaP or GaAs and the absolute changes in the impurity energy are expected to shrink accordingly. We believe, therefore, that under these circumstances the question concerning the lattice relaxation effects in Si remains open.

ACKNOWLEDGMENTS

It is a pleasure to thank Claude M. Penchina and Hans J. Stocker for many discussions.

^{*}Supported in part by ONR under Contract No. N00014-76-0890.

¹On leave of absence from Dept. of Theoretical Physics, the University, Newcastle upon Tyne, U.K.

¹C. T. Sah, L. Forbes, L. L. Rosier, and A. F. Tasch, Jr., *Solid State Electron.* **13**, 759 (1970).

²C. T. Sah, W. W. Chan, H. S. Fu, and J. W. Walker, *Appl. Phys. Lett.* **20**, 193 (1972).

³H. Kukimoto, C. H. Henry, and F. R. Merritt, *Phys. Rev. B* **7**, 2486 (1973).

⁴C. H. Henry, H. Kukimoto, G. L. Miller, and F. R. Merritt, *Phys. Rev. B* **7**, 2499 (1973).

⁵A. M. White, P. Porteous, and P. J. Dean, *J. Electron. Mater.* **5**, 91 (1976).

⁶A. M. White, P. J. Dean, and P. Porteous, *J. Appl. Phys.* **47**, 3230 (1976).

⁷H. G. Grimmeiss and L.-Å. Ledebø, *J. Appl. Phys.* **46**, 2155 (1975).

⁸M. Jaros, *J. Phys. C* **8**, 2455 (1975).

⁹M. Jaros and S. Brand, *Phys. Rev. B* **14**, 4494 (1976).

¹⁰K. Huang and A. Rhys, *Proc. R. Soc. A* **204**, 406 (1950).

¹¹T. H. Keil, *Phys. Rev.* **140**, A601 (1965).

¹²W. Kohn, *Solid State Phys.* **5**, 257 (1957).

¹³M. Jaros and S. F. Ross, *J. Phys. C* **6**, 3451 (1973); and also S. F. Ross, Ph.D. thesis (Newcastle University, U.K., 1975) (unpublished).

¹⁴Note that $\sum A_{n,\vec{k}} \langle f_j | \phi_{n,\vec{k}} \rangle = a_j$, and we have two homogeneous equations with unknown coefficients a_1 and a_2 to solve. The sums involving the matrix elements of h are then evaluated with different values of the wavefunction parameter α until the usual condition $\text{Det}=0$ is satisfied.

¹³M. Jaros and S. F. Ross, *Proceedings of the Twelfth International Conference on the Physics of Semiconductors* (Teubner, Stuttgart, 1974), p. 401.

¹⁴S. F. Ross and M. Jaros, *Phys. Lett. A* **45**, 355 (1973).

¹⁵M. Jaros and G. P. Srivastava (unpublished).

¹⁶H. B. Bebb, *Phys. Rev.* **185**, 1116 (1969).

¹⁷V. Heine and C. H. Henry, *Phys. Rev. B* **11**, 3795 (1975).

¹⁸G. Lucovsky, *Solid State Commun.* **3**, 299 (1965).

¹⁹A. A. Kopylov and A. N. Pikhin, *Fiz. Tverd. Tela* **16**, 1837 (1974) [*Sov. Phys.-Solid State* **16**, 1200 (1975)].

²⁰D. R. Penn, *Phys. Rev.* **128**, 2093 (1962); J. A. Van Vechten and J. C. Phillips, *Phys. Rev. B* **2**, 2180 (1970).

²¹V. Heine and R. O. Jones, *J. Phys. C* **2**, 719 (1969).

²²K. Huang and A. Rhys, *Proc. R. Soc. A* **204**, 406 (1950).

²³G. Björklund and H. G. Grimmeiss, *Solid State Electron.* **14**, 589 (1971).

²⁴S. Brown and H. G. Grimmeiss, *Solid State Commun.* **12**, 657 (1973).

²⁵H. C. Henry and D. V. Lang, *Phys. Rev. B* (to be published).

²⁶D. V. Lang and C. H. Henry, *Phys. Rev. Lett.* **25**, 1525 (1975).

²⁷C. D. Thurmond, *J. Electrochem. Soc.* **122**, 1133 (1975).

²⁸P. J. Dean, C. H. Henry, and C. J. Fosch, *Phys. Rev.* **168**, 812 (1968).

²⁹G. T. Pantelides, *Solid State Commun.* **14**, 1255 (1973).

³⁰D. V. Lang and R. A. Logan, *J. Electron. Mater.* **4**, 1053 (1975).

³¹Alice L. Lin, E. Omelianovski, and R. H. Dube, *J. Appl. Phys.* **47**, 1852 (1976).

³²Alice L. Lin and R. H. Dube, *J. Appl. Phys.* **47**, 1859 (1976).

³³M. Jaros, *J. Phys. C* **8**, L264 (1975).

³⁴J. M. Herman III and C. T. Sah, *J. Appl. Phys.* **44**, 1259 (1973).

³⁵T. H. Nigh and C. T. Sah, *Phys. Rev. B* **14**, 2528 (1976).

³⁶S. Braun and H. G. Grimmeiss, *J. Appl. Phys.* **45**, 2658 (1973); O. Engström and H. G. Grimmeiss, *Appl. Phys. Lett.* **25**, 413 (1974); D. C. Wong and C. M. Penchina, *Phys. Rev. B* **12**, 5840 (1975).

³⁷C. M. Penchina and J. S. Moore, *Phys. Rev. B* **9**, 5217 (1974).

³⁸D. V. Lang, *Proceedings of the International Conference on Radiation Effects in Semiconductors*, Dubrovnik, Yugoslavia, Sept. 1976 (unpublished).

³⁹J. A. Van Vechten and C. D. Thurmond, *Phys. Rev. B* **8**, 3539 (1976).

32

A CASE FOR LARGE AUGER RECOMBINATION CROSS SECTIONS ASSOCIATED WITH DEEP CENTERS IN SEMICONDUCTORS

M. Jaros^{*†}

Department of Physics and Astronomy, University of Massachusetts, Amherst, MA 01003, U.S.A.

(Received 31 October 1977 by L. Hedin)

It is argued that the recent quantitative results concerning localized defects in semiconductors (e.g. GaAs) are consistent with the possibility of large Auger-type cross sections associated with recombination at these centers.

It is proposed that many of the capture cross sections reported to be in the range 10^{-13} – 10^{-16} cm², which exhibit only weak temperature dependence, and which do not depend on carrier concentration, might be explained by this mechanism.

RECENTLY, we have reported pseudopotential calculations of the energies and wave functions associated with deeply bound carriers in GaAs and GaP [1, 2]. We have shown that, for instance, a gallium vacancy (V_{Ga}), or a complex involving an impurity and V_{Ga} , may deeply bind one or two particles in the forbidden gap. We have also shown that owing to the close spatial localization of the bound particles, their interaction energy is a significant fraction of the band gap energy (e.g. 0.1–0.2 eV per electron in GaAs). These quantitative results may enable us to make a fresh assessment of the role of deep centers in recombination. In particular, we will show here that these results are consistent with the possibility of large Auger-type capture cross sections ($\sim 10^{-14}$ cm²) at many a deep center.

The process under consideration is one in which the capture of a free hole by a center binding deeply two electrons is accompanied by ejection of the remaining localized electron into the conduction band. This capture cross section has only *weak* temperature dependence and is *not* a function of carrier concentration. It seems plausible to propose that capture cross sections of the order of 10^{-13} – 10^{-16} cm², which do not depend strongly on temperature, and which are related to deep levels in the midgap region, could be explained by this mechanism. Reports of such capture cross sections have recently appeared in recent literature on deep levels in semiconductors [3–8].

Deep centers in GaP and GaAs are not expected to exhibit such large Auger cross sections. Nonetheless, Jess [9] was able to develop a simple theory which

predicted large Auger effects for highly localized centers. In spite of the physical insight provided by Bess' work, his result has been overlooked in recent literature [10–15] and the commonly held view is that Auger cross sections are generally of the order of 10^{-18} cm² or less [3]. The present study shows that the predictions of Bess are consistent with the results of our recent calculations and that Auger-type transitions at deep defects in semiconductors might occur with cross sections in the range 10^{-13} – 10^{-16} cm².

Nonradiative capture via *shallow* centers (i.e. those characterized by a long-range Coulomb potential) has been understood thanks to the cascade mechanism proposed by Lax [11]. The presence of closely spaced highly extended states enables an electron to lose energy by dropping through the levels and emitting one phonon during each such transition. The cascade capture cross section *increases* rapidly with *decreasing* temperature. The occurrence of this mechanism can therefore be well identified. During a nonradiative capture at a *deep* center, a large energy must be dissipated in one step. Such a transition may occur via a multiphonon emission. Indeed, in a recent paper, Henry and Lang [3] presented in great detail both theoretical and experimental evidence, convincingly supporting the idea that such multiphonon processes are commonly occurring in GaP and GaAs. The multiphonon process is thermally activated so that $\sigma \sim \sigma_0 e^{-E_B/kT}$, i.e. the cross section *increases* with *increasing* temperature, with a characteristic barrier energy E_B . The threshold of the exponential temperature dependence is usually observed at or above 250 K. The essential ingredient of the theory of multiphonon capture is the assumption that the deep center is strongly coupled to the lattice. Then for sufficiently large lattice vibrations the deep level can cross into the relevant band and capture a carrier. This situation is

* Present address: Department of Theoretical Physics, The University, Newcastle upon Tyne, U.K.

† Supported in part by ONR, under contract No. N00014-76-0890

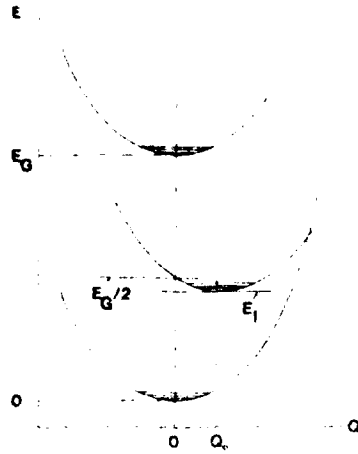


Fig. 1. A standard configuration-coordinate diagram showing a deep level of an equilibrium energy E_1 in the band gap (E_G), as a function of the lattice coordinate Q .

conveniently illustrated in a one-dimensional configuration-coordinate diagram (Fig. 1). The existence of the large lattice relaxation implied in the diagram can be verified independently since the diagram also predicts a large Stokes shift in the optical spectra.

Henry and Lang do point out that not all observed capture cross sections associated with deep levels in GaP and GaAs exhibit the multiphonon capture. There are numerous reports [3-5, 7] of commonly occurring deep traps in GaAs and GaP with capture cross sections in the range of 10^{-13} - 10^{-16} cm² which do not show appreciable temperature dependence. For example, Lang and Logan [4] show four such hole capture cross sections associated with two unidentified (but commonly present) levels, and Cu and Fe related deep levels in *p*-type GaAs. The optical spectra of Fe and Cu related levels in III-V semiconductors do not indicate exceptionally large Stokes shifts. Similar observations have been reported for deep centers in Si and Ge [6, 8].

There are only two other mechanisms that might be plausible in explaining a large energy dissipation which takes place in the capture into a deep level, namely the radiative and Auger ones. However, the radiative capture cross section at deep levels is never larger [16] than $\approx 10^{-19}$ cm² and thus does not appear to be relevant. The Auger effect in GaP and GaAs has been studied extensively during the last decade and identified - for example - as an important quenching mechanism in GaP (Zn, O) [12]. Those Auger processes which involve a collision of two free particles, have cross sections characterized by their particular dependence on the carrier concentration and as such can be easily identified [10]. These processes have been shown experimentally to be no larger than 10^{-18} cm² and will not be

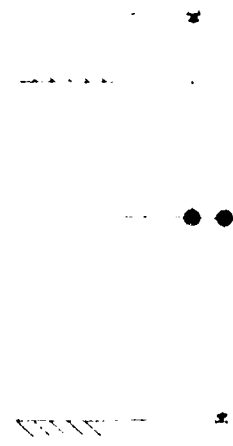


Fig. 2. The transitions are indicated of a non-radiative Auger-type recombination at a deep center binding two electrons in the forbidden gap of the host crystal.

considered here.

Nevertheless, we can think of a number of Auger processes which should not have cross sections depending on carrier concentration. As an example, we can consider the familiar model of a He-type defect, e.g. a center binding deeply two electrons. The recombination process (Fig. 2) will then consist of a free hole moving with thermal velocity and approaching the two-electron defect. It is then possible for one of the electrons and the free hole to annihilate each other, the excess energy being carried away by the other electron which will be ejected into the conduction band. This energetic electron will subsequently lose its kinetic energy through various collisions with phonons. The transition probability for this process is

$$w = \frac{2\pi}{h} |\langle b, h | \frac{e^2}{k|r_1 - r_2|} | c, h \rangle|^2 \rho_c \quad (1)$$

where b , c and h represent the wave functions of the bound electrons, the energetic electron and the free hole, resp. ρ_c is the density of states in the conduction band, associated with the final electron state. The capture cross section σ is related to w by

$$\sigma = \left(\frac{\Omega}{v} \right) w \quad (2)$$

where v is the thermal velocity of the hole and Ω is the volume of the crystal. The discussion of this problem is usually presented without any reference to capture cross sections [10]. Instead, the ratio of the Auger-to-radiative transition probabilities is evaluated and compared with measured lifetimes. We feel, however, that with the advent of the deep level transient spectroscopy

(13) and related techniques which yield directly the capture cross sections and their temperature dependence, the above formulation might be a useful one.

The integral in (1) is normally evaluated with the effective mass (hydrogenic) wave functions and plane waves representing b 's and e, h , respectively [14]. However, our recent computer calculations [1, 2] concerning the wave functions associated with deep centers in GaP and GaAs, have shown that the wave functions of deep centers are much more localized. Also their localization is *not* simply related to the apparent one electron ground state energy as anticipated in the effective mass theory. It is because both the conduction and valence bands play a significant part in the formation of the impurity energy and wave function. Since their contributions have in general opposite signs, the energy of the level with respect to the band edges represents only a fraction of the actual interactions involved. In brief, the localization of the wave functions of a given symmetry may vary very little from defect to defect although the position of the level in the gap may not. The calculations show that in general the wave functions are well localized within the nearest neighbor distance from the defect (≈ 5 at. units). However, the nodal and angular structure of the wave function strongly reflects the symmetry of the defect and therefore might change quite substantially from center to center. Also, the wave functions of deep centers are strongly hybridized with the valence band states. Both these aspects make a quantitative estimation of the electron-electron interaction very difficult. However, a detailed calculation of the electron-electron interaction was carried out for several centers. It revealed that this interaction (Hartree) energy should be about 0.1–0.2 eV per electron in GaAs and GaP. This result gives us an opportunity to make a realistic assessment of the magnitude of the integral in (1). If we choose, for example, to represent the localized wave function (b) by a hydrogenic function with an effective radius $\alpha = 5$ a.u., we can then adjust the screening constant χ so as to ensure that the electron-electron (Hartree) term computed with these functions falls in the realistic range of energies. The potential V_1 seen by the second electron due to the first is

$$V_1 = \frac{1}{r} \int_0^r r'^2 |R_1(r')|^2 dr' + \int_r^\infty r'^2 |R_1(r')|^2 dr'. \quad (3)$$

It is now determined so that the interaction energy is $\langle 2|V_1|2 \rangle = 0.2$ eV. (4)

With $\alpha = 5$ a.u., χ becomes 17. As we mentioned earlier, the valence electrons strongly interact with the defect. Consequently, the valence band wave functions representing the free hole function h must be altered. Physi-

cally, this means that the hole wave function will be somewhat changed in the relevant volume region ($\sim \alpha^3$) around the center and the matrix element in (1) altered. (This correction may not be so important for the energetic electron.) The relevance of these effects was anticipated by Bess. In his elegant study [9], he derived a formula for the matrix element in (1) for the He-type defect, with the hole wave function containing a pre-factor

$$\exp(-2(\pi)^{1/2} \{1 - \text{erf}[(r/\alpha)^{1/2}]\}) \quad (5)$$

to account for the localization of the hole in the vicinity of the defect. Using his result, with equations (1) and (2), we have

$$\begin{aligned} \sigma &= 4\pi(\alpha^2/\alpha_0)^2 (p m_h^*/\kappa^2 p_h m^*) \\ &\times [F^2(p\alpha/2) \{1 + 9F(p\alpha)\} - (16/81)F^2(p\alpha/3) \\ &\times \{1 + (25/4)F(p\alpha/2)\}]^2 \quad (6) \end{aligned}$$

where $\alpha_0 = 0.529 \times 10^{-8}$ cm, p, p_h and m^*, m_h^* are the momenta and effective masses of the free electron and hole, resp., and $F(x) = [1 + (x/\kappa)^2]^{-1}$. The largest cross section is expected for a level at the center of the forbidden gap. Then $p/p_h \approx 1$ and $(\alpha p/\kappa)^2 \ll 1$. Taking $p_h(300 \text{ K})/\hbar c = 0.77 \times 10^7 \text{ cm}^{-1}$, $\alpha = 2.65 \times 10^{-8}$, $\kappa = 17$, and setting $m_h^*/m^* = 1$ for simplicity, we obtain $\sigma \approx 4 \times 10^{-16} \text{ cm}^2$. The temperature dependence of the cross section σ is given by that of the hole thermal velocity v and the density of states ρ_e .

The necessary condition for the above recombination process to take place is the fulfillment of the energy conservation relation, i.e. the energy released in the electron-hole annihilation must be sufficient to lift the remaining electron into the conduction band. It might seem that only a few centers could satisfy the above condition. However, we must remember that practically any deep center exhibits some coupling to the lattice. Indeed, in many cases this coupling is so strong as to allow at high temperatures for capture via crossing of the deep level into the relevant band. Let us turn to the situation pictured in Fig. 1. Clearly, in this case the equilibrium energy E_T of the level at $Q \equiv Q_0$ is such that the Auger transition cannot take place. However, with the help of the electron-phonon interaction, the level can cross the critical energy value ($E_G/2$) so that the Auger transition can occur at $Q = 0$. To accomplish the process, only modest lattice vibrations may be needed since, for example, most deep levels in GaAs have their equilibrium positions only about ~ 0.1 – 0.2 eV from the midgap position. Therefore, even the phonon-assisted Auger transitions may show very little temperature dependence. Hence Fig. 1 might correspond to a case where the multiphonon recombination is quenched at low temperatures by the weakly temperature dependent,

powerful Auger process. At high temperatures, the multi-phonon mechanism may take over, showing the characteristic exponential rise of σ . As we have already noted, the model chosen for the estimate of the order of magnitude of the Auger-type capture cross section was an oversimplified one. In particular, for a phonon-assisted transition the symmetry of the problem may be such as to reduce the cross section. We might, therefore, expect the observed values of σ to fall in most cases in the region of $10^{-14} - 10^{-16}$ cm².

The predicted magnitude and temperature dependence of the capture cross sections are not the only signature of the Auger process offered by the theory for identification of the mechanism. The energy conservation rule and the fact that the center should have several charge states separated by $\approx 0.2 - 0.5$ eV in the forbidden

gap provide an *additional scope* for judicious interactive experiments along the line of [15] and [16]. Studying the kinetics of the rise and decay of the photocurrent after an injection of minority carriers may be another way of detecting this recombination mechanism [8].

Finally, it is worth remarking that the one-center, He-like model considered here may constitute only one of the numerous cases where a deep defect(s) may be two highly localized, strong interacting particles in a suitable position in the forbidden gap, thereby making the Auger process possible. Vacancies, transition metal ions, and complexes formed by these in combination with other chemical impurities may be some other candidates, capable of producing a two-center defect with several tightly bound carriers.

REFERENCES

1. JAROS M. & BRAND S., *Phys. Rev.* B14, 2294 (1976).
2. JAROS M., *Phys. Rev.* B16, 3694 (1977).
3. HENRY C.H. & LANG D.V., *Phys. Rev.* B15, 989 (1977).
4. LANG D.V. & LOGAN R.A., *J. Electron. Mater.* 4, 1053 (1975).
5. HAMILTON B., PEAKER A.R., BRANWELL S., HARDING W. & WIGHT D.R., *Appl. Phys. Lett.* 26, 701 (1975).
6. EVWARAYE A.O., *Phys. Rev. B*.
7. MIRCEA A. (private communication and to be published).
8. SHEINKMAN M.K., *Fiz. Tverd. Tela* 7, 28 (1965); *Rev. Phys. Solid State* 7, 18 (1965).
9. BESS L., *Phys. Rev.* 111, 121 (1958).
10. LANDSBERG P.T., *Phys. Status Solidi* 41, 437 (1970).
11. LAY M., *Phys. Rev.* 119, 1812 (1960).
12. NEUMARK G.F., DE RIFE T.O., DE RAGAZZANA R.N. & HARNACK P.M., *Phys. Rev.* B15, 3147 (1977).
13. LANG D.V., *J. Appl. Phys.* 58, 3111 (1970).
14. NEUMARK G.F., *Phys. Rev.* B7, 3402 (1973).
15. HENRY C.H., KUKIMOTO H., MULLER G.L. & WERRITT E.R., *Phys. Rev.* B7, 2699 (1973).
16. BRAUN S. & GRIMMELSS H.G., *J. Appl. Phys.* 45, 2655 (1974); TASCIA A.F. Jr & SAH C.T., *Phys. Rev.* B1, 800 (1970); etc.

36

Trapping characteristics and a donor-complex (*DX*) model for the persistent-photoconductivity trapping center in Te-doped $\text{Al}_x\text{Ga}_{1-x}\text{As}$

D. V. Lang and R. A. Logan

Bell Laboratories, Murray Hill, New Jersey 07974

M. Jaros*

Department of Physics and Astronomy, University of Massachusetts, Amherst, Massachusetts 01003

(Received 25 January 1978)

Photocapacitance measurements have been used to determine the electron photoionization cross section of the centers responsible for persistent photoconductivity in Te-doped $\text{Al}_x\text{Ga}_{1-x}\text{As}$. The cross-section data, which have been obtained at various temperatures and for crystals of various alloy compositions, are fitted by a theoretical line shape that is valid for large lattice relaxation. The line shape and thermal broadening can best be fit by a binding energy of 0.10 ± 0.05 eV and a Franck-Condon energy of 0.75 ± 0.1 eV. These values are in good qualitative agreement with the large-lattice-relaxation model of persistent photoconductivity which we recently proposed. We show that the 0.10-eV binding energy is also consistent with experiments that locate this energy relative to the Fermi level. The dependence of the properties of the persistent-photoconductivity center on the donor doping of the samples leaves little doubt that this center involves a donor atom, but because the center is not effective-mass-like, we believe that it is a complex also involving another constituent. Accordingly, we designate it as a "*DX*" center. The anomalously-large Franck-Condon energy (Stokes shift) and apparent fact that the unoccupied state of the *DX* center is resonant with the conduction band, yet sufficiently localized to produce a large relaxation, are thus well established. These considerations lead us to propose that the most likely model for *DX* centers in $\text{Al}_x\text{Ga}_{1-x}\text{As}$, and perhaps in other compound semiconductors as well, is a complex involving a donor and an anion vacancy. We show that such a model is qualitatively consistent with the overall trends in persistent-photoconductivity behavior observed in a variety of III-V and II-VI semiconductors.

I. INTRODUCTION

In this paper we will discuss the thermal and optical properties of the persistent-photoconductivity center in Te-doped $\text{Al}_x\text{Ga}_{1-x}\text{As}$. The dominant features of this type of defect are: (a) an apparently enormous Stokes shift (thermal depth from the conduction band ~ 0.1 eV, optical depth ~ 1 eV), and (b) a very small thermally activated electron-capture cross section ($< 10^{-30}$ cm²), for temperatures below about 77 K. These features could be semiquantitatively explained by a somewhat unorthodox configuration coordinate (CC) model which postulated a lattice relaxation that was very large for such an apparently shallow center, i.e., the Franck-Condon energy d_{FC} was proposed to be much larger than the apparent electronic binding energy E_0 .¹ We will present here temperature-dependent optical data for this center which lend further support to the lattice-relaxation model of Ref. 1 and leave little doubt as to its overall qualitative validity.

The verification of this model, however, raises more questions than it answers. For within the framework of the traditional understanding of point defects in semiconductors, based on the effective-mass theory, the model of Ref. 1 is physically untenable. The fact that $d_{FC} \gg E_0$ is

hard to explain, since for all cases where it has been measured, d_{FC} is some fraction, typically 0.1–0.5, of E_0 . Second, the CC model of Ref. 1 requires that the defect charge density be sufficiently localized to produce a large lattice relaxation even when the state is resonant with the conduction band. This is even harder to explain, since the conventional wisdom has it that such resonant states are highly delocalized, and hence the electron-lattice interaction could not possibly produce such a large relaxation. We will show that a proper view of the origin and structure of defect wave functions can resolve these apparent contradictions.

The dependence of the properties of the persistent-photoconductivity center on the donor doping of the samples leaves little doubt that this center involves a donor atom. But because the center is not effective-mass-like and because its concentration is not always a fixed fraction of the donor concentration, we believe that it is a complex involving another constituent as well. Accordingly we designate it as a *DX* center. Based on the current theoretical understanding of deep levels in semiconductors, we will present arguments which we believe show that *DX* centers are most likely complexes involving a donor atom and an anion vacancy, e.g., Te- V_{As} for Te-doped

$\text{Al}_x\text{Ga}_{1-x}\text{As}$.

In Sec. II we will discuss the experimental methods and in Sec. III we will present the experimental results. Section IV is a brief discussion of the optical-line-shape theory used to fit the data. Finally, the resolution of the theoretical inconsistencies mentioned above and our proposal for the microscopic structure of DX centers are presented in Sec. V. The paper is summarized in Sec. VI.

II. EXPERIMENTAL METHODS

A. Crystal growth and sample preparation

The $\text{Al}_x\text{Ga}_{1-x}\text{As}$ samples used in this study were grown on n^+ GaAs substrates by liquid-phase epitaxy (LPE) from gallium solution at 850 °C. Schottky barriers were fabricated on single n -type epitaxial layers by evaporating a semitransparent (~10% transmission) gold film through a mask with 250- and 500- μm diam circular openings. Some of the n layers were covered with a second p -type epitaxial layer doped with Ge ($N_A - N_D = 2 \times 10^{18} \text{ cm}^{-3}$). The p -type layer was either of the same aluminum content x (for p - n homojunctions) or of pure GaAs (for single p - n heterojunctions). These p - n junctions were formed into mesa diodes by applying conventional metallized Ohmic contacts, sand blasting, and chemical etching. They were then mounted on TO-18 headers with leads attached to the metallized Ohmic contacts by thermocompression bonding. Some of the p - n junctions were mounted on edge so that the junction space-charge layer could be uniformly illuminated through the substrate. In a few of the samples the substrate was removed by selective chemical etching in order to avoid the effects of the substrate absorption for $h\nu > 1.4 \text{ eV}$. For $h\nu < 1.3$ no essential differences were seen in the experiments performed on the three types of samples—homojunctions, heterojunctions, or Schottky barriers. The predominant dopant in the n -type $\text{Al}_x\text{Ga}_{1-x}\text{As}$ epitaxial layer was

$$\text{Te} (5 \times 10^{16} < N_D - N_A < 2 \times 10^{18} \text{ cm}^{-3}),$$

although a few preliminary results were obtained on samples doped with Se, Si, and Sn. Unless otherwise noted, all results in this paper will be for the Te-doped samples.

B. Capacitance spectroscopy techniques

The samples were studied by various forms of capacitance spectroscopy, namely, deep-level transient spectroscopy^{2,3} (DLTS) and thermally stimulated capacitance² (TSCAP) for the thermal-

emission and capture data, and photocapacitance for the optical cross-section data. The net shallow-level doping concentration was measured by a Miller feedback profiler.^{2,4} These techniques are especially well suited for the measurement of deep-level concentrations. Thus, there is no doubt that the thermal and optical data relate to the same center, since this center dominates the behavior of our samples.

In order to explain how the data in Sec. III were taken, we show typical DLTS and TSCAP curves in Figs. 1(a) and 1(b), respectively. As is well known,^{2,3} these techniques correspond to the same physical phenomena—thermal emission or capture of trapped carriers in the junction space-charge layer, observed on different time scales. Thus, the DLTS peaks in Fig. 1(a) correspond to thermal electron emission following a zero-biasing voltage pulse (negative peak) and electron capture following a forward-bias injection pulse (positive peak), both with a 2.7-msec time constant. The TSCAP data in Fig. 1(b), on the other

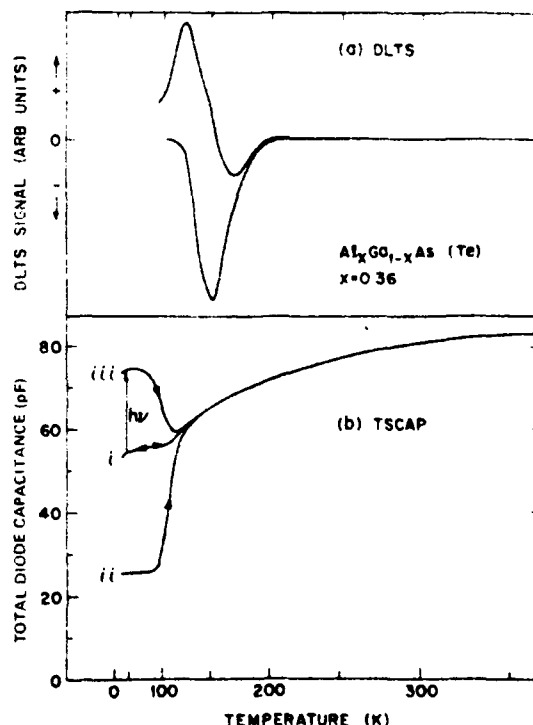


FIG. 1. DLTS and TSCAP data for a typical sample of Te-doped $\text{Al}_x\text{Ga}_{1-x}\text{As}$ with $x=0.36$. The DLTS spectra correspond to a rate window of 366 sec^{-1} ; the TSCAP heating rate was $\sim 1 \text{ K/sec}$. Increases in C correspond to fewer trapped electrons, while decreases in C imply more trapped electrons. The photocapacitance transition is indicated by the arrow labeled $h\nu$.

38

hand, correspond to time constants of the order of seconds. This explains the shift of the DLTS data to higher temperatures. The positive going TSCAP step, corresponding to initial condition (ii) (defined below) is the same physical phenomenon (thermal electron emission) as the negative DLTS peak. From the magnitude of this TSCAP step one can calculate the concentration of deep levels which are emitting electrons with rates of the order of seconds in the temperature range of the step. Similarly, the negative going TSCAP step corresponding to initial condition (iii) (also defined below) arises from the same effect as the positive DLTS peak. We have found that this is due to electron capture in the case of DX centers in $\text{Al}_x\text{Ga}_{1-x}\text{As}$.

Usually a positive DLTS peak or a negative TSCAP step is due to minority-carrier emission (holes in this case). However, the fact that initial condition (iii) can be established in *n*-type Schottky barriers by illumination with photons of energy as low as 0.6 eV totally rules out the possibility of hole emission in this temperature range, since <1.5 eV light would be needed to empty hole traps close enough to the valence band to emit holes at the same temperature as the positive DLTS peak. The fact that electron capture can give a signal that looks so much like hole emission is due to the peculiar nature of the DX center, i.e., its electron-capture cross section is very small and thermally activated at low temperatures.¹

Since most of the data in this paper have been obtained by the techniques shown in Fig. 1(b), it is important to consider in some detail the procedures used in establishing the initial conditions for the three $C(T)$ curves. Curve (i) is the steady-state zero-bias capacitance recorded as a function of temperature. This curve is reversible for increasing or decreasing temperature scans. Curves (ii) and (iii), on the other hand, are irreversible thermal scans corresponding to initial conditions at the lowest temperature of completely filled or completely empty DX centers, respectively. Initial condition (ii) is obtained by cooling the sample from about 200 K to about 50 K with +1 V bias. This bias corresponds to a narrowing of the junction space-charge layer so that nearly all DX centers (which are donors in $\text{Al}_x\text{Ga}_{1-x}\text{As}$) are below the Fermi level, tend to be filled with electrons, and hence are neutral. At the lowest temperature, the bias is returned to 0 V, where the filled DX centers in the space-charge region constitute a nonequilibrium state which is metastable because the electron thermal-emission rate is vanishingly small at 50 K. Thus, as shown in Fig. 2(a), the space-charge layer of width W_1 is made up only of ionized "normal"

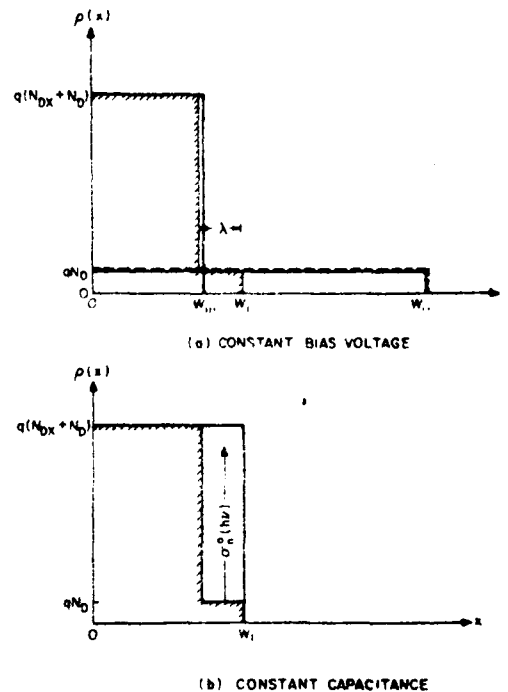


FIG. 2. Charge density vs distance in the abrupt-depletion approximations (a) for the junction space-charge layer corresponding to the three TSCAP initial conditions in Fig. 1, and (b) for the constant-capacitance condition of the photoionization measurements.

donors of net concentration N_D . When the temperature is increased to the vicinity of 100 K, the DX centers begin to thermally emit their trapped electrons and hence become positively charged. Since $N_{DX} \gg N_D$ in most of our samples, this corresponds to a drastic rearrangement of the space charge at constant bias which finally results in the equilibrium width W_1 , shown in Fig. 2(a) as the step-wise charge distribution with shaded boundaries. The step at $W_1 - \lambda$ corresponds to the point where the DX energy level passes through the Fermi level in the edge region of the space-charge layer.^{2,6} Thus between 0 and $W_1 - \lambda$, the DX centers are above E_F and are empty in equilibrium so that the positive space charge is $q(N_{DX} + N_D)$; In the edge region from $W_1 - \lambda$ to W_1 , the energy level of the DX centers is below the Fermi level so that the equilibrium space charge is only qN_D . The steady-state capacitance change of curve (i) as a function of temperature corresponds primarily to the temperature dependence of the Fermi level, and consequently of λ . As λ changes with temperature at constant-bias voltage, the space-charge distribution, and hence W_1 in Fig. 2(a), must change accordingly.

Initial condition (iii) in Fig. 1(b) corresponds to all DX centers empty. This is illustrated in Fig. 2(a) with the space-charge distribution $q(N_{DX} + N_D)$ from 0 to $W_{(ii)}$ with no edge region. Condition (iii) is obtained at low temperature from the steady-state condition (i) by emptying the DX centers either *optically*, by exciting the electrons to the conduction band, or *electrically*, by recombination of the electrons with injected holes under forward bias. The optical emptying path is illustrated in Fig. 1(b) and is utilized in the following photocapacitance method to measure the electron photoionization cross section $\sigma_n^0(h\nu)$.

In the low-temperature limit, where thermal-emission and capture rates are negligible, the concentration of occupied DX centers $n_{DX}(t)$ is given by²

$$n_{DX}(t) = N_{DX} \exp(\sigma_n^0 \Phi t), \quad (1)$$

where Φ is the optical intensity in photons/cm² sec. In the limit where $N_{DX} \gg N_D$, the capacitance is a complicated function of $n_{DX}(t)$; thus the time dependence of C from (i) to (iii) in Fig. 1(b) is far from the simple exponential relationship of Eq. (1). This is dramatically illustrated by the typical photocapacitance transient at constant bias voltage shown in Fig. 3. If, however, instead of measuring the capacitance, we monitor the bias voltage change necessary to maintain a constant capacitance, the resulting voltage transient has the simple exponential form of Eq. (1). This virtue of constant capacitance measurements in the

concentrated deep-level limit was first pointed out by Goto *et al.*⁷ We use the constant-depletion mode of a Miller feedback profiler¹ to record the constant-capacitance data.

The experimental sequence is as follows. The sample is first cooled at zero bias to reach condition (i), and then the profiler is switched to the constant-depletion mode with the depletion depth set at W_1 . When the monochromator is turned on, the DX centers in the edge region are emptied according to Eq. (1), as shown in Fig. 2(b). The photoionization transient is measured by recording the feedback bias voltage as shown in Fig. 3. The optical cross section σ_n^0 can then be obtained from the time constant of the voltage transient if Φ is known. In these experiments the light source was a Bausch and Lomb high-intensity monochromator. The monochromator output was measured with a calibrated thermopile.

A peculiar property of DX centers, which is the cause of persistent photoconductivity,¹ is that when emptied at low temperatures it is impossible to refill the centers without warming the sample. The thermal barrier due to lattice relaxation essentially stops all electron capture below about 77 K, and the fact that the empty DX state is not in the gap makes it impossible to optically refill the level from the valence band. Thus in order to measure σ_n^0 at a different photon energy after the system is in state (iii), it is first necessary to warm the sample to some temperature above the negative-going electron-capture TSCAP step in Fig. 1(b). As shown in Ref. 1, this electron-capture step is the same physical phenomenon as the thermal quenching of persistent photoconductivity. State (iii) in Fig. 1(b), therefore, corresponds to the persistent-photoconductivity state seen by photo-Hall or photoconductivity measurements.¹ As a consequence, in the measurements of $\sigma_n^0(h\nu)$, which are discussed in Sec. III, the temperature cycle from the measurement temperature T up to 150–200 K along curve (iii) and back to T along curve (i) is required for each value of $h\nu$.

C. Determination of concentrations

The capacitance values corresponding to conditions (i), (ii), and (iii) in Fig. 1(b) can be put on a more quantitative basis in order to determine the DX center and net normal-donor concentrations. The necessary relationships are based on a double integral of Poisson's equation giving the voltage drop across a spatially uniform charge distribution ρ of width x as $\rho x^2/2\epsilon$, where ϵ is the dielectric constant of the medium. The step-function charge distributions in Fig. 2 are based on the so-called abrupt-depletion approximation which is

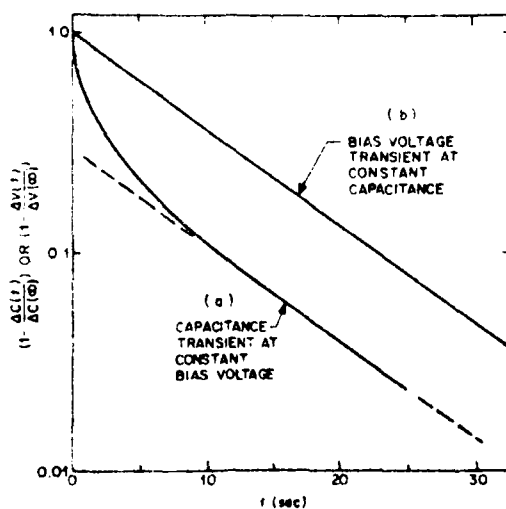


FIG. 3. Transients due to the photoionization of DX centers as observed for the same experimental conditions by two methods of measurement: (a) capacitance transient at constant bias and (b) bias-voltage transient at constant capacitance.

reasonably accurate for all conditions except forward bias.⁸ From Fig. 2 we have

$$2\epsilon(V_{bi} + V) = q[W_0^2 N_D + (W_0 - \lambda)^2 N_{DX}], \quad (2)$$

$$2\epsilon(V_{bi} + V) = qW_{11}^2 N_D, \quad (3)$$

$$2\epsilon(V_{bi} + V) = qW_{11}^2 (N_{DX} + N_D), \quad (4)$$

where V_{bi} is the so-called built-in potential which is on the order of the band gap, and V is the bias voltage. The depletion-layer width W is related to the capacitance by

$$C = \epsilon A / W, \quad (5)$$

with A the area of the junction. Since the capacitance values in Fig. 1(b) all correspond to the same bias voltage, Eqs. (2)–(4) are all equal to each other. Thus from Eqs. (3) and (4) we have

$$\frac{N_{DX}}{N_D} = \left(\frac{C_{111}}{C_{11}} \right)^2 - 1. \quad (6)$$

From the double integral of Poisson's equation in the uniform concentration limit, we have

$$\lambda = (2\epsilon\phi_{FT}/qN_D)^{1/2}, \quad (7)$$

where $\phi_{FT} = (E_F - E_T)/q$, and E_T is the energy of the deep level of interest. For the DX -center case $E_T = E_C - E_0$, where E_0 will be defined in Sec. IV. Thus by using the value of N_{DX}/N_D from Eq. (6), the fact that the bias voltage is zero for the case of Fig. 1(b) and the experimental value of C_{111} , we can solve Eq. (2) to obtain λ and ϕ_{FT} . For the data in Fig. 1(b), we find $N_{DX}/N_D = 8$ with $N_{DX} + N_D \sim 10^{18} \text{ cm}^{-3}$, and $\phi_{FT} = 44 \text{ mV}$ at 100 K. The charge-density diagrams in Fig. 2 correspond to these values.

The steady-state capacitance change between 100 and 300 K can also be explained quantitatively by Eqs. (2)–(4). As the temperature increases from 100 K, the Fermi level drops in the gap so that ϕ_{FT} , and hence λ , become smaller. Thus, from Eq. (2), W must become smaller to maintain the same voltage drop. In the limit of $\lambda \rightarrow 0$, $W \rightarrow W_{111}$ in Eq. (4). As we can see in Fig. 1(b) this approximates the experimental situation. We expect and observe that the higher-temperature capacitance is actually somewhat larger than C_{111} since the band gap, and hence V_{bi} , decreases with increasing temperature. Another effect will cause the room-temperature capacitance to be given by Eq. (4) even if $\phi_{FT} \neq 0$; namely, at approximately 250 K the extrapolated thermal-emission rate e_n^i from the DX center¹ becomes equal to $\omega_{FT} = 2\pi \times 10^6 \text{ sec}^{-1}$, corresponding to the capacitance measurement frequency of 1 MHz. In this case, when the deep-level occupation can follow the measurement frequency, the capacitance is given by Eq. (4), which includes both the shallow- and deep-

level concentrations as if λ were zero, even if it actually is not.⁸ Normally, the transition from the high- to the low-frequency limit is accompanied by a well-defined step in the C vs T curve, and is the basis of the admittance spectroscopy technique.⁹ For the DX center, however, no such step is seen near 250 K. Apparently, ϕ_{FT} is close enough to zero at 250 K and/or the $\omega_{FT} \sim e_n^i$ step is broad and small enough so as not to be noticeable.

Note that the very fact that $C(T)$ gradually decreases from 300 to 100 K is unusual, and relates to the DX center being the dominant donor in these samples. Our measurements on samples with normal donors of approximately the same depth ($\sim 0.1 \text{ eV}$), e.g., n -GaP, show a relatively temperature-independent $C(T)$ curve down to about 80–100 K. At that point the capacitance abruptly drops to zero because either e_n^i of the donors or the device RC time constant can no longer follow ω_{FT} . Most ~ 0.1 -eV-deep levels can follow ω_{FT} above 100 K and hence contribute to the space-charge-layer capacitance, even if the carrier concentration in the bulk is much lower than $N_D - N_A$, i.e., capacitance measures $N_D - N_A$, not n . For the class of ~ 0.1 -eV-deep donors the gradual $C(T)$ curve in Fig. 1 is only seen for DX centers; this is further evidence that the DX thermal-emission depth is considerably greater than its equilibrium depth.¹ Indeed, the edge-region photocapacitance technique used here [see Fig. 2(b)] would not be possible for normal donors because the recapture of electrons in the edge region is typically much faster than the photoionization rate for all but the most intense light sources, e.g., tunable ir lasers. The fact that the DX center is the cause of persistent photoconductivity, i.e., has a vanishingly small electron-capture rate at 50 K, is the only reason why the somewhat unusual techniques used here work at all.

III. EXPERIMENTAL RESULTS

A. Optical line shape

The electron-photoionization cross section $\sigma_{ph}^0(h\nu)$ measured by the constant-capacitance bias-voltage-transient technique of Figs. 2(b) and 3 is shown in Fig. 4 for an $x=0.37$ Schottky-barrier sample with the substrate removed. These data were taken for two temperatures, 44 and 78 K. The solid lines in Fig. 4 are a theoretical fit according to the phonon-broadened line-shape theory to be outlined in Sec. IV. The small temperature range of 44–78 K was dictated by the experimental constraint that the thermal-emission and capture rates be small compared to the optical-emission rate. The modest thermal broadening in Fig. 4 is actually quite large for such a small temperature

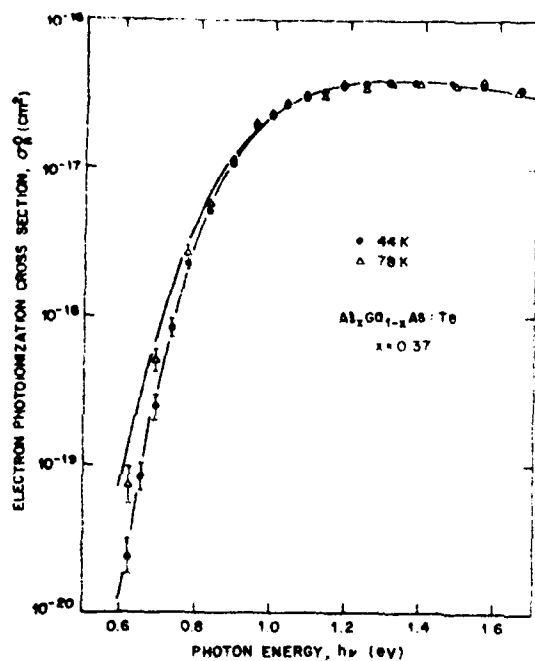


FIG. 4. Normalized electron-photoionization cross-section $\sigma_n^0(h\nu)$ for two temperatures. The solid lines are theoretical fits to the data.

rise and, as we will discuss in Sec. IV, verifies the qualitative features of the large-lattice-relaxation model of Ref. 1. The maximum cross section of 4×10^{-17} cm² is typical of other deep levels as reported in the recent review by Grimmeiss.¹⁰

Figure 5 shows data from five samples of different aluminum content ($0.27 \leq x \leq 0.60$) all taken at 44 K. We have normalized all the data to unity at 1.2 eV without having measured the absolute cross-section changes from sample to sample. The heavy line drawn through the data is the 44-K theoretical fit shown in Fig. 4. The lighter lines for $x = 0.27$ and $x = 0.30$ are not fits but are intended to show how these samples, well into the direct-gap composition range, have distinguishable shifts in the threshold region for $\sigma_n^0 < 10^{-2} \sigma_{\text{max}}$. As we will discuss in Sec. IV, these weak tails at low values of $h\nu$ most likely correspond to transitions to the low density of states at Γ . It is noteworthy that the remainder of the curves shows essentially no consistent variation with crystal composition. Indeed, the three curves for $x = 0.37, 0.42,$ and 0.60 are practically indistinguishable.

B. Variations of DLTS spectra

The small sample-to-sample variations that are seen in Fig. 5, other than the direct-gap tails, may be attributable to the fact that the *DX* center

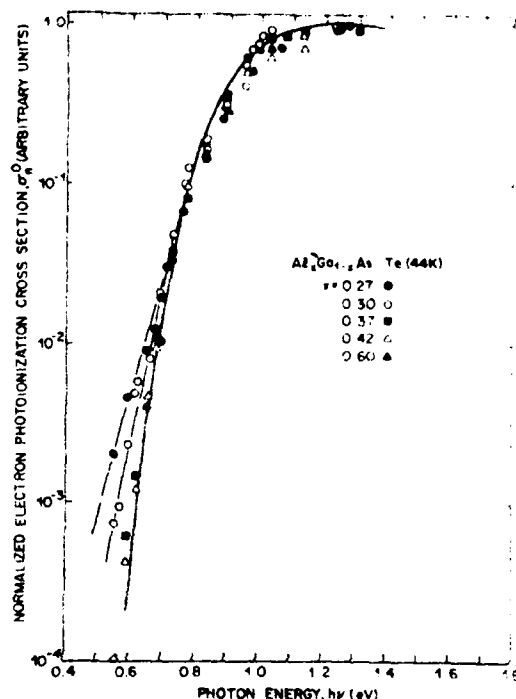


FIG. 5. Normalized electron-photoionization cross-section $\sigma_n^0(h\nu)$ at 44 K for five samples with different Al fractions. The heavy curve is the same theoretical fit as in Fig. 4.

does not seem to be a single well-defined center, but rather a closely related family of defects with a slight spread in binding energies. The range of possible Te-related *DX* centers is shown in the selected DLTS electron-emission spectra shown in Fig. 6. Note that some samples actually show two resolved DLTS peaks, while most show a single peak of varying width located somewhere between the extremes of the double-peak examples. The range of peak positions in Fig. 6 corresponds to a shift of about 60 meV in the thermal-emission activation energy of ~ 0.3 eV. There is no systematic correlation of these peak positions, and hence of thermal-emission energies, with mixed crystal composition. Apparently, the dominant type of *DX* center in any given sample is determined more or less at random. The only possible correlation with x is that the very few double-peak examples seem to occur more readily at the extremes of the composition range, i.e., in the $x = 0.20-0.30$ or $x > 0.6$ range. Perhaps the relative probabilities of particular Ga or Al arrangements around the defect play a role in the slight shifts of its properties.

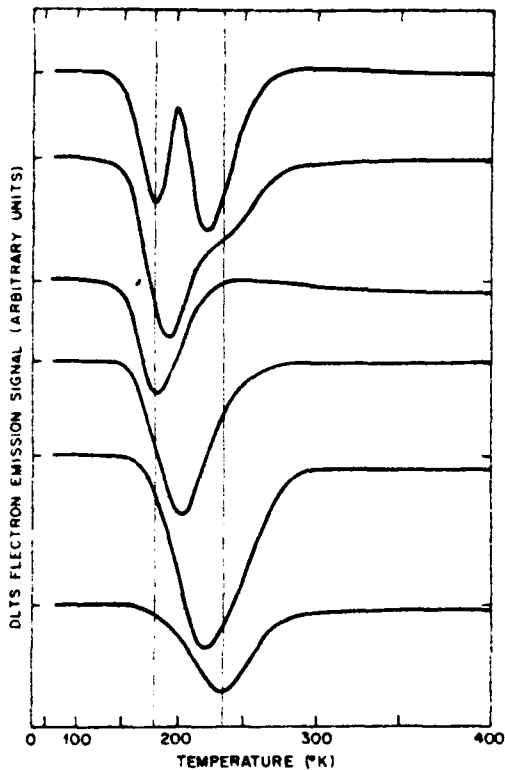


FIG. 6. DLTS spectra of the DX centers in six Te-doped $Al_xGa_{1-x}As$ samples selected to show the typical range of peak positions and line shapes commonly observed. The rate window was $3.7 \cdot 10^5 \text{ sec}^{-1}$, with a 2-V reverse bias and a 3-V majority-carrier pulse of 10- μ sec duration.

C. DX signal versus x and stress

Let us now discuss a set of data which are valuable in assessing the reasonableness of the energies to be determined in Sec. IV from the optical fit. These data, as shown in Fig. 7, are the magnitudes of the DLTS signal due to DX centers in a large number of samples of various Al content. Note that there is quite a bit of scatter in the points. This corresponds to fluctuations in the N_{DX}/N_D ratio from sample to sample. In fact, using the procedure of Eq. (6) we find the N_{DX}/N_D ratio to be typically of the order of 10 but to vary from less than 1 to more than 30 in different samples. This variation has only a modest correlation with x , i.e., the lower N_{DX}/N_D values tend to occur for higher Al fractions, as seen in Fig. 7.

The precipitous drop in DLTS signal below $x = 0.35$ is not due to a drop in DX concentration, however. This is shown by stress measurements. The y axis of the heavy arrow in Fig. 7 corre-

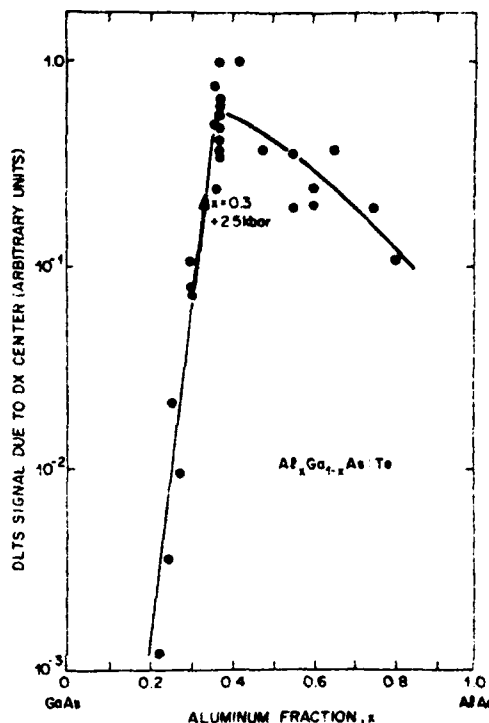


FIG. 7. DLTS signal magnitude due to DX centers in various $Al_xGa_{1-x}As$ samples vs the aluminum fraction x of the sample under the same conditions as the spectra in Fig. 6. The heavy arrow indicates the signal increase in an $x = 0.3$ sample induced by the application of a 2.5 kbar stress. The discontinuous drop in DLTS signal below $x = 0.36$ corresponds to E_0 crossing the Fermi level, as explained in the text.

sponds to the 3x increase in DLTS signal induced in an $x = 0.3$ sample by the application of 2.5 kbar of stress; the x axis of this arrow indicates the composition change which would give rise to the same shift of the Γ minimum as does 2.5 kbar of hydrostatic stress. A similar effect was seen at $x = 0.25$, but at $x = 0.37$ the same level of stress produced no effect. Thus the DLTS signal is affected by stress only in the exponential-drop-off region of $x < 0.35$.

The stress was applied to mesa diodes perpendicular to the junction plane; thus the sample dimension along the stress direction was considerably smaller than in the perpendicular dimension, so that the stress could be considered essentially hydrostatic. Under these conditions the major change induced by the stress is to raise the Γ and L conduction-band minima by 12.6 and 5.5 meV/kbar, respectively, and to lower the X minimum by 1.5 meV/kbar.¹¹ Since such an effect obviously cannot change the DX concentration, it must have

changed the DX occupation. This could only happen if the energy level of the DX center were above E_F in the $x < 0.35$ composition range, so that it would be only partially occupied during the majority-carrier pulse used to initiate the DLTS signal. The large signal change between $x = 0.35$ and $x = 0.22$ can be readily explained by an $\exp\{-[E_{DX} - E_F]/kT\}$ Boltzmann factor if E_F more or less follows the Γ minimum while $E_{DX} \approx E_X - E_0$ roughly follows the high-density-of-states X minimum E_X . The data in Fig. 7 can thus be interpreted as showing that E_{DX} crosses E_F for $0.32 < x < 0.35$ and more or less follows the X minimum in the direct-gap region (see Fig. 9). Also, this crossing point corresponds to $\phi_{FT} = 0$ so that $\lambda = 0$; indeed, we see no edge effects in the $C(T)$ curve for $x < 0.35$, as expected.

D. Donor doping effects

One of the most important observations concerning the DX -type centers is that they depend strongly on the concentration and chemical species of the donor added during LPE crystal growth.^{1,5} First, the DX concentration depends nearly linearly on the donor concentration.⁵ Despite some scatter in the data, this proportional relationship can be seen relative to both $N_D \sim N_A$ (determined by $C-V$ or Hall measurements) and the amount of Te added during crystal growth.

Even if such concentration data leave one unconvinced as to the "D" of DX centers, the dramatic shifts induced by changing the chemical type of donor should leave no doubt that DX centers involve donor atoms as a constituent. We have examined several samples having n layers doped with Se, Si, Sn (or undoped) instead of the Te doping which all of our other results are based. A complete treatment of the various dopants is planned, but the preliminary data can be briefly summarized as follows. The samples doped with Se show behavior such as in Fig. 1, which is essentially identical to that of the Te-doped samples. The Si- and Sn-doped samples, on the other hand, are very different, both from Te and Se, and from each other. For example, the DLTS spectra of Sn-doped samples always show two peaks. With the same rate window ($3.7 \times 10^3 \text{ sec}^{-1}$) as the Te data in Fig. 6, the Sn-doped spectra have a small peak ($N_{DX} \ll N_D$) at ~ 245 K and a very large peak ($N_{DX} > N_D$) at about 130–140 K. The TSCAP curves, such as in Fig. 1(h), are also very different for Sn doping, i.e., the negative step from C_{III} occurs at about 40 K, indicating a smaller barrier to electron capture than in the Te case. In general, the Sn-related DX center appears to be somewhat closer to the conduction band than the Te- or Se-

related centers. The Si-related DX center is even deeper than the Te and Se centers, with the positive TSCAP step from state (i) at ~ 160 K and the negative step from state (iii) at ~ 140 K.

The unknown background donor, which is always present in the mid- 10^{16}-cm^{-3} range in our samples, does not produce any of the effects reported above. Nonintentionally doped samples show no DLTS peaks in the region where the peaks due to DX centers appear, and, in addition, do not appear to exhibit persistent photoconductivity or show the qualitative TSCAP behavior of Fig. 1(b). This might mean either that the DX concentration depends nonlinearly on the donor concentration, in spite of our concentration data, or that the background donor is *not* Te, Se, Sn, or Si, but another element—perhaps C—which does not produce a DX center with states in the gap. The suggestion of C as the background donor in $\text{Al}_x\text{Ga}_{1-x}\text{As}$ is not unreasonable, since the LPE growth boat is constructed from graphite.

IV. THEORETICAL FIT OF THE PHOTOIONIZATION DATA

The experimental results of a photocapacitance or optical-absorption study can be presented in terms of the normalized cross section σ per incident photon of energy $h\nu$, as in Eq. (1) and Figs. 4 and 5. It is our prime task to find a link between the characteristic properties of $\sigma(h\nu)$ and the quantum-mechanical parameters associated with a particular defect. In the present study, we will adopt a recently developed¹² approach which has been successfully applied to a number of deep-level spectra. Accordingly, we will restrict ourselves to a brief outline of the most important considerations particularly relevant to the problems we are trying to solve here.

In the absence of an electron-phonon interaction, it is a standard approximation to write the cross section σ as

$$\sigma(h\nu) = \frac{\text{const}}{h\nu} \sum_{n,\vec{k}} |\langle \psi | \exp(-i\vec{k}_1 \cdot \vec{r}) \vec{\epsilon}_1 \cdot \vec{p} | \Phi_{n,\vec{k}} \rangle|^2 \times \delta(\epsilon_0 + E_{n,\vec{k}} - h\nu), \quad (8)$$

where \vec{k} is the wave vector of the radiation field and λ is the polarization direction. In the usual dipole approximation we have $\exp(-i\vec{k}_1 \cdot \vec{r}) \approx 1$. The momentum matrix element in Eq. (8) really indicates an average over all degenerate initial and final states. ϵ_0 , $E_{n,\vec{k}}$, and $\Phi_{n,\vec{k}}$ stand for the impurity energy, band energy, and wave function associated with a band n and reduced wave vector \vec{k} , respectively. ψ represents the impurity wave function.

In the event of strong coupling between the impurity and lattice, the transition probability can be expressed following the model of Huang and Rhys.¹³ In this model, the equations for the electronic and phonon functions separate. Only the electron-phonon interaction which is linear in the lattice coordinates is included. The cross section σ becomes

$$\sigma(h\nu) = \frac{1}{h\nu} \sum_{n, \mathbf{k}} |\langle \psi | \exp(-i \mathbf{k} \cdot \mathbf{r}) \tilde{\epsilon}_\lambda \cdot \tilde{\mathbf{p}} | \Phi_{n, \mathbf{k}} \rangle|^2 J_{n, \mathbf{k}}, \quad (9)$$

where the function $J_{n, \mathbf{k}}$ carries the information about the vibrational states and for the model in question can be evaluated exactly.¹³ For strong electron-phonon coupling, the expression for $J_{n, \mathbf{k}}$ simplifies to

$$J_{n, \mathbf{k}} = (\pi U)^{-1/2} \exp\{-[h\nu - (|E_n| + E_{n, \mathbf{k}})]^2/U\},$$

where

$$U = 2S(h\omega)^2 / \tanh(h\omega/2kT). \quad (10)$$

Here $h\omega$ refers to the phonon energy, k is the Boltzmann constant, S is the Huang-Rhys factor, and the terms $S\hbar\omega = d_{FC}$ and $E_n = E_0 + d_{FC}$ are defined in the configuration coordinate (CC) diagram shown in Fig. 8. The preexponential term in Eq.

(10) obviously does not affect the shape of the optical cross section, and for our purposes can be omitted.

In Ref. 12 a series of simplifying approximations were introduced which, for a sufficiently localized ψ , allow one to express Eq. (9) in the form

$$\begin{aligned} \sigma(h\nu) = & \frac{1}{h\nu} \int_n dE \rho(E) \\ & \times \left[\frac{(1+\eta)E^{1/2}}{E_p + E} + \frac{(1-\eta)E_p}{E_p - E - (E_p + E_A)/2} \right] \\ & \times U^{-1/2} \exp\left\{-\left[\frac{h\nu - (|E_p| + E)}{U}\right]^2\right\}. \end{aligned} \quad (11)$$

where $\rho(E)$ represents the density of electron states, E_p is the free-electron Fermi energy, E_c is the forbidden band gap, and E_A is the average or Penn gap. The function $\eta(E)$ interpolates between its apparent values at $E=0$ and $E=\infty$, and was chosen simply as $\eta(E) = \exp(-2E/E_A)$. The required choice of + or - depends on the nodal character of ψ and corresponds to valence-band-like or conduction-band-like deep states for the upper and lower signs, respectively. In addition, $\rho(E)$ and E_p may be functions of temperature as well. We have neglected this possibility over the limited temperature range of our measurements.

The cross section $\sigma(h\nu)$ observed at several values of temperature can be fitted with Eq. (11) by using the optical ionization energy $E_0 = E_n + d_{FC}$ and the Franck-Condon shift d_{FC} as adjustable parameters. Since E_0 appears to be of the order of 0.1 eV from thermal measurements,¹ it is clear that the line shape in Fig. 4 can only be fit by Eq. (11) for $d_{FC} \approx E_0$. For if d_{FC} were less than E_0 , the cross-section curves would literally disappear from the figures, with σ_{max} occurring at $h\nu \approx 0.2$ eV!

In the limit of a large d_{FC} , the formula for $\sigma(h\nu)$ in Eq. (11) is dominated by the lattice-relaxation Gaussian and the details of the electronic part in Eq. (8) become unimportant. The approximations in Ref. 12 concerning Eq. (8) are therefore perfectly acceptable in this case. A difficulty may arise, however, at $h\nu \approx 1.5$ eV, since above that energy the drop in the crystal density of states¹⁵ at around 2 eV above the conduction-band edge begins to affect the cross section. In order to represent the cross section well at $h\nu \approx 1.5$ eV we would have to abandon our simple model and perform a more rigorous calculation of the electronic part in which the true variation of the electronic matrix element and the density of states farther from the band edge is better accounted for. However, our main objective here

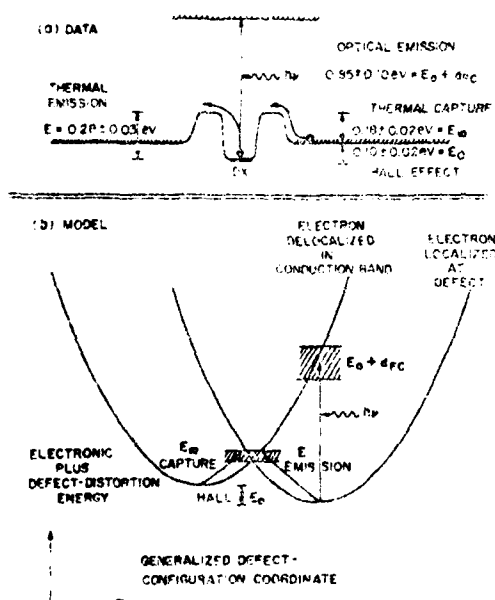


FIG. 8. (a) Summary of the experimentally determined thermal and optical energies for the FV center in Te-doped Al₂O₃. (b) CC diagram constructed to fit the data. The ranges of uncertainty in the data are shown as shaded regions.

is to determine the magnitude of d_{FC} and E_0 from the thermal broadening and composition dependence of $\sigma(h\nu)$. We are first of all interested in σ between its apparent threshold and maximum, therefore we will take $\rho(E) \propto E^{1/2}$. The theoretical fit for a valence-band-like state, shown in Fig. 4 with the experimental data, was obtained with $d_{FC} = 0.75 \pm 0.1$ eV, $E_0 = 0.10 \pm 0.05$ eV, and $\hbar\omega = 10$ meV. The other parameters were fixed at the values for GaAs ($E_A = 5.2$ eV, $E_F = 11.5$ eV) and $\text{Al}_{0.37}\text{Ga}_{0.63}\text{As}$ ($E_F = 2.05$ eV). This result seems to essentially confirm the original model which we proposed for this center.¹ The thermal and optical energies of the Te-related DX center may thus be summarized in Fig. 8(a). The extent to which these data are consistent with a simple CC diagram is shown in Fig. 8(b), where the estimated ranges of error are shown as shaded regions. The values of $E_0 + d_{FC}$ in such a diagram, are quite sensitive to the values chosen for E_A and E_F . However, since the CC diagram is totally determined by only two parameters, we can see that the internal consistency among the data in Fig. 8(b) is quite impressive for so simple a model.

The estimated errors for d_{FC} and E_0 are primarily due to the fact that the experimental data cover only a small range of temperatures. Data at higher temperature would provide a means of testing our model more thoroughly. In addition, it may well be that the linear model is not entirely adequate for such large relaxations. However, the magnitude of the broadening with increasing temperature seems in good accord with the large value of d_{FC} required to fit the shape of $\sigma(h\nu)$ (Fig. 4).

The large value of d_{FC} means that modest variations in the density of states due to variations in composition should not introduce any sharp features in $\sigma(h\nu)$. In particular, the appearance of the tail of low density of states due to the Γ valley being lowered in energy with decreasing x should have no such effect on σ and on the actual position of the level in the gap. We would thus expect that the optical spectrum should be practically unchanged as x increases from 0.4 to 0.6, and should shift only slightly towards lower energies as we move into the direct-gap range. Indeed, this is the behavior of the data in Fig. 5. It occurs because the level does not follow the band edge but rather the higher-lying regions of large density of states primarily associated with the X valley, as indicated in Fig. 9. Any quantitative assessment of the shift of σ towards lower energies with decreasing x is obscured by the large scatter of the data for different compositions. As pointed out in connection with Fig. 6, it would seem that the

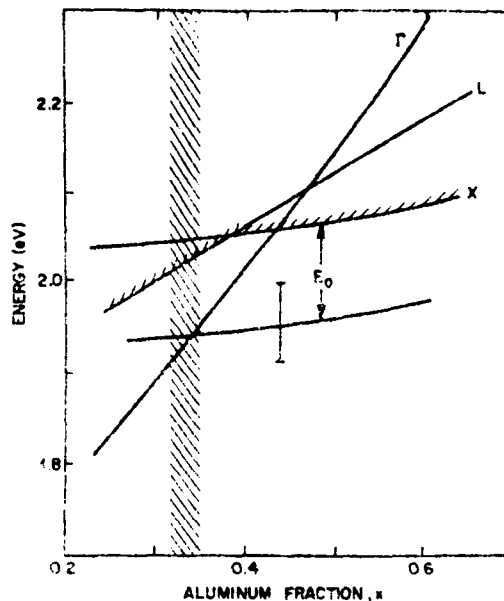


FIG. 9. Equilibrium energy E_0 of DX centers in $\text{Al}_x\text{Ga}_{1-x}\text{As}$ as deduced from the fit to the optical data in Figs. 4 and 5 with estimated error bar. The shaded region $0.32 < x < 0.35$ indicates the range of composition where E_0 crosses the Fermi level, according to the data in Fig. 7. The lowest high-density-of-states minimum relevant for optical transitions is shown shaded. The $\text{Al}_x\text{Ga}_{1-x}\text{As}$ band structure is from Dingle *et al.* (Ref. 16).

material contains several Te-related DX-type centers of very similar energies and overall properties which may vary somewhat from sample to sample.

In Fig. 9 the range of x where we think E_0 crosses E_F according to the data in Fig. 7, is shown. The $\text{Al}_x\text{Ga}_{1-x}\text{As}$ band structure in Fig. 9 is taken from Dingle *et al.*¹⁶ Unfortunately, it is difficult to know the precise position of the Fermi level in our material. Clearly, that would provide a test of our prediction, for if our result $E_0 = 0.10 \pm 0.05$ eV were correct, the point where the impurity level crosses the Fermi level should occur at a composition x such that the separation between the Fermi level and the bottom of the X valley is on the order of 0.10 eV. With the estimated error of about 50 meV in E_0 , we see that the Fermi level must be in the range $-0.05 < E_F - E_X < +0.05$ eV at $x \approx 0.33$, to be consistent with these data. Hall data^{17,18} on $\text{Al}_x\text{Ga}_{1-x}\text{As}$ samples with similar Te concentrations indicate E_F values in this range for the conditions of our measurements. If we can assume that these Hall data were taken on samples with large DX concentrations, then the E_F values in Refs. 17 and 18 are a mea-

46

sure of E_0 , as well. For $x > 0.5$, where a one-band Hall analysis is valid, the ionization energy extrapolated to low doping levels (which is the appropriate value to compare with optical measurements) is $E_D = 0.105$ eV.¹⁸ The estimate of $E_0 \sim 0.1$ eV in Ref. 1 is also consistent with these values, but is subject to considerable uncertainty since it is the difference of two large numbers.

Thus four independent measurements of E_0 —(a) DLTS emission and capture measurements, (b) Hall measurements, (c) the fit to the data of Fig. 4, and (d) the E_F crossing point in Fig. 7—all place this equilibrium thermal energy depth between 0.05 and 0.15 eV. This leaves absolutely no doubt as to the reality of the large Stokes shift associated with DX centers.

V. MODEL FOR THE STRUCTURE OF DX CENTERS IN COMPOUND SEMICONDUCTORS

A. Inadequacy of effective-mass theory for deep levels

There are two principal features of the DX-center CC diagram of Fig. 8(b) which are difficult to explain using the traditional views of defect states in semiconductors. They are (a) the extremely large lattice relaxation in which the energy of relaxation d_{FC} is much larger than the apparent binding energy E_0 and (b) the fact that before the capture of an electron the unoccupied DX state is resonant with the conduction band, yet still sufficiently localized to force a lattice relaxation of ~ 0.75 eV after electron capture.

These apparent inconsistencies can be readily resolved when viewed with our current understanding of deep states in semiconductors. In the past it had always been assumed, in the spirit of the effective-mass theory, that the localization of the wave function could be simply related to the depth of the impurity level in the forbidden gap. Thus the envelope function would be $f \sim \exp(-\alpha r)$, where $\alpha \sim (2m^*E_0)^{1/2}$ in atomic units.^{19,20} An effective-mass-like defect state obviously could never be localized if it were resonant with a band. However, if the defect state is properly viewed as arising from many bands and not simply from band states of the nearest minimum, then the degree of localization is no longer related in any simple way to the position of the energy level in the forbidden gap.

In this more general view of deep levels there is no problem in accepting the possibility of a strong lattice relaxation originating from a resonant state, such as the unoccupied DX center. Baraff and Appelbaum²¹ have shown that even though a bound state changes discontinuously in character when it moves into the band and be-

comes a broadened resonance of scattering states, the change in the charge density associated with the potential is continuous. This is a manifestation of the Kohn-Majumdar theorem.²² According to recent calculations of the energies and wave functions associated with deep states in III-V semiconductors,^{12,23,24} it is quite reasonable to expect that a bound state near the conduction-band edge could be sufficiently localized to produce the lattice relaxation required of the DX center. The results of Baraff and Appelbaum allow us to accept such localization for a resonant state as well. Indeed, the DX center might be viewed as an experimental example of the situation described by the Kohn-Majumdar theorem. Of course, we do not intend to imply that a resonant state can ever be truly localized. Indeed, any defect resonance has a delocalized Bloch-wave component in its wave function in addition to a localized component. We define a localized resonant state to be one in which the corresponding electronic charge density is predominantly found in the immediate vicinity of the defect.

When a state is viewed as arising from the overall density of states and not necessarily related in any important way to states at a particular band minimum, we can then understand why $d_{FC} \gg E_0$. This is because the value of E_0 determined for the DX center is not really a measure of the strength of the DX potential, but rather is a measure of the position of the state in the gap with respect to an arbitrary energy reference point, namely the conduction-band minimum at X. In a sense this is the "binding energy", since the net change in free energy necessary to ionize a DX center is E_0 . The energy with which d_{FC} should be compared, however, is not E_0 , but some measure of the electronic strength of the DX potential. For effective-mass-like defects, these energies are the same, but not for deep levels. For well-characterized deep levels, the Franck-Condon energy is some fraction of the strength of the purely electronic part of the defect potential. For transition elements in GaAs, for example, d_{FC} is of the order of $0.1 E_0$,²⁵ where E_0 in this case is of the order of the intra-*d*-level crystal-field splitting. Other examples, e.g., ZnO or O in GaP, exhibit values of d_{FC} between 0.1 and $0.5 E_0$.²⁶ Thus our value of $d_{FC} \approx 0.75$ eV would be quite reasonable if the true strength of the DX potential were of the order of 2 eV. In this context, also, the 60 meV range of energies in Fig. 6, which seems large compared to the equilibrium depth of $E_0 \sim 0.1$ eV or the thermal-emission depth of $E \sim 0.3$ eV, is almost negligible if the DX center is considered to have a potential strength of ~ 2 eV.

47

B. Discussion of DX model

We have seen above that the apparently peculiar properties of the DX center need not be considered at all unusual when viewed within the non-effective-mass framework of deep levels. Indeed, based on recent state-of-the-art computer calculations of deep levels,^{12,23,24} there exists a very common and plausible type of defect which exhibits all of the qualitative features of the DX center, namely, the donor-anion-vacancy complex. In fact, any complex containing an anion vacancy is dominated by this defect and has properties qualitatively similar to the isolated vacancy. Thus any complex of an anion vacancy plus an impurity or even a divacancy (alone or with an impurity) will behave roughly like an anion vacancy. The model which we will propose is merely the simplest form of donor-vacancy complex. The data do not preclude more complicated anion-vacancy-related defects.

The unrelaxed As vacancy in GaAs has a gap of ~ 2 eV between the a_1 and t_2 states which are available for the dangling electrons, as shown schematically in Fig. 10.²⁴ This splitting is a measure of the strength of the V_{As} potential and is the energy with which $d_{FC} \sim 0.75$ eV should be compared. Calculations of impurity-vacancy complexes²⁴ show that the presence of the impurity, e.g., a Te-donor atom, does not strongly affect

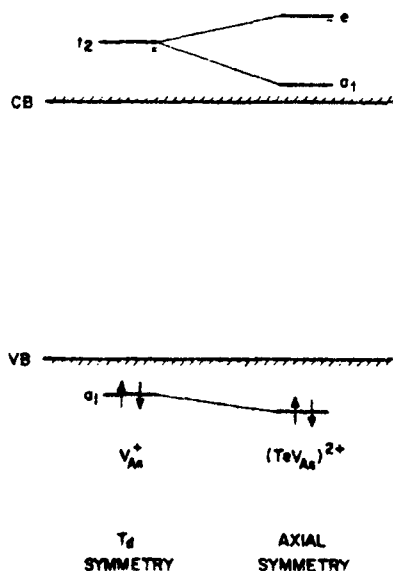


FIG. 10. Schematic single-electron energy-level diagram for the unrelaxed positive arsenic vacancy and TeV_{As}^{2+} complex in GaAs and $Al_xGa_{1-x}As$. The relative ordering of the a_1 and e states of TeV_{As} depends on the sign of the axial distortion. Note that the energies shown are intended to be of only qualitative significance.

the overall properties of the complex, which is still basically V_{As} -like both in its energy and wave function. The similarity between isolated vacancies and impurity-vacancy complexes, as well as the insensitivity of such complexes to the details of the impurity potential, are well known experimentally for cation-vacancy complexes.^{27,28} Indeed, the existence of the donor-cation-vacancy complex has been very well established; it is the so-called self-activated luminescence center in II-VI semiconductors.²⁸ Anion vacancies or their complexes, on the other hand, have not been unambiguously identified except in a few very wide-gap II-VI compounds such as BeO, ZnO, and ZnS.²⁸ This is consistent with the theoretical picture in which the much stronger potential at the anion site pushes the anion-vacancy levels farther up from the valence band than is the case for the cation vacancy. Thus in all but the wider-gap materials, the anion vacancy and its associated complexes have deep states originating in the valence band and pushed all the way up through the gap and into the conduction band, i.e., these valence-band-like anion-vacancy states are deeper than E_g . In those materials where these highly localized states are located near the edge of the conduction band, it is possible to have DX -like behavior with the unoccupied level resonant with the conduction band, while the occupied level relaxes to a bound state in the gap. Such is the essence of persistent photoconductivity.

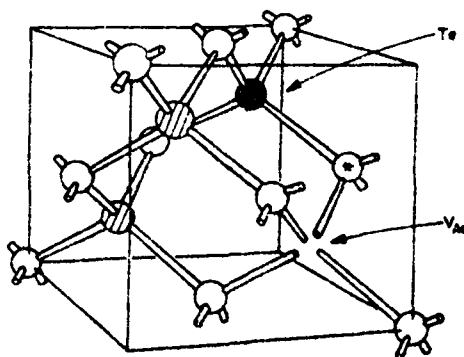


FIG. 11. Crystal model of one of the 12 equivalent second-nearest-neighbor positions for the Te donor in the simplest form of TeV_{As} complex in $Al_xGa_{1-x}As$. The As atoms are shown shaded with the Ga(Al) atoms plain. The Ga(Al) atom marked by an asterisk moves in response to the Te donor and hence produces the axial distortion of the vacancy. Different locations of the Te donor and/or different local Al-Ga distributions are likely to produce the range of DX energies observed in Fig. 6. Sn or Si donors occupy Ga sites which are first nearest neighbors of the As vacancy and hence give rise to shifted DX energies, as explained in the text.

Thus, we propose a model in which the microstructure of DX-like centers is a complex involving a donor and an anion vacancy. An example of one possible donor-anion-vacancy complex is shown for Te donors in $\text{Al}_x\text{Ga}_{1-x}\text{As}$ in Fig. 11. Experimental data, of course, can never actually prove that such a model is correct, but within the general trends that have emerged from the recent calculations of native defects and deep impurities in III-V compounds^{12,23,24,29} our proposal is the only defect model among those which have been studied which is consistent with the observations.

Let us first briefly discuss the other defect models which have been theoretically analyzed in order to show that they cannot even qualitatively explain the DX-center data, i.e., they cannot produce a "deep" highly localized state above the conduction-band edge in $\text{Al}_x\text{Ga}_{1-x}\text{As}$. We will consider substitutional chemical impurities, antisite defects cation-vacancy complexes, and interstitials.

None of the substitutional chemical impurities and/or their pairs appear to be likely candidates. Deep levels due to most chemical defects have been found in the gap. Even in cases where the electronegativity difference between the host and impurity atoms is large (i.e., ZnTe:O , GaP:O), a level exhibiting lattice relaxation appears in the forbidden gap.²³ The exceptions are transition-metal elements and perhaps the elements from the rare-earth groups. However, these are known to exhibit only small Stokes shifts and their behavior is generally determined by the *d* and *f* character of their incomplete shells.

An antisite defect, if it exists, should behave as a simple double donor or acceptor, since it has only a weak short-range potential.

The gallium vacancy and its complexes have weak potentials and are expected to produce levels in the gap.²⁴ Such a level has been observed in electron-irradiated $\text{Al}_x\text{Ga}_{1-x}\text{As}$ and identified as being due to V_{Ga} .³⁰ The donor- V_{Ga} complexes are apparently the source of the well-known 1.2-eV luminescence band in As-rich GaAs.²⁷

Very little is known about interstitials, especially bonded interstitials. Impurity interstitials generally behave as shallow effective-mass donors, but self interstitials have never been identified in semiconductors, except as close-pair Frenkel defects in ZnSe.²⁸

Let us now discuss the behavior of the Te- V_{As} model of Fig. 11 vis-à-vis the DX centers in Te-doped $\text{Al}_x\text{Ga}_{1-x}\text{As}$, keeping in mind that the actual defect structure might differ somewhat in detail from that shown but still be dominated by V_{As} . The attractive donor potential will lower the symmetry of V_{As} and split the triply degenerate t_2 state as

shown in Fig. 10. The position of these energy levels may vary perhaps within a few tenths of a volt or so with different chemical donors or donor locations, but the overall properties are determined by the symmetry and by the strength of the vacancy potential. The shifts in E_0 due to different donors, as well as the ~60 meV fluctuations in the energy of the Te-complex in Fig. 6, are consistent with this expectation. Indeed, the experimental donor-related shifts seen in the donor- V_{Zn} self-activated luminescence centers in ZnS and ZnSe are also 40–50 meV.²⁷ According to the extrapolation of Fig. 9, the donor- V_{As} complexes as well as isolated V_{As} should be located well up into the conduction band in pure GaAs, and are thus relatively inactive electrically. This may explain the relative weakness of the recovery stage apparently associated with V_{As} in irradiated GaAs.¹¹

It is natural to ask whether this defect model is adequate to explain the persistent-photoconductivity centers seen in other materials, i.e., S-doped $\text{GaAs}_{1-x}\text{P}_x$,³² S-doped GaSb,³³ and Cl- and Ga-doped $\text{Cd}_{1-x}\text{Zn}_x\text{Te}$,³⁴ and CdTe.²⁵⁻²⁷ Since we would expect most anion vacancies in III-V and II-VI compounds to give rise to states near the conduction-band edge for material with E_g in the general vicinity of 2 eV, the model proposed here should be suitable to explain all such data (except perhaps GaSb with its very small gap, where V_{Ga} could be near the conduction band). The relatively small differences in the strength of the interactions and their effect on the actual position of the energy levels may have important consequences, however. In particular, if the states originating from the t_2 levels associated with the vacancy are not pushed as deeply into the conduction band as in Fig. 10 or 12(a), one of the levels might be in the gap and the complex might show acceptor behavior, as indicated in Fig. 12(b). Indeed, the defects in $\text{GaAs}_{1-x}\text{P}_x$ (Ref. 32) and $\text{Cd}_{1-x}\text{Zn}_x\text{Te}$ (Ref. 34) exhibit an increase in mobility after photoexcitation, i.e., behave as acceptors. On the other hand, the DX center in Te-doped $\text{Al}_x\text{Ga}_{1-x}\text{As}$ is a donor by virtue of a decrease in mobility after excitation.⁵ We would expect from our model, in agreement with experiment³² that the DX center in $\text{GaAs}_{1-x}\text{P}_x$ should be an acceptor since V_{P} in GaP produces a state in the gap²⁹ and hence is like Fig. 12(b). Thus in wide-gap materials like GaP or CdS we would not expect to find DX-like high-mobility persistent-photoconductivity behavior, for in those cases the anion-vacancy potential is not strong enough to push the state above, or as far as, the conduction-band edge, and the DX center should behave like a normal deep level in the gap. This again is consistent with experiment, for persistent photoconductivity

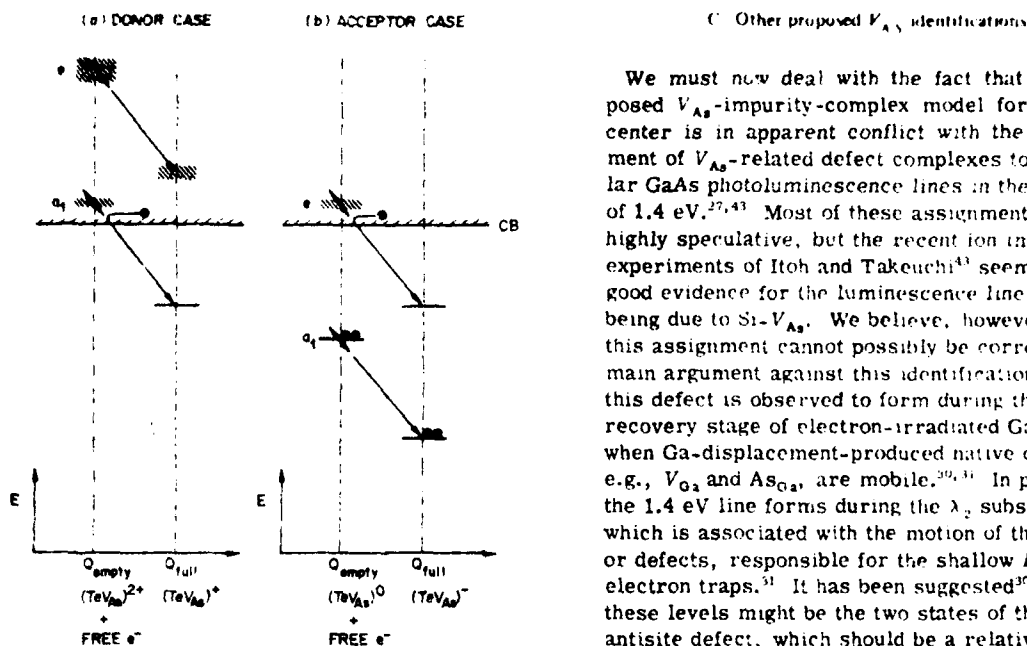


FIG. 12. Schematic single-electron energy-level diagrams of TeV_{As} showing the possibility of either donor (a) or acceptor (b) behavior depending on the position of the axially split a_1 and e states relative to the edge of the conduction band.

has not been seen in GaP. In CdS the persistent-photoconductivity state exhibits extremely low mobility³⁸ and most likely involves impurity-banding effects, and not defect centers which are resonant with the conduction band.

Very large relaxation effects, defined by a CC diagram such as Fig. 8(b), in which $d_{FC} = S\hbar\omega > E_0$, are of course quite common in ionic materials. The well-known carrier self-trapping phenomenon in these materials is a typical example. Another more recent example is that of In in CdF_2 .³⁹ This along with the *DX* centers in III-V compounds, might be considered an example of what Toyozawa calls the *extrinsic self-trapping of an electron*.⁴⁰ Even though the microscopic models of the various defects may be quite different in these very different materials, there seems to be a general trend in which defects exhibit either relatively small or very large relaxation with few, if any, intermediate cases. This behavior has, in fact, been predicted on very general theoretical grounds for strongly coupled electron-lattice systems.^{41,42} The *DX* centers are thus striking evidence that such behavior, which had been largely confined to ionic materials, also exists in the rather covalent III-V semiconductor compounds as well.

We must now deal with the fact that our proposed V_{As} -impurity-complex model for the *DX* center is in apparent conflict with the assignment of V_{As} -related defect complexes to particular GaAs photoluminescence lines in the vicinity of 1.4 eV.^{27,43} Most of these assignments are highly speculative, but the recent ion implantation experiments of Itoh and Takeuchi⁴³ seem to give good evidence for the luminescence line at 1.4 eV being due to $Si-V_{As}$. We believe, however, that this assignment cannot possibly be correct. The main argument against this identification is that this defect is observed to form during the 500-K recovery stage of electron-irradiated GaAs:Si when Ga-displacement-produced native defects, e.g., V_{Ga} and As_{Ga} , are mobile.^{30,41} In particular, the 1.4 eV line forms during the λ_2 substage, which is associated with the motion of the defect, or defects, responsible for the shallow *E1* and *E2* electron traps.³¹ It has been suggested³⁰ that these levels might be the two states of the As_{Ga} antisite defect, which should be a relatively shallow double donor. In any event, they are certainly not due to V_{As} , which is thought to become mobile during the recovery stages at 235 and 280 K.⁴¹

How, then, do we explain the observation of Itoh and Takeuchi⁴³ that As^+ ion implantation reduces the 1.4 eV luminescence while Ar^+ implantation does not. These data are clear evidence that the concentration of the defect responsible for the 1.4 eV line is depressed by excess arsenic. Conversely, the increase in this line within 1 μm of the surface as a result of high-temperature annealing treatments, is consistent with the defect concentration being enhanced by an arsenic deficiency. While the above data are certainly consistent with the defect in question involving V_{As} , they are also equally consistent with the defect involving Ga_i , Ga_{As} , or any chemical impurity which is substitutional on an arsenic site. Watkins²⁸ has shown for ZnSe (which in many ways is very similar to GaAs) that the vacancies and vacancy-impurity complexes which have been identified by EPR typically have very broad optical line shapes. He specifically points out that one should not expect any vacancy-related defect to produce sharp luminescence lines. This is consistent with our assertion that the relatively sharp 1.4 eV luminescence line is not related to an arsenic vacancy.

We believe that the most reasonable model for the defect giving rise to the 1.4 eV line is a Si_{As} acceptor, plus whatever it is which gives the (*E1*, *E2*) deep-level pair, perhaps As_{Ga} . This would explain the 500-K annealing data³¹ as well as the

implantation data of Itoh and Takeuchi,⁴³ since then the As⁺ implantation can be seen to diminish the 1.4 eV line by reducing the Si_{As} concentration due to a suppression of the V_{As} concentration. The tendency for an As_{Ga} double donor and Si_{As} acceptor to pair would be substantial because of their strong Coulomb attraction. Indeed, the (E1, E2) defect shows a strong tendency during the 500-K stage to pair with acceptors, e.g., Cd and Zn.³¹ Thus, we believe that the stoichiometric arguments for the identification of V_{As} and its complexes are weak and at best ambiguous, with alternate explanations possible which are equally valid. When we consider additional factors such as the damage-rate orientation dependences, the optically induced EPR in related materials, and the expected quantum-mechanical properties of vacancy-related states, we see that the donor-V_{As} model is most appropriate for the DX center and not the sharp 1.4 eV luminescence line in GaAs.

VI. CONCLUSIONS

The electron photoionization cross section σ_n^0 of DX centers in Te-doped Al_xGa_{1-x}As has been measured as a function of temperature and composition by the photocapacitance technique. The line shape and temperature dependence of $\sigma_n^0(h\nu)$ can be consistently fit by a phonon-broadened line-shape theory and can imply a considerable lattice relaxation associated with the capture or emission of an electron at the defect. The best fit is for an equilibrium depth $E_0 = 0.10 \pm 0.05$ eV with a relaxation energy $d_{FC} = S\hbar\omega = 0.75 \pm 0.1$ eV. This is consistent with the large-lattice-relaxation model for persistent photoconductivity which we have recently proposed. This fact, together with the evidence discussed in Ref. 1, leaves very little doubt that such a model correctly describes the overall qualitative features of the DX centers, which give rise to persistent-photoconductivity effects in a number of III-V and II-VI semiconductors.

In addition to the optical data, we presented data on the variations of the DLTS signal due to the DX centers both as a function of Al fraction x and applied stress. These data locate the composition range where the occupied DX energy level crosses the Fermi level in our samples at approximately $0.32 < x < 0.35$. This, along with estimates of the position of E_F from Hall data on similar samples in the literature, is in reasonable agreement with the value of E_0 determined from the optical fit.

From an analysis of TSCAP and photocapacitance data we find that the concentration of DX centers in our samples is large—about ten times the normal net shallow-donor-concentration N_D in most

samples, and typically within the range $1 < N_{DX}/N_D < 30$. Thus, since the DX center is itself a donor, it is usually the dominant donor in Te-doped Al_xGa_{1-x}As. In Te-doped samples the DX concentration is roughly proportional to the Te concentration. Doping with Se gives the same effect as Te. In samples doped with Sn or Si, on the other hand, a different but closely related type of DX center is produced, again proportional to the donor concentration. These observations are strong evidence that the DX center involves a donor atom, hence the "D" of DX.

Finally, we have argued that the verification of the model of Ref. 1 forces us to assume that a defect state exists which is resonant with the conduction band when unoccupied, but which relaxes to a point nearly 0.8 eV deep in the gap after the capture of an electron. Thus the defect wave function must be sufficiently localized, even when it is a resonance in the continuum states of the band, to produce a very substantial lattice relaxation. We believe that the existence of such a state supports the view, based on recent calculations, that the localization of a deep-level wave function is not necessarily related to the position of the corresponding energy level in the forbidden gap. This is contrary to the picture of defect wave functions in semiconductors based on the effective-mass theory.

Based on experience gained from recent computer calculations of the energies and wave functions of various native defects and chemical impurities in III-V compounds, we believe that the simplest consistent model for the microstructure of DX-type defects is a complex involving a donor and an anion vacancy. For the case of Te-doped Al_xGa_{1-x}As which we are studying, this corresponds to Te-V_{As}. We propose that such a model for the structure of DX centers may be quite valid in general and can explain the data on persistent photoconductivity and other effects due to DX centers in a number of III-V and II-VI semiconductors.

ACKNOWLEDGMENTS

We wish to acknowledge the assistance of H. G. White and A. J. Williams, who have been instrumental in growing, processing, and testing the dozens of samples used in this study. Special thanks are due Ann Silversmith who took much of the photocapacitance data. We have also benefited from various stimulating discussions with our colleagues, in particular, V. Narayanamurti, G. A. Baraff, M. Schluter, C. H. Henry, J. L. Merz, and J. P. van der Ziel. One of us (M. J.) would like to thank ONR for their partial support under Contract No. N00014-76-0890.

51

- *Present address: Dept. of Theor. Phys., The University, Newcastle Upon Tyne, U. K.
- ¹D. V. Lang and R. A. Logan, *Phys. Rev. Lett.* **39**, 635 (1977).
- ²G. L. Miller, D. V. Lang, and L. C. Kimerling, *Ann. Rev. Mat. Sci.* **7**, 377 (1977).
- ³D. V. Lang, *J. Appl. Phys.* **45**, 3023 (1974).
- ⁴G. L. Miller, *IEEE Trans. Electron Devices* **19**, 1103 (1972).
- ⁵R. J. Nelson, *Appl. Phys. Lett.* **31**, 351 (1977).
- ⁶C. T. Sah and V. G. K. Reddi, *IEEE Trans. Electron Devices* **11**, 345 (1964).
- ⁷G. Goto, S. Yanagisawa, O. Wada, and H. Takanashi, *J. Appl. Phys.* **13**, 1127 (1974).
- ⁸K. Hesse and H. Strack, *Solid-State Electron.* **15**, 767 (1972).
- ⁹D. L. Losee, *Appl. Phys. Lett.* **21**, 54 (1972); *J. Appl. Phys.* **46**, 2204 (1975).
- ¹⁰H. G. Grimmeiss, *Ann. Rev. Mat. Sci.* **7**, 341 (1977).
- ¹¹D. E. Aspnes, *Phys. Rev. B* **14**, 3331 (1976).
- ¹²M. Jaros, *Phys. Rev. B* **16**, 3694 (1978).
- ¹³K. Huang and R. Rhys, *Proc. R. Soc.* **204**, 406 (1950).
- ¹⁴T. H. Kell, *Phys. Rev.* **140**, A601 (1965).
- ¹⁵J. R. Chelikowsky and M. L. Cohen, *Phys. Rev. B* **14**, 556 (1976).
- ¹⁶R. Dingle, R. A. Logan, and J. R. Arthur, Jr., *GaAs and Related Compounds (Edinburgh)*, 1976 (Inst. Phys. Conf. Ser. No. 33a, 1977), p. 210.
- ¹⁷A. J. SpringThorpe, F. D. King, and A. Becke, *J. Electron. Mat.* **4**, 101 (1975).
- ¹⁸Yu. E. Maronchuk and N. A. Yakuseva, *Fiz. Tekh. Poluprovodn.* **10**, 1349 (1976) [*Sov. Phys. Semicond.* **10**, 800 (1976)].
- ¹⁹W. Kohn, *Solid State Phys.* **5**, 259 (1957).
- ²⁰V. Heine and C. H. Henry, *Phys. Rev. B* **11**, 3795 (1975).
- ²¹G. A. Baraff and J. A. Appelbaum, *Phys. Rev. B* **5**, 475 (1972).
- ²²W. Kohn and C. Majumdar, *Phys. Rev.* **138**, A1617 (1965).
- ²³M. Jaros, *J. Phys. C* **3**, 2455 (1975).
- ²⁴M. Jaros and S. Brand, *Phys. Rev. B* **14**, 4494 (1976).
- ²⁵J. I. Pankove, *Optical Processes in Semiconductors*, (Prentice-Hall, Englewood Cliffs, 1971), p. 142.
- ²⁶C. H. Henry and D. V. Lang, *Phys. Rev. B* **15**, 989 (1977).
- ²⁷E. W. Williams and H. B. Bebb, in *Semiconductors and Semimetals*, edited by R. K. Willardson and A. C. Beer (Academic, New York, 1972), Vol. **8**, p. 321.
- ²⁸G. D. Watkins, *Radiation Effects in Semiconductors*, 1976 (Inst. Phys. Conf. Ser. No. 31, 1977), p. 95.
- ²⁹M. Jaros and G. P. Srivastava, *J. Phys. Chem. Sol.* **38**, 1399 (1977).
- ³⁰D. V. Lang, R. A. Logan, and L. C. Kimerling, *Phys. Rev. B* **15**, 4874 (1977).
- ³¹D. V. Lang, *Radiation Effects in Semiconductors*, 1976 (Inst. Phys. Conf. Ser. No. 31, 1977), p. 70.
- ³²M. G. Craford, G. E. Stillman, J. A. Rossi, and N. Holonyak, Jr., *Phys. Rev.* **168**, 867 (1968).
- ³³A. Ya. Vul', L. V. Golubev, L. V. Sharonova, and Yu. V. Shmartsev, *Fiz. Tekh. Poluprovodn.* **4**, 2347 (1970) [*Sov. Phys. Semicond.* **4**, 2017 (1971)]; L. Dmowski, M. Baj, M. Kubalski, R. Piotrkowski, and S. Porowski, Fourteenth International Conference on the Physics of Semiconductors, Edinburgh, 1974 (to be published).
- ³⁴B. C. Burkey, R. P. Khosla, J. R. Fischer, and D. L. Losee, *J. Appl. Phys.* **47**, 1095 (1976).
- ³⁵M. R. Lorenz, B. Segall, and H. H. Woodbury, *Phys. Rev.* **134**, A751 (1964).
- ³⁶H. F. MacMillan, Ph.D. Thesis (Stanford University, 1972) (unpublished).
- ³⁷G. W. Iseler, J. A. Kafalas, A. J. Strauss, H. F. MacMillan and, R. H. Bube, *Solid State Commun.* **10**, 619 (1972).
- ³⁸H. C. Wright, R. J. Douney, and J. R. Canning, *J. Phys. D* **1**, 1593 (1968).
- ³⁹C. Piekara, J. M. Langer, and B. Krukowska-Fulda, *Solid State Commun.* **23**, 583 (1977).
- ⁴⁰Y. Toyozawa, Proceedings of the International Conference on Recombination in Semiconductors, Southampton, 1978 (to be published).
- ⁴¹A. Sumi and Y. Toyozawa, *J. Phys. Soc. Jpn.* **35**, 137 (1973).
- ⁴²D. Emin and F. Holstein, *Phys. Rev. Lett.* **36**, 324 (1976).
- ⁴³T. Itoh and M. Takeuchi, *Jpn. J. Appl. Phys.* **16**, 227 (1977) and references therein.

LETTER TO THE EDITOR

Fine structure in the cathodoluminescence spectrum from chromium-doped gallium arsenide

E C Lightowers† and Claude M Penchina‡

† Wheatstone Physics Laboratory, King's College, Strand, London WC2R 2LS

‡ Department of Physics and Astronomy, University of Massachusetts, Amherst, Massachusetts 01003, USA

Received 23 January 1978

Abstract. It has been reported previously that chromium in gallium arsenide gives rise to two luminescence bands, one centred around 0.80 eV with a no-phonon line at 0.839 eV, the other centred around 0.56 eV. High-resolution cathodoluminescence measurements are reported which show that the line at 0.839 eV consists of nine components, and that there are three no-phonon components at ~0.574 eV associated with the lower energy band. Temperature dependence measurements show that there is no shift in the transition energies in the temperature range 4–25 K and indicate that splitting occurs in both the initial and final states of the transitions.

A broad luminescence band centred around 0.80 eV in chromium-doped gallium arsenide has been reported by several authors (Turner and Petit 1964, Williams and Blacknall 1967, Allen 1968, Egiazaryan *et al* 1970, Gorelenok *et al* 1971). Peka and Karkhanin (1972) and Aleksandrova *et al* (1972) have also observed a band centred around 0.56 eV which they associate with the presence of chromium. More recent high-resolution measurements at 4.2 K by Stocker and Schmidt (1976a, b) on Cr-doped GaAs grown by liquid phase epitaxy (LPE) have shown that the 0.80 eV band has a sharp no-phonon line at 0.838 eV. This has been confirmed by Koschel *et al* (1976a) who also report that the 0.80 eV system is always accompanied by the 0.56 eV band in Cr-doped semi-insulating bulk material, but the lower energy band was not detected in the n-type LPE layer which they also investigated. Koschel *et al* (1976a, b) have suggested that the 0.56 and 0.80 eV systems may be identified with transitions between the crystal-field split levels of Cr^{3+} and Cr^{2+} ions respectively, located on gallium sites. On the other hand, Stocker and Schmidt (1976b) consider that the 0.56 eV band is associated with an internal ${}^5\text{E} \rightarrow {}^5\text{T}_2$ transition at Cr^{2+} whereas the 0.80 eV system may be identified with a transition from the conduction band to the Cr^{2+} ground state.

We have studied the luminescence from several samples of GaAs obtained from different sources. These include a Cr-doped LPE sample from Stocker and Schmidt, some O-doped and Cr-doped bulk material from RSRE, and semi-insulating bulk samples from the Sumitomo Company. The crystals were mounted in indium on the cold finger of a helium flow cryostat. The luminescence was excited by a 50 keV electron beam focused to ~0.5 mm diameter with a typical beam current of 1.8 μA . A study of the spectral variation with beam current indicated that, near 4.2 K, a 1.8 μA beam raises the

effective temperature of the emitting region by ~ 1 K above that of the cold finger. This heating effect decreases at higher temperatures as the thermal conductivity of GaAs increases. The luminescence was dispersed by a Spex 1401 monochromator with a 600 groove per mm grating blazed at $1.6 \mu\text{m}$, and detected by a cooled PbS cell.

Spectra obtained from the n-type LPE sample of Stocker and Schmidt showed the presence of the 0.56 eV system, which they did not observe, in addition to the 0.80 eV system. However, since the penetration of the electron beam is substantially greater than the 488 nm photoexcitation they employed, we cannot rule out the possibility that some of the cathodoluminescence originated in the substrate. Bulk samples of O-doped semi-insulating GaAs from the Sumitomo Company (impurity concentration in atomic ppm: O, 4.5; Si, 0.5; Cr, 0.2; Fe, 0.03; Cu, 0.02) showed the same spectral features with about six times greater intensity, allowing much higher resolution measurements to be made. It was these samples which were used for all the detailed studies of fine structure reported in the Letter. The fact that the Cr spectra were so much more intense in the O-doped sample than in the intentionally Cr-doped samples was noted with interest. To test that these spectra are really due to chromium rather than oxygen or some other impurity, we studied the luminescence of some O-doped and Cr-doped bulk samples from RSRE. The Cr-doped samples showed the expected luminescence features whereas the O-doped samples showed very different broad spectra which will be reported elsewhere.

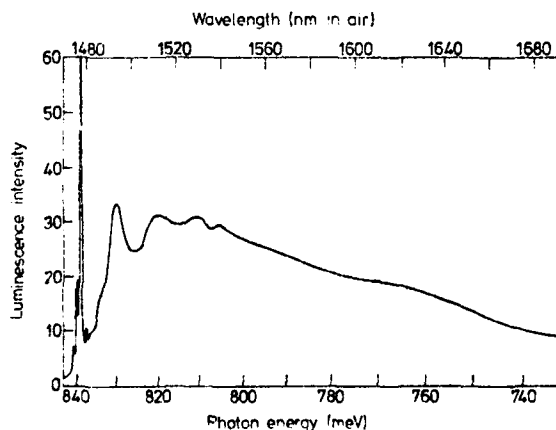


Figure 1. Cathodoluminescence spectrum of the 0.80 eV system, uncorrected for the transfer function of the optical system, obtained from Sumitomo semi-insulating GaAs with a cold finger temperature of 4.8 K and beam current of $2.0 \mu\text{A}$. The temperature of the emitting region was 6.0 ± 0.5 K. The no-phonon structure is distorted by the slitwidth of the monochromator and the system response time. The main peak at 839.30 meV has a height of ~ 1.50 on this scale.

Figure 1 shows a relatively low resolution spectrum of the 0.80 eV system obtained with a cold finger temperature of 4.8 K (temperature of the emitting region 6.0 ± 0.5 K). Some fine structure can be seen in the no-phonon region at ~ 0.839 eV. The broader structure at the high-energy end of the sideband has been identified with phonon-assisted transitions involving intrinsic zone boundary and zone centre phonons (Stocker and Schmidt 1976a, Koschel *et al* 1976a). The broad hump seen around 750 meV is of about the same strength as reported by Stocker and Schmidt (1976a) for their Cr doped GaAs.

even though the sample used in our experiments had more oxygen than chromium and had a photoconductivity spectrum dominated by oxygen (Tyler *et al* 1977). This casts some doubt on their suggestion that the hump is 'possibly due to transitions to the energy level associated with oxygen.'

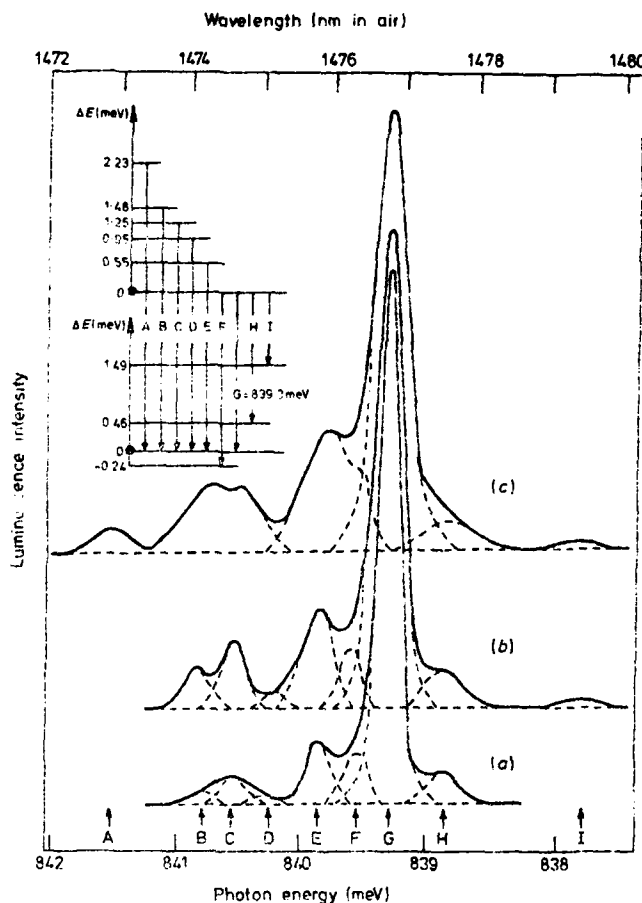


Figure 2. Cathodoluminescence spectra of the 0.839 eV no-phonon structure, obtained from Sumitomo semi-insulating GaAs with cold finger temperatures of: (a) 5.0 K; (b) 10.3 K; and (c) 14.4 K. The beam current was $\sim 1.8 \mu\text{A}$ in all cases and the electron beam heating of the emitting region $\lesssim 1$ K. The monochromator slitwidth was $100 \mu\text{m}$ giving a spectral resolution of 0.2 nm . The energy level scheme inferred from the temperature dependence of the relative line strengths is shown as an insert.

Higher resolution spectra of the no-phonon structure are shown in figure 2. It can be seen that there are nine closely spaced no-phonon lines, labelled A-I, some clearly resolved and some overlapping. The strongest no-phonon line, labelled G in figure 2, is at $1476.82 \pm 0.05 \text{ nm}$ ($839.30 \pm 0.03 \text{ meV}$) with a linewidth (FWHM) of $\sim 0.3 \text{ nm}$ (0.35 nm apparent width with a spectrometer resolution of 0.20 nm) at $\sim 4.2 \text{ K}$. The wavelength of this line is independent of the temperature, within 0.1 nm accuracy, from

4.2 to 25 K. The lines broaden with increasing temperature so that above ~ 25 K the nine lines appear almost as one. A study of the temperature dependence of the strengths of the various no-phonon lines indicates that lines A-E thermalise with respect to the main line G. Lines F, H and I, on the other hand, maintain the same strength relative to G at all temperatures. From these data we deduce the energy level scheme, shown as an insert in figure 2.

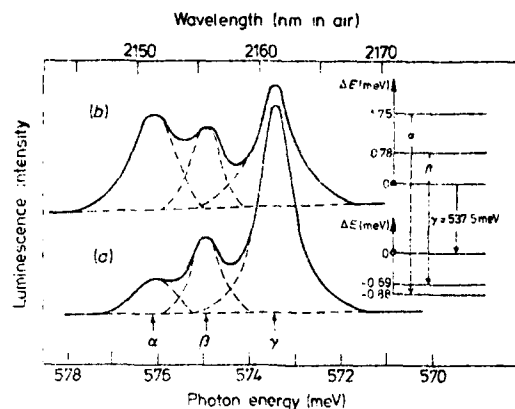


Figure 3. Cathodoluminescence spectra of the no-phonon structure near 0.573 eV obtained from Sumitomo semi-insulating GaAs with cold finger temperatures of: (a) 7.7 K; and (b) 21.2 K. The beam currents were (a) 2.3 μ A and (b) 1.8 μ A, and the monochromator slitwidths (a) 500 μ m and (b) 400 μ m for a resolution of (a) 1 nm and (b) 0.8 nm. The energy level scheme inferred from the temperature dependence of the relative line strengths is shown as an insert.

Figure 3 shows the no-phonon region of the 0.56 eV system and three distinct lines are observed. At low temperatures there is a main line at 2161.34 ± 0.06 nm (573.49 ± 0.02 meV) with two weaker lines at higher energy. Increasing the temperature produces a relative increase in the strengths of the higher energy lines but the thermalisation is less than would be expected if all the splitting were in the initial state of the transition. The

Table 1. Relative transition probabilities of the lines shown in figures 1 and 2 normalised to the strongest line at low temperature.

Transition	Wavelength (nm in air)	Photon energy (meV) ± 0.03	Normalised transition probability
A	1472.91 ± 0.06	841.53	0.28
B	1474.23 ± 0.05	840.78	0.44
C	1474.67 ± 0.05	840.53	0.49
D	1475.13 ± 0.06	840.25	0.12
F	1475.86 ± 0.05	839.85	0.37
F	1476.40 ± 0.05	839.54	0.11
G	1476.82 ± 0.05	839.30	1.0
H	1477.63 ± 0.06	838.84	0.10
I	1479.45 ± 0.05	837.81	0.05
γ	2151.46 ± 0.14	576.12 ± 0.04	2.1
β	2155.82 ± 0.01	574.96 ± 0.03	1.0
α	2161.34 ± 0.06	573.49 ± 0.02	1.0

estimated splittings of the initial and final states are shown in the energy level scheme in figure 3. Note, however, that the final states of the transitions labelled α and β may really be the same level since the splitting shown is within the uncertainty caused by signal noise and beam heating. Scatter of the data causes about 0.05 meV uncertainty and an error of 1 K in sample temperature would cause ~ 0.13 meV error in the energy levels.

Extrapolation of the relative line strengths to infinite temperature gives the relative transition probabilities. These are listed in table 1 together with the wavelengths and photon energies of the various transitions observed.

It is apparent from the data presented here that both the 0.80 eV and 0.56 eV luminescence systems may be ascribed to transition between bound states of the chromium defect. A more detailed understanding requires, as a first priority, a more thorough study of the role, if any, of oxygen and the effect of conductivity type.

We wish to thank Hans J Stocker and A Michael White for supplying some of the samples used in this study, and Alan T Collins and Martin O Henry for their aid at various stages of the experiments. This work was supported in part by the Office of Naval Research under contract N00014-76-C-0890, and by the Science Research Council and the University of London Central Research Fund.

References

- Aleksandrova G A, Vil'kotskii V A, Domanevskii D S and Tkachev V D 1972 *Sov. Phys.-Semicond.* **6** 266-9
Allen G A 1968 *J. Phys. D: Appl. Phys.* **1** 593-602
Egiazaryan G A, Murygin V I, Rubin V S and Stafeev V I 1970 *Sov. Phys.-Semicond.* **3** 1389-92
Gorelenok A T, Tsarenkov B V and Chiabrishvili N G 1971 *Sov. Phys.-Semicond.* **5** 95-9
Koschel W H, Bishop S G and McCombe B D 1976a *Solid St. Commun.* **19** 521-4
--- 1976b *Proc. 13th Int. Conf. Physics of Semiconductors, Rome* ed F G Fumi (Rome: Tipografia Marves) pp 1065-8
Peka G P and Karkhanin Yu I 1972 *Sov. Phys.-Semicond.* **6** 261-5
Stocker H J and Schmidt M 1976a *J. Appl. Phys.* **47** 2450-1
--- 1976b *Proc. 13th Int. Conf. Physics of Semiconductors, Rome* ed F G Fumi (Rome: Tipografia Marves) pp 611-4
Turner W J and Petit G D 1964 *Bull. Am. Phys. Soc.* **9** 269
Tyler E, Jaros M and Penchina C M 1977 *Appl. Phys. Lett.* **31** 208-10
Williams E W and Blacknall D M 1967 *Trans. Metall. Soc. AIME* **239** 387-94

TEMPERATURE DEPENDENCE OF THE FINE STRUCTURE IN THE LUMINESCENCE AND ABSORPTION SPECTRA OF CHROMIUM-DOPED GALLIUM ARSENIDE[‡]

Edward C. Lightowers and Martin O. Henry
Physics Department, King's College, Strand, London WC2R 2LS UK
Claude M. Penchina, Department of Physics and Astronomy,
University of Massachusetts, Amherst, Mass. 01003, USA

High resolution luminescence measurements on the 839meV no-phonon line in Cr-doped semi-insulating GaAs have revealed the presence of 13 components. Corresponding structure has also been found in the absorption spectrum. An energy level scheme and relative transition rates have been determined from thermalization measurements.

We have reported previously¹ that the no-phonon line at 839meV^{2,3} in the luminescence spectrum from Cr-doped semi-insulating (SI) GaAs contains nine components, and a tentative energy level scheme was proposed based on thermalization measurements. In the present work we report a higher resolution luminescence study in which thirteen lines have been identified. We report also the existence of most of these lines in absorption. A modified energy level scheme is proposed based on temperature dependence measurements of both the absorption and emission spectra.

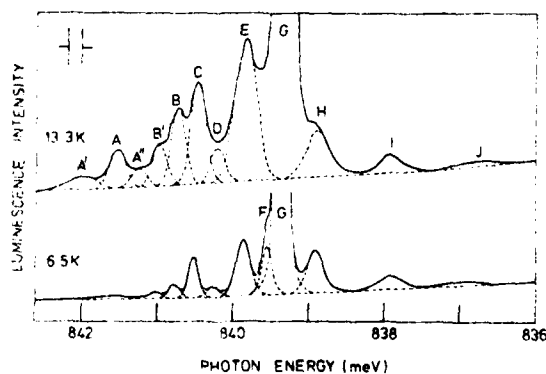


Fig. 1. Cathodoluminescence spectra of SI GaAs:Cr. The ordinate scales for the two temperatures differ.

The luminescence was excited by 50keV electrons as described previously¹, but a significant gain in signal strength was obtained by using samples shaped as Weierstrass over-hemispheres⁴. A path length of 50mm was

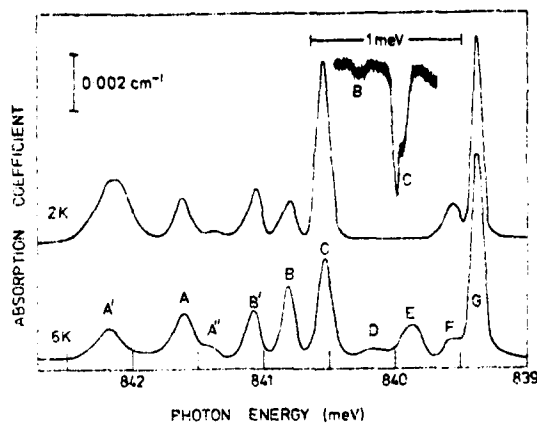


Fig. 2. Absorption coefficient for the 839meV no-phonon system in SI GaAs:Cr(10^{23}cm^{-3}). The lines are superimposed on a much stronger background absorption similar to that described by Bois and Pinard⁵.

employed in the absorption measurements because of the small transition oscillator strength.

Luminescence spectra obtained at 6.5K and 13.3K are shown in Fig. 1. The intensities of the lines A' to E increase relative to G with increasing temperature whilst the lines F, H, I and J do not appear to thermalize. Corresponding absorption spectra obtained at 2.0K and 6.0K are shown in Fig. 2. Lines A', C and F decrease relative to G with increasing temperature, and line E increases. The thermalization of the other lines is less clear. The lines on the low energy side of G, observed in the luminescence spectrum, could not be detected in absorption. All of the experimental measurements are

summarized in Table 1.

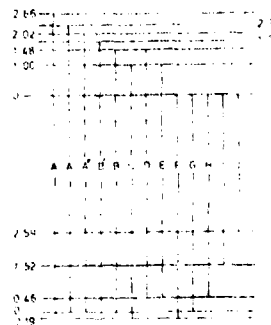


Fig. 3. Energy level scheme based on the data in Table 1. Line G occurs at 839.37 ± 0.05 meV at 2K.

Table 1. Energy separations and intensities of lines relative to line G.

Line	Spectroscopic energy separation (meV)	Thermal activation energy(meV)		Relative transition probability	
		Absorption	Luminescence	Absorption	Luminescence
A'	+2.85 ± 0.02	-0.25 ± 0.06	+2.9 ± 1.1	0.24 ± 0.04	~0.4
A	+2.31 ± 0.02	+0.06 ± 0.04*	+2.01 ± 0.11	0.61 ± 0.16	0.39 ± 0.06
A''	+2.02 ± 0.08		+2.87 ± 0.66		~0.3
B'	+1.74 ± 0.02	-0.07 ± 0.06*	+1.72 ± 0.10	0.25 ± 0.02	0.25 ± 0.03
B	+1.48 ± 0.01	+0.12 ± 0.08*	+1.90 ± 0.14	0.48 ± 0.20	0.60 ± 0.11
C	+1.20 ± 0.01	-0.19 ± 0.04	+1.12 ± 0.06	0.38 ± 0.04	0.46 ± 0.03
D	+0.92 ± 0.06		+1.44 ± 0.17		0.18 ± 0.04
E	+0.52 ± 0.02	+0.44 ± 0.18	+1.06 ± 0.04	0.45 ± 0.16	0.77 ± 0.04
F	+0.19 ± 0.02	-0.22 ± 0.04	0	0.06 ± 0.01	0.08 ± 0.01
H	-0.46 ± 0.02		0		0.12 ± 0.03
I	-1.52 ± 0.01		0		0.05 ± 0.006
J	-2.59 ± 0.20		0		0.02 ± 0.005

* Assumed to be zero for the purpose of figure 3.

The proposed energy level scheme based on the data in Table 1 is shown in Fig. 3. The transitions indicated with full lines appear to be clearly defined by the thermalization data. However, experimental uncertainties, particularly in the absorption measurements, prevent an unambiguous assignment of the transitions indicated by broken lines. It is likely that some of the difficulties in analysing the absorption spectra arise from unresolved structure. This is apparent in the higher resolution transmission spectrum for line C inset in Fig. 2.

Electrical transport, local mode absorption and mass spectroscopic studies by Brozel et al⁶ indicate that in the material used in this investigation, the chromium exists primarily as Cr²⁺ and Cr¹⁺ on gallium sites. These authors also argue that in strongly n-type material the chromium is entirely present as Cr¹⁺. We were unable to detect the 839meV absorption system in an n-type sample containing about five times the chromium concentration of the semi-insulating material, and luminescence studies by Instone and Eaves⁷ have shown that the strength of this

system decreases as the material becomes progressively n-type. This is in agreement with the conclusion of other investigators that the 839meV system is associated with chromium in the Cr²⁺ state. The transitions involved have variously been ascribed to internal ⁵E - ⁵T₂ transitions at Cr²⁺, or from a band to the Cr²⁺ ground state^{2,3,8}. However, the multiplicity of the upper level would appear to rule out the latter alternative.

The work of Vallin et al⁹ on Cr-doped III-VI compounds has shown that complex splittings can be expected for the ⁵E and ⁵T₂ states of Cr²⁺ on a tetrahedral site. The fine structure in the spectra reported here would suggest an interpretation in terms of an internal ⁵E - ⁵T₂ transition at Cr²⁺ on a gallium site in SI GaAs.

We are grateful to D.J.Stirland of the Allen Clark Research Centre and K.J.Shaw of Mining and Chemical Products for providing the GaAs used in these investigations and to L.Eaves for discussing his experimental results prior to publication.

I Supported in part by the Office of Naval Research under contract N 00014-76-C-0890, by the Science Research Council, and the University of London Central Research Fund.

1. Lightowers E C and Penchina C M 1978 *J.Phys.C* 11 L405-9
2. Stocker H J and Schmidt M 1976 *J.Appl.Phys.* 47 2450-1
3. Koschel W H, Bishop S G and McCombe B D 1976 *Solid St.Commun.* 19 521-4
4. Collins A T 1977 *J.Phys.D* 10 1143-50
5. Bois D and Pinard P 1974 *Phys.Rev. B* 9 4171-7
6. Brozel M R, Butler J, Newman R C, Ritson A, Stirland D and Whitehead C 1978 *J.Phys.C* 11 1857-63
7. Instone T and Eaves L 1978 Private communication
8. Kaufmann U and Koschel W H 1978 *Phys.Rev.B* 17 2081-4
9. Vallin J T, Slack G A, Roberts S and Hughes A E 1970 *Phys.Rev.B* 2 4313-33

Study of the main electron trap in $\text{Ga}_{1-x}\text{In}_x\text{As}$ alloys

A. Mircea, A. Mitonneau, and J. Hallais

Laboratoires d'Electronique et de Physique Appliquée 3, Avenue Descartes, 94450 Limell-Brevannes, France

M. Jaros

Department of Theoretical Physics, The University, Newcastle-upon-Tyne, United Kingdom

(Received 11 February 1977)

Transient-capacitance-spectroscopy experiments yielded electron-emission-rate and electron capture cross-section versus temperature data for the main electron trap in vapor-phase epitaxial $\text{Ga}_{1-x}\text{In}_x\text{As}$ layers with $0 < x < 0.21$. The ionization energy $E_C - E_T$ was obtained from these. Theoretical calculations using the pseudopotential method were performed for substitutional oxygen donor in GaInAs, and the calculated energy levels were compared with the experimental ones. The electron-capture cross sections, as well as optical photoionization data are also discussed from the theoretical point of view. It is argued that most of the experimental evidence is not consistent with the idea that the observed electron trap is simple (substitutional) donor oxygen.

I. INTRODUCTION

The deep levels may play an important role in the operation of specific semiconductor devices, particularly in optoelectronics. In recent years, largely due to improvements in the experimental techniques which tend to become more quantitative, and also due to the development of efficient tools for theoretical investigation, some progress has been made towards understanding the electronic and optical properties of these levels, their physicochemical origin, and the physical configuration of the corresponding defects.

Most of the recent studies deal with III-V semiconductors, in view of their applications in optoelectronics. A recent review of the situation in GaAs and GaP has been prepared by Ikoma and co-workers.¹

Particle irradiation of semiconductors is a convenient means for creating defects (and therefore deep levels) in a controlled fashion. A recent review on irradiation defects in III-V semiconductors has been presented by Lang.² Equally important, but more difficult is the study of the defects which appear spontaneously in as-grown materials, since the means available for controlling the presence and concentration of these defects are limited. Since none of the deep levels corresponding to these "natural" defects have electronic properties identical with those of the defects created by irradiation, one may conclude that they are not simple lattice defects, e.g., anion or cation vacancies or interstitials; more likely, they are due to impurities and impurity-lattice defect complexes.

In the case of III-V semiconductors, one of the useful ways of investigation of the "natural" deep levels is to follow the variation of their properties as a function of composition in pseudoternary

alloys. The first such tentatives have been accomplished by Lang³ and Majerfeld⁴ for the system $\text{Ga}_{1-x}\text{Al}_x\text{As}$.

We present here a study of this type, concerning the system $\text{Ga}_{1-x}\text{In}_x\text{As}$ and the deep level, already well known for GaAs, labeled electron trap "A" in our previous publications⁵ or "O" in recent papers by Lang⁶; the last label points to the fact that this deep level may be due to oxygen, either in the simplest configuration of a substitutional atom on arsenic site, or in an impurity-lattice defect complex. An attempt to discover whether the level can be identified with the simple substitutional oxygen impurity has been one of the motivations of this study. In addition to the new experimental results which will be presented for the alloys, we have endeavored to compare the experimental results with detailed, specific theoretical calculations, hoping to establish a new tradition and make a step forward with respect to previous work. In Sec. II, we briefly discuss the existing evidence concerning the origin of electron trap A and its possible relation to oxygen. In Sec. III, we describe the techniques used in the experimental study, as well as the experimental results concerning the emission and capture rates for level A in GaInAs alloys of various compositions. Section IV deals with the theoretical calculations and their comparison with experiment. Section V is a summary.

II. REVIEW OF THE EXPERIMENTAL EVIDENCE ON DEEP LEVELS POSSIBLY RELATED TO OXYGEN IN GaAs

The deep electron trap which forms the object of the present study has been known for a long time and it seems to be by far the most common of the unintentionally created deep levels in GaAs, both

bulk grown and vapor-phase epitaxial (VPE). The level has been studied most often by two different techniques in two different types of material, namely, photoconductivity in high-resistivity samples and capacitance transients in p - n junctions, or Schottky barriers, in low-resistivity ones. For discussions of previous studies of the second kind we refer to Lang *et al.*⁹ and Mircea *et al.*⁸

The tentative attribution of this level to oxygen is strongly supported by the investigation of the high-resistivity bulk-grown material, since the concentration of the level greatly increases when the material is deliberately doped with oxygen.⁷⁻⁹ The photoionization spectral response data taken on such samples often reveal^{7,8,30} two distinct contributions with threshold energies at 0.75–0.8 eV and around 1.05 eV. Grimmeiss *et al.*⁹ have recently shown that the same thresholds are also observed in p - n junctions on low-resistivity material and that they correspond to transitions from the deep levels into the conduction band.

The question then arises whether both these levels belong to the same defect center, more generally, whether they are both related in some way to the presence of oxygen in the semiconductor.

The concentrations of these deep levels in bulk-grown material are usually rather high, typically in the 10^{18} - cm^{-3} range, so that they are easily observed, but other levels are generally present as well in this kind of material,^{7,10} which renders the interpretation more difficult. In this respect, the situation is clearer with epitaxial material. From our previous photoconductivity and transient capacitance experience with VPE, GaAs^{11,12} and its comparison with deep level transient spectroscopy (DLTS) work by Lang and Logan,⁶ photo-capacitance work by Bois and Boulou,¹³ photo-capacitance and transient-capacitance work by Sakai and Ikoma,¹⁴ as well as with Grimmeiss and Ledebor,⁹ and Lin *et al.*,³⁰ we draw the following conclusions: (i) the two levels referred to above are also present in undoped VPE material, although at much lower concentrations, typically 10^{12} – 10^{14} cm^{-3} ; (ii) the two levels are independent from one another. The level with photoionization threshold at 1–1.05 eV from E_c (and 0.42–0.45 eV from E_v) is directly related to copper.^{6,12} Therefore, the hypothesis of a double level (a defect with two ionization states) proposed by Bois^{13,15} is not verified. However, it is shown in Sec. III B 2 below that the "A" electron trap, which is the level with photoionization threshold at 0.75–0.8 eV, seems to have at least one of the features which are characteristic for a defect with two ionization states.

As further evidence for the fact that the "oxygen" level in bulk-grown GaAs is indeed the same as

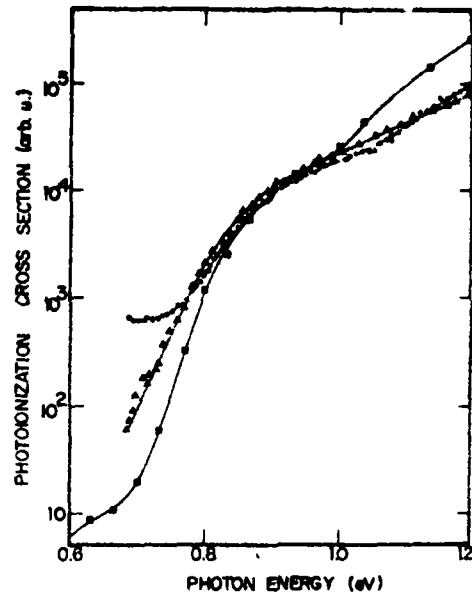


FIG. 1. Extrinsic photoconductivity in GaAs at 100 K. Triangles—high-resistivity oxygen-doped bulk (Ref. 9); crosses and circles—two different low-resistivity (1Ω cm) VPE layers with the substrate etched off (Ref. 11).

"A" electron trap in high-purity VPE material, we present in Fig. 1 photoconductivity spectra measured on thin (10^{-2} mm) epilayers with the substrate removed.¹¹ The two photoionization curves for two different epilayers are essentially identical in the range 0.75–1.0 eV and are in agreement with the recent data for oxygen-doped bulk. The threshold at 1–1.05 eV is strong only in one of the two epilayers, in agreement with statement (ii) above.

III. EXPERIMENTAL STUDY OF THE A ELECTRON TRAP

A. Preparation of semiconductor material and samples

The material was prepared at *Laboratoire d'Electronique et de Physique applique (LEP)* by vapor phase epitaxial growth using the AsCl_3 process under hydrogen flow. The substrates were n^+ doped and oriented 3° off (100). The source and substrate temperatures were 800 and 720 $^\circ\text{C}$, respectively. Growth rate was 10 $\mu\text{m}/\text{h}$. In order to reduce the effects of lattice mismatch, the In content was increased in steps.¹⁶ The dislocation density in the final, constant composition layer was in the 10^2 - cm^{-2} range.

The epilayers were visually examined, then their composition was determined by using the x-ray measurement of the lattice parameter. The band

gap was estimated from the infrared absorption threshold at room temperature in the so-called "water-droplet" experiment,¹⁷ this measurement being subsequently used as a routine check of alloy composition. Preliminary electrical characterization included conductivity type and free-carrier-concentration profile determinations using a mercury Schottky barrier.

Without intentional doping, the layers were *n* type with electron concentrations of 10^{13} – 10^{16} cm^{-3} . For our study, low electron concentrations are highly desirable, in order to be able to measure the electron-capture rates (see Sec. III B 2 below); however, for compositions with large indium content it has not been possible to obtain low doping levels. On the layers chosen for transient-capacitance experiments, the doping profile measurements were repeated, with better accuracy, on the permanent Schottky barriers used in these experiments.

The barriers were circular gold plots with a diameter of 0.9 mm, obtained by vacuum evaporation through a nickel mask in an oil-free vacuum setup. No cleaning procedure was applied to the wafers prior to evaporation, but considerable care was taken to reduce surface pollution as much as possible. The Ohmic contact was made by soldering a tin ball on the edge of the sample. The connection to the barrier was realized with a gold wire fastened with silver paste. A more detailed description of the sample mounting has been given in a previous report.¹⁸

In Table I, we summarize the main characteristics of the samples chosen for this study. A range

TABLE I. Survey of $Ga_{1-x}In_xAs$ wafers used in this study.

Wafer n^d	x^a	E_g^b (eV)	n^c (cm^{-3})	w^d (μm)	N_t^e (cm^{-3})
1	0.046	1.320	1.2×10^{16}	10	2×10^{13}
2	0.077	1.265	8×10^{15}	20	7×10^{13}
3	0.099	1.245	7.5×10^{15}	20	10^{14}
4	0.140	1.215	7×10^{15}	3	4×10^{13}
5	0.21	1.115	1.5×10^{16}	20	4×10^{13}
6	0.24	1.075	2×10^{16}	11	4×10^{13}
GaAs	0	1.37	2×10^{15}	20	2×10^{14}

^a Composition as deduced from x-ray lattice parameter measurements.

^b Band gap evaluated at room temperature from the spectral response of a water-droplet barrier on semiconductor.

^c Free-carrier (electron) concentration at room temperature; accurate to within 20%.

^d Thickness of the layer of $GaInAs$ with uniform composition.

^e Concentration of deep electron trap *A* calculated from the height of the DLTS peak.

of indium content from (0–24)% has been explored. The samples listed in the table had fairly uniform electron concentration profiles.

B. Transient-capacitance experiments

We have measured the emission rates (from deep level to conduction band) and the capture rates (from conduction band to deep level) as a function of temperature.

1. Emission rates

We have mainly worked with the dynamic, differential measurement of capacitance transients introduced by Lang¹⁹ under the name DLTS. Two different experimental systems were used. The first, semiautomatic system based on a Hewlett-Packard model 9821 calculator has been described previously¹⁶; it can measure from very small emission rates (starting at 10^{-3} s^{-1} or so) up to 10 s^{-1} . The second system, extending the range from about 10 s^{-1} to 5×10^3 s^{-1} , is an analog one and is based on the use of a network analyzer (HP model 8407 A), as capacitance meter with a signal of 0.1 V applied to the sample, and a lock-in detector (PAR model 128) as filter selecting the fundamental of the repetitive transient. This last setup, schematically shown in Fig. 2, is characterized by an excellent signal-to-noise ratio, due to the efficient use of information and in spite of the relatively high level of noise coming from the network analyzer.

In Fig. 3, we show the DLTS spectra, taken with

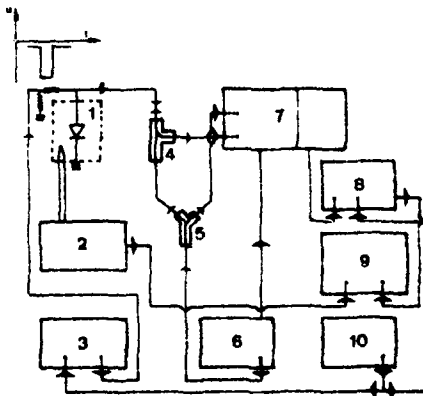


FIG. 2. Schematic drawing of the electronic setup for transient capacitance spectroscopy at moderately high emission rates. (1) Sample in cryostat, (2) digital thermometer CRL 204, (3) pulse generator HP 8015 A, (4) directional coupler HP 8721 A, (5) power splitter, (6) rf generator HP 8601 A, (7) network analyzer HP 8407 A with display 8412 A, (8) lock-in detector PAR 128, (9) x-y recorder, (10) square-wave generator.

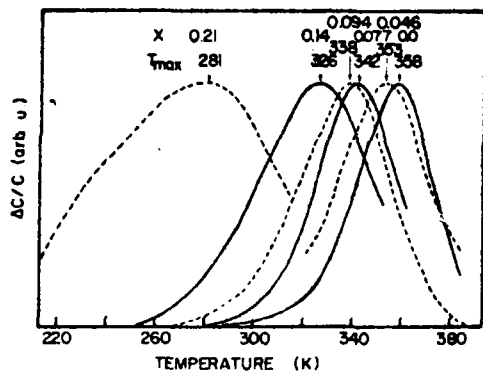


FIG. 3. DLTS spectra with a fixed-emission-rate window as a function of alloy composition. C is the capacitance of the barrier.

an emission-rate window centered at 7.5 s^{-1} ; on samples made from pure GaAs and from alloys 1, 2, 3, and 4. For easier comparison, the spectra have been redrawn with normalized amplitudes, while in reality the peaks were of course unequal—the peak height being proportional to N_t/n , where N_t is the deep-level concentration. In the range of temperatures investigated (-190 to $+160^\circ\text{C}$), a single electron trap peak was observed for each sample. Also, the peak position monotonously moves toward lower temperatures as the indium fraction x increases, which is exactly what one expects if the same defect is responsible for the peaks observed in the different samples. From these observations, and taking into account that the layers were grown in the same reactor under similar conditions, we conclude with a high degree of credibility that the same defect is observed over the whole composition range.

The temperature T_{max} corresponding to the DLTS peaks of Fig. 3 are plotted as a function of indium

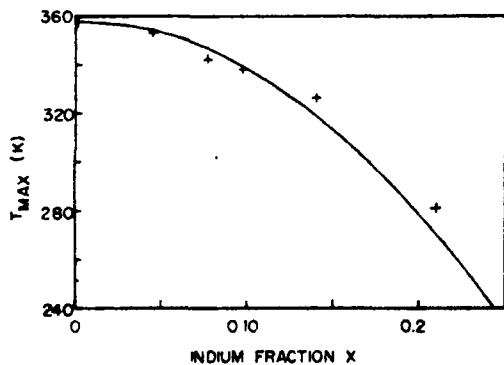


FIG. 4. Plot of temperatures T_{max} of Fig. 3, corresponding to an emission rate of 7.5 s^{-1} vs indium fraction x .

fraction x in Fig. 4. A parabolic law

$$T_{\text{max}} = T_{\text{max}}(0) - T_{\text{max}}(x) = ax^b$$

with $b=2$, $a=2000 \text{ K}$, allows one to reproduce the experimental results quite faithfully; this empirical fit is also shown in Fig. 4. Still, nonsystematic differences, significantly larger than the experimental error, exist between the smooth fit and the data. These differences have probably to do with two "secondary effects" which we have observed:

(i) Even in the simplest case of the binary semiconductor GaAs ($x=0$), the dependence of emission rate versus temperature $\epsilon_n(T)$ is not unique; it can slightly, but significantly vary from layer to layer, even if these are of a similar kind (VPE, doping in the 10^{15}-cm^{-3} range, relative trap concentration N_t/n much smaller than unity).

(ii) While, in the case of pure-GaAs samples the emission transients are rigorously exponential, this is no more true for our alloy samples, in which more complex transients with several time constants are obtained.

Since these effects—especially the first one, which we have already signalled in a previous publication—may present some intrinsic interest, we have looked at them in more detail. To illustrate the first effect, Fig. 5 shows DLTS spectra taken on five different GaAs layers with all samples mounted at the same time under identical conditions in the crystal. The reproducibility of the temperature measurement is within 1°C . Two different positions of the peak may be clearly seen. Most of the layers (including the one of Fig. 3) behave as samples (a), (d), or (e), while (b) and (c) have a larger emission rate, in spite of the fact that they are in fact less doped—thus, excluding the possibility of electric-field-assisted emission. We stress again that for all these GaAs samples the emission transient is rigorously exponential.

The temperature difference obtained between the two groups of GaAs samples is of the same order as the one measured between GaAs and $\text{Ga}_{0.95}\text{As}$ (Fig. 3); therefore, one must be careful

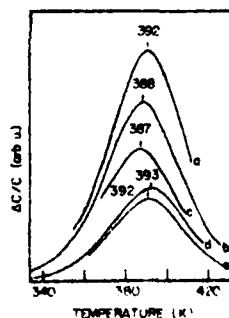


FIG. 5. Emission-rate variations from sample to sample in GaAs. Doping levels are (a) $1.5 \times 10^{15} \text{ cm}^{-3}$, (b) and (c) $8.10^{14} \text{ cm}^{-3}$, (d) and (e) $2.10^{15} \text{ cm}^{-3}$. All samples are VPE layers. The spectra were taken with all samples mounted simultaneously and identically in the cryostat. Reverse bias 5 V, emission window 120 s^{-1} .

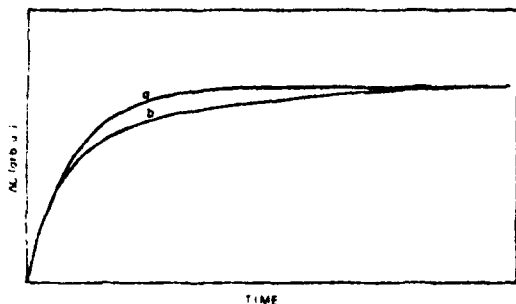


FIG. 6. Linear plot of capacitance transients at 27°C. (a) GaAs, (b) ternary $x=1$ ($x=0.046$).

not to rely too heavily on the exact position of experimental points in Fig. 4.

These small emission-rate variations may be due to the effect of internal crystal strain.

The second "secondary effect" (nonexponential emission transients) has been observed to date only on the ternary samples. To look at this aspect more carefully, we performed accurate measurements at a fixed temperature, using the calculator system as transient averager in order to improve the signal-to-noise ratio. Typical observations are shown in Figs. 6 and 7. In Fig. 6, we plot in linear scales the transients observed at 27°C for GaAs and for layer #1 ($x=0.5$). In the second case, the nonexponential variation is easily seen.

In Fig. 7, we show semilogarithmic plots for three transients. Generally it appears feasible to describe the experimental curve as a sum of two or three pure exponentials. However, we have not been able to determine a regular variation of each time constant as a function of temperature, which would have conferred a physical meaning to this decomposition.

This completes the description of the secondary

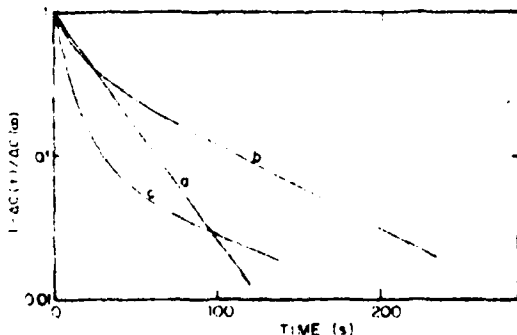


FIG. 7. Semilogarithmic plot of capacitance transients. (a) GaAs, (b) #1, (c) ternary $x=1$ at 27°C, (d) ternary $x=2$ at 27°C.

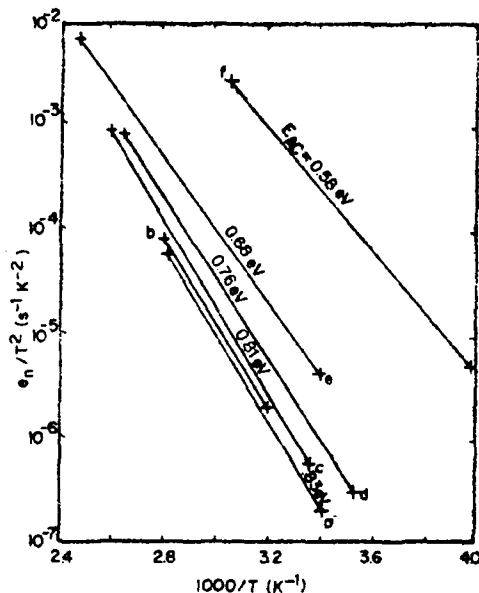


FIG. 8. Arrhenius plots of experimental emission rates of electron trap A vs temperature. (a) GaAs, standard; (b) ternary $x=1$ ($x=0.046$); (c) GaAs, high-emission-rate layer (see text); (d) ternary $x=2$ ($x=0.077$); (e) ternary $x=4$ ($x=0.14$); (f) ternary $x=5$ ($x=0.21$).

effects which loaded our investigation. In spite of these difficulties, from the DLTS data taken with different emission-rate windows it has been possible to obtain straight-line plots of $e_n/T^2 = f(1/T)$, characteristic for the deep electron trap A in alloys of increasing indium fraction. These are shown in Fig. 8. According to the discussion above, curve (b) for the ternary with weak indium content, falls within the range of uncertainty observed for pure GaAs. It would then be pointless to seek for better accuracy in the position of curve (b).

The activation energies E_{AC} associated with the plots of Fig. 8 are marked in this figure. They remain more or less constant for indium fractions lower than 8%, then start decreasing. It is known that these activation energies are related to the energetical difference between the conduction band and the deep level, $E_{TC} = E_C - E_T$. However, as discussed by Henry and Lang a correction E_B due to the variation of capture cross section versus temperature must be applied:

$$E_{AC} = E_{TC} + E_B. \quad (1)$$

Therefore, before comparing the experimental results to the theoretical predictions concerning E_{TC} , it is necessary to measure the capture cross sections and detect possible variations of E_B as a function of x .

2. Electron-capture rates and cross sections

The capture cross sections were obtained using either dynamic or static measurements of the capture rates.

The dynamic method consists of sweeping across the DLTS peak with different durations of the refilling pulse, then plotting the peak amplitude versus pulse duration. This method can only be used within a limited temperature range where the emission rate is not too small so that a DLTS peak is obtained in a reasonable time.

At lower temperatures, the capture rate may be obtained by the static method, provided that the deep level under study is the only one present—which has been shown above to be the case for our samples, Fig. 3—and provided that the trap concentration is sufficient so that the corresponding ΔC is well above the noise level. In the static measurement, one empties the trap by heating the sample under reverse bias, then one cools it down to the desired temperature; when this is reached a succession of refilling pulses of equal duration is applied and a capacitance reading is taken after each pulse.

Irrespective of the measuring method, if $N_t \ll n$ one expects the capacitance variations to follow an exponential dependence on refilling time. We have found, however, that the variations we observed were more complex, even in the case of pure GaAs as shown in Fig. 9. The reason for this behavior is not clear. We indicate in Fig. 9 that the experimental curves can be described as sums of two pure exponentials with approximately equal amplitudes. This of course suggests the successive capture of two electrons. Although this hypothesis should not be ignored, for the needs of the present study we have decided to circumvent the difficulty simply by taking, as a measure of the refilling time constant, the duration

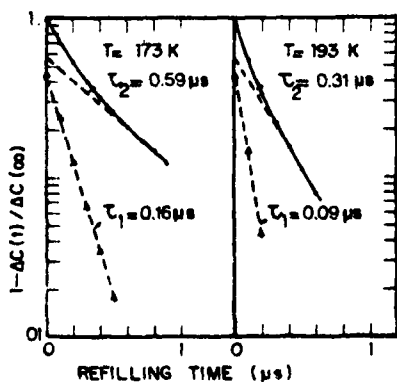


FIG. 9. Illustrating the nonexponential character of trap refilling in GaAs sample.

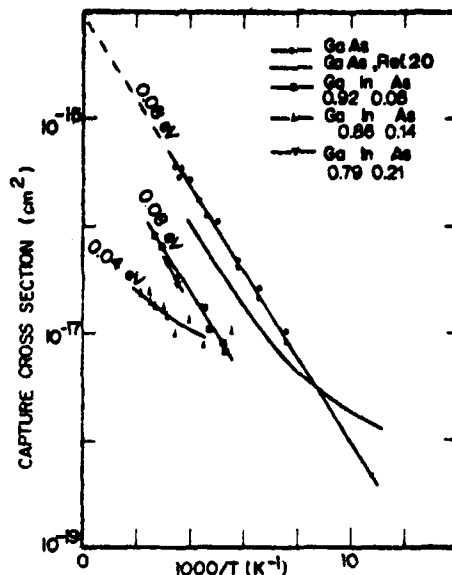


FIG. 10. Capture cross section vs inverse temperature for electron trap A in $\text{Ga}_{1-x}\text{In}_x\text{As}$.

necessary for reducing the capacitance variation to $1/e$ of its initial value. The reasons for this are: (i) the ratio between the two time constants in Fig. 9 is not very large; (ii) this ratio does not seem to vary with temperature; (iii) as shown above, the emptying process is strictly exponential, at least in pure GaAs, tending to discourage the idea of a two electron trap. We have been able to obtain capture cross-sections σ_n for GaAs and for three alloy compositions—samples #51, 55, and 62 of Table I. When calculating σ_n from the capture rates, we have neglected the weak variation of electron effective mass versus x , using in all cases the same expression of the thermal velocity v_{th}

$$v_{th}(\text{cm/s}) = 2.6 \times 10^6 T^{1/2}(\text{K}). \quad (2)$$

The $\sigma_n(T)$ results are gathered in Fig. 10. For comparison, we have reproduced in this same figure the curve found by Lang and Henry²⁰ for GaAs. In view of the above discussed difficulties, the agreement seems satisfactory. In particular, the slope (activation energy E_b) of 0.08 eV is the same for the two series of experiments on GaAs.

The change induced in the capture cross sections by the increase of indium fraction x is remarkable. Up to $x = 0.14$, σ_n decreases by a large factor. For the sample with $x = 0.077$, the activation energy E_b is still essentially the same as in GaAs, but for the sample $x = 0.14$ it has decreased significantly, so that the two curves cross at low temperatures. Finally the (unfortunately very limited) data that

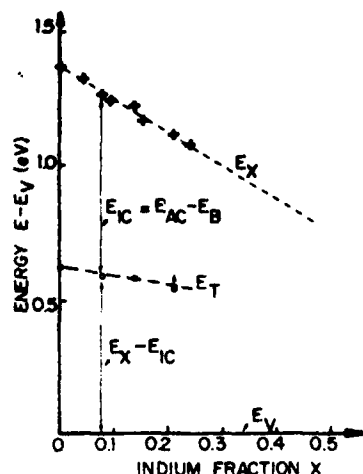


FIG. 11. Dependence on Indium fraction x of the bottom of the conduction band E_C and of the deep level E_T for electron trap A. Reference is top of the valence band.

we have been able to get for $x = 0.21$ seem to indicate that σ_n increases again, but this point may need further verification.

C. Ionization energies

From the above data on emission activation energy E_{AC} , Fig. 8, and capture cross-section activation energy E_B , Fig. 10, we calculate the ionization energy E_{IC} of deep electron trap A as a function of indium fraction x , according to Eq. (1). The result is presented graphically in Fig. 11, where we plot both the band gap E_x (as from Table I) and $E_x - E_{IC}$ vs x . As suggested by the arrow pointing upwards, the point at $x = 0.21$ is probably an inferior limit, since E_B could not be reliably estimated in this case, so that we have simply taken $E_{IC} \approx E_{AC}$.

The simplest smooth-curve approximations to the data, both for the conduction band and the deep level, are straight lines. From $x = 0$ to $x = 0.20$, the band gap varies by 18%, while $E_x - E_T$ varies by only 9%; that is to say, as x increases the deep level tends to come nearer to the conduction band.

This completes the description of experimental work. In Sec. IV, the results will be compared with theoretical predictions.

IV. CALCULATIONS OF DEEP-LEVEL STATES

A. Energy level of oxygen in GaAs

In previously reported²¹ deep-level calculations, we have found an ionization energy of 0.78 eV for GaAs:O, in good agreement with the experimental data discussed in Sec. II above. Clearly the re-

sults reported here for $Ga_{1-x}In_xAs$ give us an opportunity to put the above hypothesis to a test; if the close agreement between the activation energy for trap A and the calculation for GaAs:O is not mere coincidence, then a similar agreement must exist in $Ga_{1-x}In_xAs$. Although this calculation cannot prove that trap A is due to oxygen (or any other chemical impurity), a disagreement between the calculated and observed activation energies in $Ga_{1-x}In_xAs$ might be a strong indication that the trap is not simple substitutional donor oxygen.

The details of pseudopotential calculations of impurity levels associated with deep traps in GaP and GaAs have been described in our previous publications^{21,22} and will not be repeated here. The essence of the method consists of writing the impurity wave function ψ as an expansion in terms of the unperturbed Bloch functions of the host crystal, $\delta_{n\mathbf{k}}\xi$. Here n , \mathbf{k} indicate the band and reduced wave vector, respectively. The one-electron Schrödinger equation, i.e.,

$$(H_0 + h)\psi = \epsilon\psi \quad (3)$$

with

$$\psi = \sum_{n,\mathbf{k}} A_{n,\mathbf{k}} \delta_{n,\mathbf{k}} \xi \quad (4)$$

is then solved numerically. The functions $\delta_{n,\mathbf{k}}\xi$ are obtained from a local empirical pseudopotential band-structure calculation.²³ Here h is the impurity pseudopotential which in this particular case is just the difference between the self-consistent (screened) pseudopotentials of oxygen and arsenic. The expansion in (4) requires ten bands and several thousand sampling points in the reduced zone to converge.

When we come to consider oxygen in $Ga_{1-x}In_xAs$

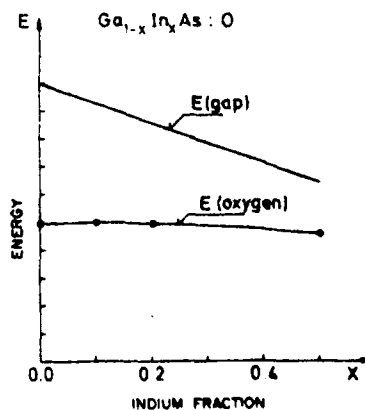


FIG. 12. Calculated ground-state energy of a single donor oxygen in $Ga_{1-x}In_xAs$. The position in the direct gap is shown.

68

for $x \neq 0$, we maintain our sampling procedure and the potential \hbar unchanged. The band-structure parameters, i.e., the functions $\delta_{n,i}$ and energies $E_{n,i}$ are obtained as before, i.e., by solving

$$H_0 \delta_{n,i} = E_{n,i} \delta_{n,i}. \quad (5)$$

The crystal potential H_0 for the alloy is set up according to the virtual-crystal approximation. This involves simple linear interpolation of the lattice constant and the pseudopotential form factors between GaAs and InAs values. The calculations were performed for $x = 0.0, 0.1, 0.2$, and 0.5 and the results are shown in Fig. 12. This figure shows both the calculated direct band gap and the impurity-ground-state energy as a function of the indium concentration x .

B. Comparison of theory with experiment

Comparison of the calculated (Fig. 12) activation energies with the experimental ones in Fig. 11 is not favorable enough and can hardly support our hypothesis that the trap is O donor at the As site. We must now closely examine our results in the light of all existing experimental information, for there may be evidence which might contradict our conclusions about the activation energy or some consequences of such a conclusion. However, before we do so we must critically assess the calculation itself.

As we have pointed out earlier,²¹ the absolute position of an impurity level in the forbidden band gap is very difficult to calculate accurately. This is because the impurity-ground-state energy arises as a result of cancellations which take place when contributions coming from different parts of the wave-vector space are added up. Convergence properties of such a system are difficult and tedious to study. Furthermore, our calculation is not self-consistent in the usual sense and the reliability of the potential \hbar depends to some extent on the validity of linear screening approximation. The close agreement of our theory with experiment as far as GaP:O is concerned must be at least to some degree fortuitous. In GaAs, the precision with which we can position a deep donor level can only be lower. The density of states near Γ_1 (conduction band) is very low and our sampling procedure does not really represent this part of the band structure very well. Fortunately, the ground-state wave function spreads over a large area in k space²¹ and such parts as Γ_1 affect the ground state only very little. Positions of deep levels in the gap merely reflect a change in those parts of the band structure where the density of states is high. This argument which is not difficult to accept on intuitive grounds, has been well supported

by all our calculations. Finally, the details of the band structure are not well described by the local empirical pseudopotential employed here. For instance, some very recent experiments²⁴ show that the secondary conduction-band minimum at X_1 is above that at L_1 (0.475 and 0.285 eV above the bottom of the conduction band of GaAs, respectively). Since we really calculated the impurity energy with respect to the lowest conduction-band valley with large density of states more accurately than with respect to Γ_1 , all impurity energies shown in Fig. 12 should be reduced by about 50 meV. We do not believe that such corrections are of importance here since (a) they only represent a systematic error, and (b) this error is smaller than the expected (systematic) error due to sampling and impurity potential which amounts to at least ± 0.1 eV.

We shall now concern ourselves with the relative changes in the ground-state energy. In Fig. 13, we can see the changes in the positions of the secondary minima at X_1 and L_1 as a function of x . A glance at Figs. 12 and 13 shows that—as expected— E (oxygen) does not follow the band edge but seems to “follow” the valence band. What really happens is that this level which is primarily associated with the conduction band²¹ simply is not very sensitive to the low density of states area near Γ_1 .

Of course, as x increases, the interaction with the Γ_1 valley should slowly increase in importance since Γ_1 comes closer to the level in the gap.

There is some uncertainty as far as the positions of X_1 and L_1 with respect to Γ_1 in InAs are concerned. Obviously, the relative change in the position of the deep level with x does depend on the change at X_1 and L_1 . Hence, our predictions concerning the relative change in E (oxygen) also contain some uncertainty. However, the main result of our calculation, namely, that E (oxygen) does not follow either X_1 , L_1 , or Γ_1 and that $E_{\nu} - E$ (oxygen) \approx (const) for $x = 0.0-0.2$ (i.e., the range in which the experiment was performed), can hardly be altered by the above consideration significantly enough to render comparison with the experiment impossible. On the other hand, it may be argued

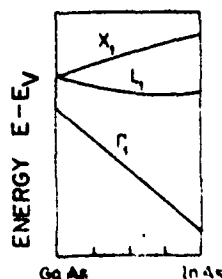


FIG. 13. Position of the conduction-band minima with respect to the top of the valence band in $Ga_{1-x}In_xAs$ from a simple virtual-crystal model employed in this calculation

that the above behavior of $E(\text{oxygen})$ is not necessarily peculiar to oxygen. All deep states of this symmetry, dominated by short-range potentials, should be expected to follow such a trend, and it may well be beyond the sensitivity of our impurity calculation to distinguish one from another if only a small range of concentrations is studied. Recent work by Lang *et al.* on $\text{Ga}_{1-x}\text{Al}_x\text{As}$ (Ref. 3) does confirm that the changes in trap energies with concentration x may indeed be small compared to the magnitude of the change of the direct gap. However, they also found that some levels of different depth exhibited a very similar change with alloy concentration.

In our calculation, we represent the crystal potential by an average potential obtained from a linear interpolation procedure. The samples used in the present experiment do not show any bowing in the band gap versus indium fraction variation. It has been pointed out²⁵ that in a high-quality $\text{Ga}_{1-x}\text{In}_x\text{As}$ alloy, the bowing should indeed be negligible. The observed direct gap agrees well with the values calculated with our simple virtual-crystal model. Although this does not necessarily mean that there is no local disorder in the impurity cell, our calculations ignore any such correction. If the center is really the simple oxygen donor then such a correction should not be very important. Our studies²¹ on the substitutional single donor oxygen in GaP certainly indicated that the ground state is s -like and insensitive to small asymmetric fields. An axial complex, on the other hand, may respond sharply²⁶ to small changes in the local environment which may be a function of the concentration x . Since several of the deep traps observed by Lang *et al.*³ do not follow the trend predicted by our calculation for a symmetric center, our result might be taken as an indication that those centers are of lower symmetry.

As concerns our trap A, the observed variation in the impurity energy $E \equiv E(x)$ with respect to the valence band, is too fast to be consistent with our simple model (i.e., substitutional single donor oxygen), as can be seen from Figs. 11 and 12.

C. Discussion of the photoionization data

The photoionization spectrum of O-doped GaAs was shown in Fig. 1, and in Sec. II above, we argued that only the threshold in the middle of the gap, i.e., electron trap A, should be related to oxygen, the upturn above 1 eV being mainly a contribution from another level, with possibly some contribution due to the rise in the density of states in the GaAs conduction band²⁷ (Fig. 14). It is unfortunate that the presence of the second level masks this last contribution, since the exact

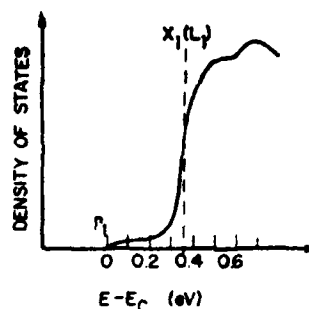


FIG. 14. Rough graph indicating the density of states near the bottom of the conduction band of GaAs.

knowledge of this part of the "oxygen" spectrum would greatly help the comparison with theory.

At this point a comment on the problem of interpretation of this kind of data may be in order. It is remarkable that in spite of great importance generally attached to experimental information concerning optical cross sections for deep levels, the theoretical aspects of the problem have been largely neglected. Nevertheless, it has been shown²⁷ that simple extensions²⁸ of the well-known effective-mass theory do not apply in many cases. The experimental work of White *et al.*²⁹ confirms these theoretical considerations. In brief, there are at least three important points that must be taken into consideration:

- (i) The wave function spreads over a large area in the wave-vector space and the optical matrix elements are significantly altered, if this fact is taken into account.
- (ii) The details of such a process are particularly important in direct-gap materials where not only the position of the maximum of the frequency-dependent cross section, but also its shape near the threshold are affected.²⁷ Because of the low density of states at the conduction-band edge, the true threshold of the cross section associated with a particular level may be obscured by a combination of the above-mentioned effects and temperature-dependent phonon broadening.
- (iii) Finally, one may expect a Franck-Condon shift of the order of 0.1 eV.

Our calculations showed that oxygen donor in GaAs is basically of similar nature as that in GaP. It is borne in mind that if such a center really exists, then it is capable of binding two electrons as well as its analog as in GaP.²¹ We did not carry out a full-length analysis of the two-electron problem in GaAs, as we had done for GaP, and are not able to offer a numerical result for the Franck-Condon shift and the equilibrium energy of the two-electron state. However, as far as calculations are concerned, the degree of similarity between

GaP:O and GaAs:O is so great that a rough prediction can be made without going through the tedious and imperfect process of the numerical procedure. Thus for GaAs:O we might expect $E_2^0 \sim 0.6$ and $E_2^1 \sim 1.0$ eV (E_2^0 and E_2^1 are energies per electron in the two-electron state before and after the lattice relaxation takes place, respectively). The presence of a two-electron state may affect the observed optical spectra and it would be worth investigating whether the above mentioned two-electron state exists in $\text{Ga}_{1-x}\text{In}_x\text{As}$.

D. Discussion of the electron-capture cross sections in $\text{Ga}_{1-x}\text{In}_x\text{As}$

In Sec. III, we described our results concerning the electron-capture cross sections and their temperature dependence in $\text{Ga}_{1-x}\text{In}_x\text{As}$. The main features of the temperature dependence of the cross section can be understood²⁰ with the help of a simple diagram in Fig. 15. The temperature dependence is dominated by an exponential factor $\exp(-E_B/kT)$. In GaAs, E_B for the level A is 80 meV. The exponential dependence is clearly seen in both Lang's and our data. In the alloy, the exponential behavior persists over a similar range of temperatures (Fig. 10). However, the barrier energy E_B changes when x is larger than 0.10. Hence, there are two important questions to ask: (i) How do we explain this variation of E_B vs. x ? (ii) Is it consistent with our hypothesis about the origin of the trap? However, the very fact that this capture mechanism is so important in $\text{Ga}_{1-x}\text{In}_x\text{As}$ raises a question. The properties of the single donor oxygen in GaP have been studied experimentally by many authors. Yet we do not know of any report suggesting that the nonradiative capture mechanism—which is characterized by the exponential temperature dependence—is important for GaP:O. Only when a second electron is captured at that center do we observe the above-mentioned behavior. Why should a single donor oxygen in GaAs be so different from that in GaP? The impurity potentials, the wave functions, and the acti-

vation energies are very similar. The symmetry is the same in both cases. In brief, we can see no simple reason why a single donor oxygen in GaAs should exhibit the observed capture cross section. Of course, in the absence of a truly quantitative description of the nonradiative capture mechanism which would relate the values of E_B to the band structure and impurity parameters, no definite conclusion can be made about the plausibility of our hypothesis. We feel, however, that the above contradiction perhaps gives the strongest hint that the trap A is of more complex nature.

Clearly the variation of E_B with x can only be explained in terms of the simple model pictured in Fig. 15 if we assume that the force constants in the impurity cell change with x . In view of the magnitude of the change in E_B , such a correction might be significant enough to affect the impurity energy not only via the band structure, but also via the impurity potential itself. It would also be interesting to know whether the results obtained in this study are peculiar to trap "A" or whether the barrier changes in a similar way for other deep traps, since it may well be that E_B is very sensitive to a small change in the force constants. The change in E_B with x —if E_B is indeed due to the same trap for all concentrations—amplifies our earlier conclusion that the trap A may possess lower symmetry.

V. SUMMARY

Transient-capacitance spectroscopy was applied to the study of the main electron trap A in vapor-phase epitaxial $\text{Ga}_{1-x}\text{In}_x\text{As}$ alloys with $0 < x < 0.21$. Emission rate versus temperature and electron-capture cross section versus temperature data were obtained as a function of x . From these results, the ionization energy $E_c - E_t$ was determined as a function of x .

The experimental evidence relating this electron trap to the presence of oxygen was discussed, and new photoconductivity data taken directly on GaAs vapor-phase epitaxial layers with the substrate removed were presented to show the identity between this trap and the deep level observed in oxygen-doped bulk-grown material.

Theoretical calculations using the pseudopotential method were performed concerning the energy level of oxygen, substitutional on As site, in GaInAs alloys. Due to a combination of contributions from the Γ and the L (or X) minima in the conduction band, which vary in a different way as a function of x , the deep level tends to remain at a more or less constant energy difference with respect to E_V . This conclusion is not in good quantitative agreement with the experimental results. How-

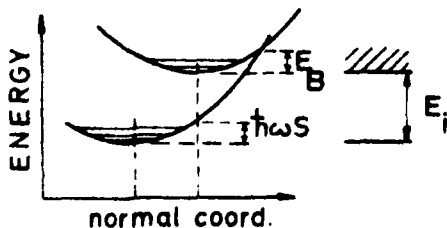


FIG. 15. Configuration coordinate diagram illustrating a capture process of a carrier from the conduction band into a deep level of energy E_t . S is the Franck-Condon shift expressed in units of lattice vibration.

71

ever, this argument alone does not allow to reject the hypothesis that the trap A is due to substitutional donor oxygen.

The experimental electron-capture cross sections in $GaInAs$ show an exponential variation with inverse temperature, typical for the multiphonon emission capture mechanism. The cross sections decrease in magnitude as x increases, at least up to $x=0.15$, and a variation of the activation energy E_a is also observed above $x=0.10$. These rather remarkable results are discussed from the theoretical point of view; it is pointed out that, at least at the present state of knowledge, the multiphonon emission mechanism should *not* apply to single donor oxygen. Moreover, since the s -like wave function associated with the ground state of

this defect should not be sensitive to small changes in the local environment due to alloying, the activation energy should not vary with composition as observed in our experiments. Therefore, we must conclude that the existing experimental evidence concerning this trap does not support the hypothesis that the trap is substitutional single donor oxygen.

ACKNOWLEDGMENTS

We are grateful to C. Schemali and C. Schiller for their hearty collaboration to this study; also to G. M. Martin, D. Bois, A. T. Vink, L. Hollan, A. M. White, J. Vannimenus, and D. V. Lang for interesting discussions.

- ¹T. Ikoma, M. Takikawa, and T. Okumura, in Proceedings of the 1976 International Conference on Solid State Devices, Tokyo, 1976 (unpublished).
- ²D. V. Lang, in Proceedings of the International Conference on Radiation Effects in Semiconductors, Dubrovnik, 1976 (unpublished).
- ³D. V. Lang, R. A. Logan, and L. C. Kimerling, Proceedings of the International Conference on the Physics of Semiconductors, Rome, 1976 (unpublished).
- ⁴A. Majerfeld (private communication).
- ⁵A. Mircea and A. Mitonneau, *Appl. Phys.* **8**, 15 (1975); A. Mircea, A. Mitonneau, L. Hollan, and A. Briere, *ibid.* **11**, 153 (1976).
- ⁶D. V. Lang and R. A. Logan, *J. Electron. Mater.* **4**, 1053 (1975).
- ⁷N. M. Kolehanova, G. N. Talulaklin, and E. A. Kretova, *Sov. Phys. Semicond.* **3**, 174 (1970).
- ⁸M. Bleicher and E. Lange, *Solid State Electron.* **16**, 375 (1973).
- ⁹H. G. Grimmeiss and L. A. Ludebo, *J. Appl. Phys.* **46**, 2135 (1975).
- ¹⁰G. P. Peka, L. G. Shepel, and L. Z. Mirets, *Sov. Phys.-Semicond.* **7**, 1439 (1974).
- ¹¹A. Mitonneau and A. Mircea, Laboratoires d'Electronique et de Physique Appliquée, Internal Report No. J607, 1974 (unpublished).
- ¹²A. Mitonneau, G. M. Martin, and A. Mircea, *Proceedings of the Conference on GaAs Related Compounds*, Edinburgh, 1976 (The Institute of Physics, Bristol, 1977), Vol. 33a, p. 73.
- ¹³D. Bois and M. Boulou, *Phys. Status Solidi A* **22**, 671 (1974).
- ¹⁴K. Sakai and T. Ikoma, *Appl. Phys.* **5**, 165 (1974).
- ¹⁵A. Humbert, L. Hollan, and D. Bois, *Appl. Phys.* **9**, 117 (1976).
- ¹⁶M. C. Boissy, D. Diquet, C. Schemali, and J. Hallais, in Ref. 12.
- ¹⁷J. S. Escher and B. F. Williams, *J. Appl. Phys.* **44**, 525 (1973).
- ¹⁸A. Mitonneau, *Philips Res. Rep.* **31**, 244 (1976).
- ¹⁹D. V. Lang, *J. Appl. Phys.* **45**, 3023 (1974).
- ²⁰D. V. Lang and C. H. Henry, *Phys. Rev. Lett.* **35**, 1525 (1975).
- ²¹M. Jaros, *J. Phys. C* **8**, 2455 (1975).
- ²²M. Jaros and S. Brand, *Phys. Rev. B* **14**, 4496 (1976).
- ²³M. L. Cohen and T. K. Bergstresser, *Phys. Rev.* **141**, 749 (1966).
- ²⁴D. E. Aspnes, C. G. Olson, and D. W. Lynch, *Phys. Rev. Lett.* **37**, 766 (1976).
- ²⁵B. J. Baliga, R. Bhas, and S. K. Ghandi, *J. Appl. Phys.* **46**, 4608 (1975).
- ²⁶M. Jaros and S. Brand, in Proceedings of the International Conference on the Physics of Semiconductors, Rome, 1976 (unpublished).
- ²⁷M. Jaros, *J. Phys. C* **8**, L264 (1975).
- ²⁸G. Lucovsky, *Solid State Commun.* **3**, 299 (1965).
- ²⁹A. M. White, P. J. Dean, and P. Porteous, *J. Appl. Phys.* **47**, 3230 (1976).
- ³⁰A. L. Lin, E. Omel'yanovskii, and R. H. Bube, *J. Appl. Phys.* **47**, 1852 (1976).

reprint from *Radiation Effects in Semiconductors 1976*
 Eds.: N.B. Urli and J.W. Corbett
 Inst. Phys. Conf. Ser. No. 31 (1977)

512 *Poster papers*

Optical modulation study of proton-bombarded GaAs[†]

Moshe Oren[‡], A R Quinton and Claude M Penchina

Department of Physics and Astronomy, University of Massachusetts, Amherst,
 Massachusetts 01002, USA

Transverse electroreflectance (ER), transverse electroabsorption (EA), and transmittance (τ) measurements were used to study the effect of proton bombardment on semi-insulating, Cr-doped bulk single-crystal GaAs. The samples were bombarded with 150 KeV protons, and water cooled during bombardment. Measurements were made at liquid-nitrogen temperature. The main experimental results are summarized as follows.

All signals decrease with increasing proton dose, including ER, EA and τ near the fundamental absorption edge E_0 , as well as ER at the E_1 critical point. Of these, ER at the E_0 critical point decreases most rapidly; the decrease is nearly linear in the logarithm of the proton dose between 10^{14} and 10^{16} protons/cm², with the signal falling below the detection limit ($\Delta R/R \sim 10^{-5}$) for doses above 2.5×10^{16} protons/cm².

The optical absorption coefficient near E_0 increases sublinearly with dose, levelling off for doses above 10^{16} protons/cm².

Broadening is evident for ER at E_0 and E_1 , but not sufficient to account for the decrease in peak-to-peak signal strength. The EA signal decreases least in amplitude, and develops a tail on the low-energy side.

[†] Supported in part by the National Science Foundation, The Office of Naval Research, and a Faculty Research Grant from the University of Massachusetts.

[‡] Present address: Simulation Physics Inc, Patriots Park, P.O. Box D, Bedford, Massachusetts 01730, USA

Poster papers

513

All electromodulation spectra shift in energy as a result of bombardment. At a dose of 5×10^{15} protons/cm², the EA and ER lines at E_0 shift to higher energies by about 4 meV, while the main ER peak at E_1 , on the other hand, shifts about 1.5 meV to lower energy.

Annealing at 300°C for up to 2 h only partially recovers the unbombarded spectra. The recovery rate decreases with annealing time.

The ER and EA spectral lines are associated with critical points in the band structure, which in turn are a manifestation of the long-range order in the crystal. The decrease of electromodulation signals upon successive bombardment would therefore indicate a decrease in the long-range order until total amorphization is achieved, when the ER and EA signals completely vanish at a dose of about 10^{17} protons/cm². The tail in the EA spectrum caused by bombardment suggests the creation of a tail in the joint density of states of the conduction and valence bands.

Effect of Proton Damage on Optical Modulation Spectra of Gallium Arsenide

Moshe Oren,¹ A. R. Quinton, and Claude M. Penchina

Department of Physics and Astronomy, University of Massachusetts, Amherst, Massachusetts 01003

ABSTRACT

We studied the effect of proton bombardment on the electroreflectance (ER), electroabsorption (EA), and transmission (T) spectra of high resistivity Cr-doped single crystal GaAs. The high resolution of ER and EA and their sensitivity to crystalline order make it possible to study shift, broadening, and gradual distortion of the spectral peaks as disorder increases with successive irradiations. The sample is bombarded with 150 keV protons. We have measured ER and EA at the absorption edge E_0 , ER at the E_1 critical point, and d-c optical absorption. All these measurements are sensitive to proton irradiation of the sample; the most sensitive one is ER at E_0 . In the range of 3×10^{14} to 5×10^{15} protons/cm², optical absorption just below the energy gap increases sublinearly with proton dose; the peak-to-peak amplitudes of ER at E_0 and E_1 vary linearly with the logarithm of the dose and hence can be used to measure the degree of damage in the sample. The EA signal at E_0 develops a tail toward the low energy side of the spectrum. The ER at E_0 has a peak shift of ~ 4 meV to higher energy while the peak of the ER signal at E_1 shifts by about 15 meV to lower energy. Broadening is evident in the ER signals at E_0 and E_1 . Annealing at 300°C for up to 2 hr only partially recovers the unbombarded state. A model based on the gradual amorphization of the sample by an increasing number of proton damaged, amorphous islands with well-defined boundaries can partially explain the experimental results.

Lattice damage in single crystals plays a major role in device applications. Lattice damage caused by ion implantation received special attention in recent years following the introduction of ion implantation as a method for doping semiconductor materials. There are several experimental techniques that can be applied to study radiation damage in semiconductors, among others: optical (1), electrical (2), Rutherford back scattering (3), and electron paramagnetic resonance (4).

The optical absorption and reflection of GaAs were found to be sensitive to ion bombardment damage but the sensitivity of such measurements (reflectivity in particular) is low, and quantitative results are difficult to obtain.

In the present work we use electromodulation (EM) spectroscopy to study the effect of proton bombardment on single crystal, semi-insulating GaAs. In electromodulation one measures the change in reflectance (ΔR) or transmittance (ΔT) when an external electric field is applied to the sample (5). The EM response is spectrally concentrated around the critical points in the band structure. A phase sensitive detection system tuned to the frequency and phase of the external field greatly enhances the sensitivity of the measurement to critical points in the spectrum. These critical points are a manifestation of the long range order in the crystal; a change in the EM signal on successive bombard-

ment would indicate, therefore, the gradual relaxation in this long range order. This relation allows a semi-quantitative measure of lattice damage to be made.

EM has been applied to date primarily to problems of intrinsic band-structure analysis (5), but as a powerful spectroscopic method it is now finding new areas of applications. Jonath et al. (6) studied electroabsorption (EA) of oxygen impurities in GaAs. Bauer (7) used EA to study the symmetry properties of defect states in nitrogen-doped GaP and their interaction with the host band structure. Gavrilenko et al. studied the influence of low energy argon ion bombardment on the electroreflectance (ER) and photoluminescence spectra of n-type $\text{Al}_x\text{Ga}_{1-x}\text{As}$ solid solution (8) and Si (9). Anderson et al. (10) used ER to detect shallow impurity levels in GaAs doped with Si, Te, Zn, or Cd impurities. A disadvantage of this method is that different types of lattice damage cannot be distinguished.

Experimental

High resistivity, n-type GaAs:Cr single crystal was used in this experiment. The sample had $\sim 10^9$ Ω -cm room temperature resistivity. For radiation damage experiments it is preferable to have the sample front surface free of any evaporated electrode or insulating layer. For that reason, the sample geometry used in the ER and the EA measurements is based on the transverse configuration (11). Slices were cut from the GaAs crystal, lapped, polished with 0.3 μ alumina powder, and then etch polished with Monsanto Syton solution. For contacts, two Au films were evaporated on the

¹ Present address: Spire Corporation, Bedford, Massachusetts 01730.

Key words: electroreflectance, electroabsorption, GaAs:Cr, amorphous GaAs, ion implantation.

polished sample surface forming a gap 1 mm wide (see insert in Fig. 1). The current voltage characteristics up to 900V show good ohmic behavior. The light beam was incident in the [111] crystal direction. The magnitude of the ER signal is a function of surface potential. Therefore, it varies from sample to sample due to slight changes in surface preparation, which may alter considerably the surface potential. To avoid this complexity, only half of the gap between the field electrodes was bombarded and the other half was used as a reference for all successive measurements. The gap height is more than twice the height of the incident light beam in order that the light will not overlap the bombarded and nonbombarded regions.

The system used for the ER and EA measurement is shown in Fig. 1. It includes the following components: 250W tungsten halogen lamp, monochromator, optics, dewars, and detectors. All measurements were made at LN₂ temperature. Two photomultipliers (PM) were permanently mounted in the sample chamber, 1P28 PM to measure ER at E₁ critical point and 7102 PM for ER at the E₀ critical point. A removable front surface aluminum mirror directs the reflected beam into the PM in use. A PbS detector was used for the EA and transmission measurements. The two PM's were wired such that higher voltage was impressed between the last dynode and the anode than on the intermediate stage of the voltage divider. This allows greater linear swing of the anode voltage, which is desirable when a small a-c signal, superimposed on a large d-c signal, is to be measured. The voltage applied to the sample was 1 kHz, 2000V peak-to-peak sine wave superimposed on 1000V d-c. For the ER measurement a d-c photon flux was used, a lock-in amplifier measured the a-c signal (I₀ · ΔR) and an electrometer measured the d-c reflection (I₀ · R). For the transmission (T) and EA measurements the incident light beam was chopped at 147 Hz; two lock-in amplifiers tuned at 1 kHz and 147 Hz measured the ΔT and T signal, respectively.

Sample bombardment was done with a 150 keV proton beam. The sample was mounted on a water-cooled holder. An in-line cold trap was used to remove oil vapor that may otherwise be carried along with the proton beam to contaminate the sample surface. In addition when a high dose was used (≥ 5 × 10¹⁵ p/cm²), a thin carbon film (~ 20 μm) was inserted in front of the sample, to further prevent possible oil contamination.

Isothermal annealing of the sample was done at 300°C in an oil-free vacuum system (~ 5 × 10⁻⁷ Torr).

Results

Transmission.—The sample transmission in the range of the fundamental absorption edge was measured at LN₂ temperature for various bombardment doses. In order to determine more conveniently the effect of proton damage on the sample transmission, the ratio of the transmitted intensity from the bombarded (T_b)

and nonbombarded (T₀) regions was determined at one wavelength. Such a graph is shown in Fig. 2 (insert). Taking into account reflection losses, R, from the sample front and back surfaces, one can write

$$T_0 = (1 - R)^2 \exp(-\alpha_0 d_0) \quad [1]$$

α_0 and d_0 are the sample absorption coefficient and thickness, respectively (multiple internal reflections are neglected). The transmission through the bombarded region is

$$T_b = (1 - R') (1 - R) \exp(-\alpha_b d_b - \alpha_0 d_0) \quad [2]$$

where R' is the reflectivity coefficient from the front surface of the bombarded region, α_b is the average value of the change in absorption coefficient over the bombarded layer thickness d_b . Measurement of I₀ · R (when R is the reflectivity and I₀ is the incident intensity) in the vicinity of the absorption edge shows a change of less than 5% due to proton bombardment. Similarly, Kalma (12) found no change in reflectivity in the vicinity of the absorption edge of GaAs following a 1 MeV electron irradiation; Sell and MacRae (1b), found a change of ~ 3% in reflectivity at 2.5 eV in argon-implanted GaAs. We assume therefore R ~ R'. Then

$$\ln(T_0/T_b) = \alpha_b d_b \quad [3]$$

α_b can be related to the number, N, of the optically active defects produced in the bombarded layer (13)

$$\alpha_b = N \sigma_b \quad [4]$$

where σ_b is the cross section for optical absorption by these defects. The best straight line fit to the data in the log-log plot of Fig. 2 (insert) provides the relation

$$T_0/T_b = \gamma \phi^\beta \quad [3a]$$

with $\ln \gamma = -16.9$ and $\beta = 0.48$. Therefore, from Eq. [3], [3a], and [4]

$$d_b N \sigma_b = d_0 \alpha_0 = \ln \gamma + \beta \ln \phi \quad [5]$$

The production rate of defects is sublinear in dose. This is due to damaged regions overlapping and possible room temperature annealing (14, 15).

If we approximate the damaged layer thickness, d_b , by the projected range (16) (~ 1.5 μ) of the proton beam, the wavelength dependence of the added absorption due to bombardment can be expressed using Eq. [3]. Such a graph is presented in Fig. 2. The featureless increase in absorption indicates that the bombardment generates a continuous distribution of energy levels right below the bandgap with no evidence of discrete levels in this range. Kalma (12) studied electron irradiated GaAs, Si, Ge, InSb, and PbTe and

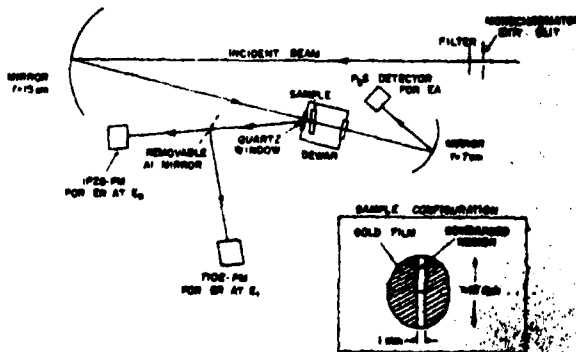


Fig. 1. Optical system used for the ER and EA measurements

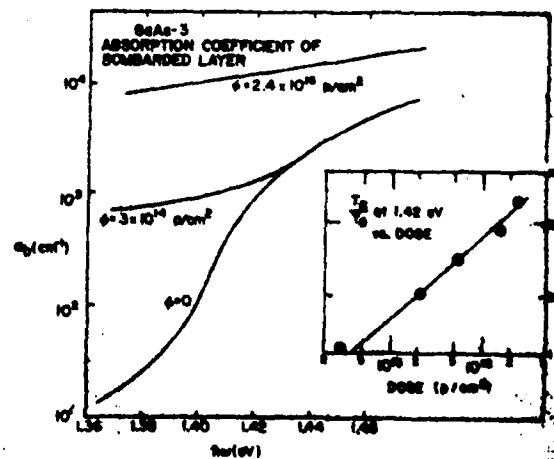


Fig. 2. Absorption coefficient of bombarded and non-bombarded regions.

suggested that increased absorption near the bandedge observed in GaAs can be attributed to tailing of the density of states into the bandgap. Note that the range of α_0 ($\sim 10^4 \text{ cm}^{-1}$) is about two orders of magnitude higher than the absorption coefficient observed in neutron damaged GaAs (17).

Theoretical Model

A simple picture of gradual amorphization of the sample by the incident radiation was used by a number of workers (3, 18) to describe the process in which long-range order in the bombarded layer is destroyed. In such a picture each incident proton produces a highly disordered region along its track in the sample. Assuming these regions have well-defined boundaries, at low dose they are separated from each other except for random overlapping. As the dose increases the overlapping increases until a completely amorphous layer is formed. The added absorption coefficient in this picture will be due to the introduction of amorphous islands with higher absorption

$$\alpha_b = \frac{A}{A_0} (\alpha_a - \alpha_0) \quad [6]$$

where A is the area of the amorphous regions, A_0 is the total sample area exposed to the beam, and subscripts a, b, and c correspond to amorphous, bombarded, and crystalline, respectively.

Based on this description we can define a quantity $\sigma(\phi)$ which is the cross section for added amorphization per proton which hits a previously undamaged area. The probability that an additional incident proton will not hit the amorphous region A is $1 - (A/A_0)$. In terms of this cross section, the change in A per incident proton, dA/dP will be therefore

$$\frac{dA}{dP} = \frac{A}{A_0} \frac{dA}{d\phi} = \left(1 - \frac{A}{A_0}\right) \sigma(\phi) \quad [7]$$

and after integration

$$1 - \frac{A}{A_0} = \exp[-\int \sigma(\phi) d\phi] \quad [7a]$$

Using Eq. [6] and [7a]

$$\exp[-\int \sigma(\phi) d\phi] = 1 - \frac{A}{A_0} = 1 - \frac{\alpha_b}{\alpha_a - \alpha_0} \quad [8]$$

Using the experimental data for α_b as expressed in Eq. [5] and taking the logarithmic derivative of Eq. [8], we get

$$\sigma_{TR}(\phi) = \frac{1}{\phi(K_2 - \ln \phi)} \quad [9]$$

with

$$K_2 = \frac{d(\alpha_a - \alpha_0)}{\beta} - \frac{1}{\beta} \ln \gamma \quad [10]$$

For $h\nu = 1.42 \text{ eV}$, $\alpha_a h \gg \alpha_0$, thus α_a approximated by α_b at high dose (where $A \rightarrow A_0$)

$$\alpha_a(1.42 \text{ eV}) \approx \alpha_b(1.42 \text{ eV}, \phi = 2.4 \times 10^{16} \text{ p/cm}^2) = 1.24 \times 10^4 \text{ cm}^{-1} \quad [11]$$

this gives

$$K_2 = 38.9 \quad [10a]$$

This same picture will be applied for the ER data, and the result compared with the results above.

ER at E_0 and E_1 Critical Points

Figure 3 shows the ER at the absorption edge E_0 , and Fig. 4 shows the ER response at the E_1 critical point. The most obvious feature of the bombarded spectrum is the reduction in signal intensity in both cases compared to the unbombarded spectrum. To better evaluate this effect, the peak-to-peak amplitude (PPA), Δ_b , of the bombarded region, normalized to the

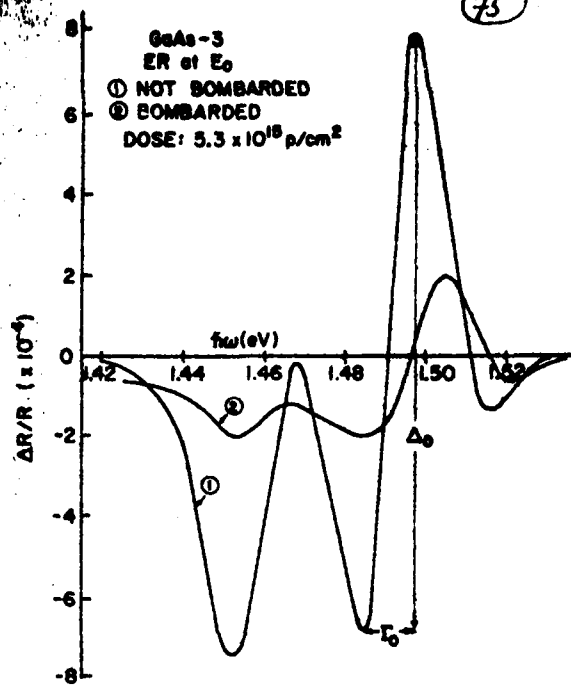


Fig. 3. ER at E_0 from the bombarded and not-bombarded regions

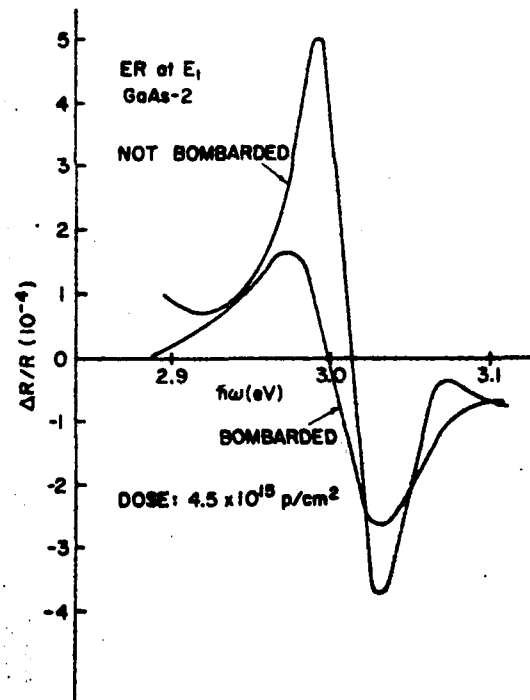


Fig. 4. ER at E_1 from the bombarded and not-bombarded regions

PPA from the nonbombarded region, Δ_0 , is plotted vs. dose in Fig. 5 for both E_0 and E_1 critical points.

It is apparent that the attenuation of Δ for a given dose is larger at E_0 than at E_1 . This can be explained qualitatively by the higher penetration depth of the light beam at E_0 . At the bandgap transition, the penetration depth of the light is of the same order as that of the proton beam range, $\sim 1.5\mu$ (19), where the induced crystalline damage is mostly concentrated. At the E_1 transition the light penetration depth is only

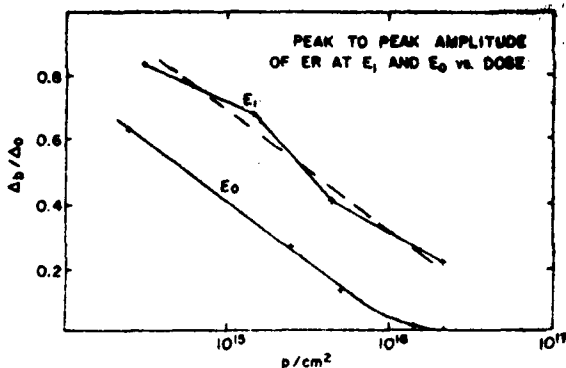


Fig. 5. Peak-to-peak amplitude (PPA) of the ER at E_1 and E_0 normalized to the PPA from the not-bombarded region.

0.017 μ (19). The ER signal at E_0 is reduced to below the detection limit ($\sim 10^{-6}$) for dose $\geq 2.4 \times 10^{16}$. This increased sensitivity of ER at E_0 to irradiation damage can be a useful tool for damage detection. The PPA will be used to give a semi-quantitative value for the amount of damage introduced into the sample, averaged over the damaged layer thickness. The ER will not distinguish, though, between the various types of damage in the sample. It is of interest to note that the linear fits of Eq. [3] to both E_0 and E_1 data are parallel, although the data at the E_1 critical point are more scattered. Between 2.5×10^{14} p/cm² and 5×10^{15} p/cm² the decrease in Δ_b/Δ_0 for E_0 is linear in the logarithm of the dose ϕ

$$\Delta_b/\Delta_0 = a \ln(\phi/\phi_0) \quad [12]$$

with: $a = -0.16$ and $\ln \phi_0 = 38.9$. For the E_1 critical point we get

$$\Delta_b/\Delta_0 = a' \ln(\phi/\phi_0') \quad [13]$$

with: $a = a' = -0.16$, $\ln \phi_0' = 38.0$.

Proton bombardment resulted in a small shift of about 15 meV toward the low energy in the ER peak at E_1 , and 4 meV shift toward higher energy in the ER peak at E_0 . A contribution to the shift at E_0 may come from the uneven attenuation of the ER peak due to strong variation in the penetration depth of the light beam near the absorption edge combined with the fact that the damaged layer peaks about 1.5 μ below the surface.

Gavrilenko et al. (9) found that bombardment of Si with 1 keV He⁺ ions causes a shift in the E_1 ER peak to higher energy; 1 keV Ar⁺ bombardment of Al₂Ga_{1-x}As solution shifts the ER peak at E_1 to lower energy (8). Figure 6 shows the increased broadening in the E_1 and E_0 ER peaks vs. bombardment dose. Here too, note the higher values obtained for E_0 compared to E_1 . Various sources can contribute to broadening of the ER signal, among others, temperature effect, local random electric field, and microstress due to defects. In our case a local electric field can be created by the proton doping of the damaged crystal.

The ER signal disappears at high dose. Based on the gradual amorphization model, the ER peak-to-peak amplitude, Δ_b , at a given dose, will be proportional to the area fraction which is still in the crystalline state

$$\Delta_b = \Delta_0 \left(1 - \frac{A}{A_0}\right) \quad [14]$$

Thus from Eq. [7a], [12], and [14]

$$\exp[-\int \sigma(\phi) d\phi] = 1 - \frac{A}{A_0} = \frac{\Delta_b}{\Delta_0} = a \ln(\phi/\phi_0) \quad [15]$$

Taking the logarithmic derivative on both sides

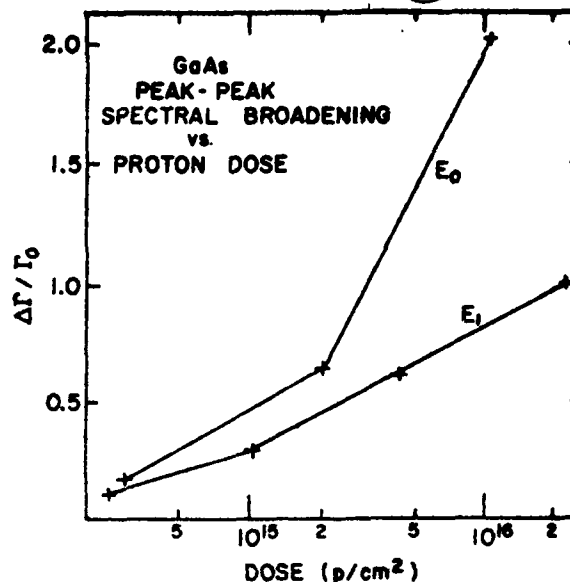


Fig. 6. Spectral broadening vs. proton dose of the ER signals at E_0 and E_1 .

$$\sigma_{ER} = \frac{1}{\phi(K_0 - \ln \phi)} \quad [16]$$

where $K_0 = \ln \phi_0$.

We previously found (Eq. [12]) that

$$K_0 = \ln \phi_0 = 38.9 \quad [17]$$

Thus, from electroreflectance at E_0 , at a dose of $\phi = 10^{15}$ p/cm² we get (Eq. [12], [16], and [17])

$$\sigma_{ER}(\phi = 10^{15} \text{ p/cm}^2) = 4 \times 10^{-16} \text{ cm}^2$$

Similarly, from transmission measurements, at this same dose we get (Eq. [9] and [10a])

$$\sigma_{TR}(\phi = 10^{15} \text{ p/cm}^2) = 2 \times 10^{-16} \text{ cm}^2$$

The relatively small discrepancy between the values obtained for σ_{ER} and σ_{TR} indicates that the simple picture used to describe the amorphization process is essentially correct in the first approximation. The result $\sigma_{ER} > \sigma_{TR}$ is to be expected because the ER is more sensitive to bombardment; partially damaged regions, neglected in the simple model, will affect the ER more than the transmission. It was suggested (20) that such partially damaged regions are caused by diffusion of defects from the outer portion of the ion track, into the undamaged bulk.

EA at the Absorption Edge E_0

The effect of proton bombardment on the band-to-band electroabsorption (EA), $\Delta T/T$, of the sample is shown in Fig. 7. Just below the bandgap, $\Delta T/T$ is negative, corresponding to a red shift of the absorption edge on application of the electric field as expected from the Franz Keldysh theory (5). Due to the high value of ad ($\sim 10^2$ - 10^3) the expected (5) oscillations in $\Delta T/T$ above the bandgap, have not been observed. Such oscillations have been seen previously by workers studying EA in thin films of GaAs (21).

The peak in the $\Delta T/T$ spectrum around 1.45 eV gradually disappears with increasing proton bombardment dose; ΔT also develops a tail toward the low energy side which is also seen in the $\Delta T/T$ spectrum below 1.45 eV. This newly created tail in the EA spectrum suggests the creation of a tail in the joint-density of states of the conduction and valence bands. This assumption is also in agreement with the results for the added absorption coefficient of the bombarded layer.

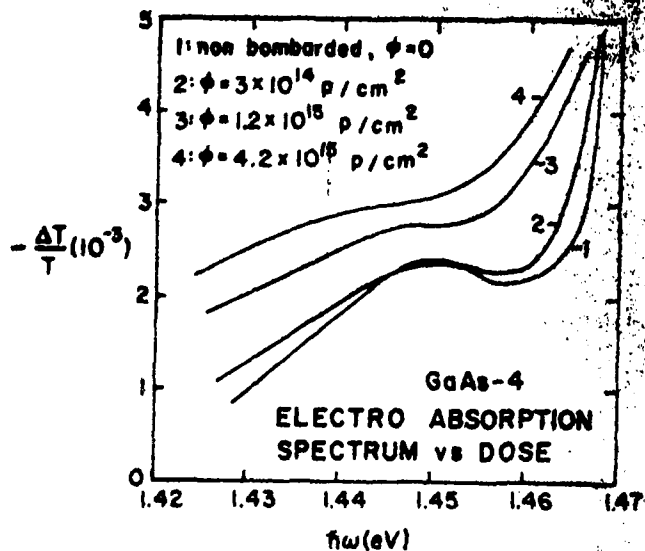


Fig. 7. EA vs. dose of bombarded and not-bombarded regions

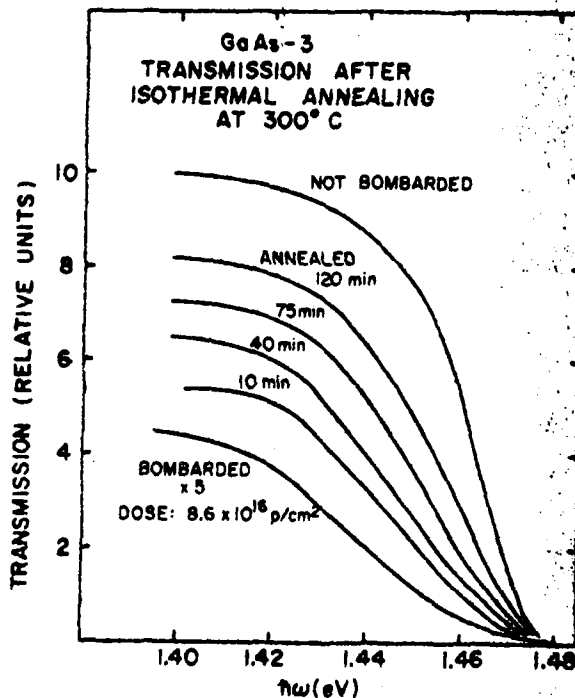


Fig. 8. Transmission from the bombarded region after isothermal annealing at 300°C.

Annealing

The effect of heat-treatment on the sample transmission in the vicinity of the E_0 critical point is shown in Fig. 8.

The sample was subjected to a bombardment dose of 8.6×10^{16} p/cm² (which completely eliminated its ER signals) and then isothermally annealed in vacuum at 300°C for up to 2 hr. The heat-treatment only partially recovers the transmission (Fig. 8) and ER signals before bombardment. For a given annealing time, the recovery of the ER signal is smaller than the recovery of the transmission; this is in agreement with our previous finding that the ER at E_0 is more sensitive to crystalline damage than the transmission.

77
does not necessarily indicate that different types of defects are involved.

Dymont et al. (22) showed that the optical absorption of proton bombarded GaAs can be annealed more easily than the resistivity. They concluded that there must be at least two types of defects involved in the bombardment process.

Summary and Conclusions

All electromodulation signals decrease in intensity following proton bombardment of the sample. Due to better overlap of the incident light beam and the damaged region, the ER at E_0 is the most sensitive to proton bombardment. The added absorption just below the energy gap increases sublinearly with dose in the dose interval between 3×10^{14} and 5×10^{15} p/cm². In the same dose interval, the peak-to-peak spectral amplitude, Δ , of the ER at E_0 and E_1 critical points both vary linearly with the logarithm of the dose and thus can be used as a measure for the degree of the sample amorphicity.

The EA at E_0 develops a tail toward the low energy side of the spectrum. The ER at E_0 has a shift of ~ 4 meV to higher energy while the peak of the ER signal at E_1 shifts by ~ 15 meV to lower energy. The origins of these shifts are not yet clear.

Annealing at 300°C for up to 2 hr only partially recovers the unbombarded state. The recovery is not linear in time.

A model based on the gradual amorphization of the sample by an increasing number of proton-damaged amorphous islands with well-defined boundaries was considered. The change in absorption coefficient, α_0 , or the change in the ER signal, in this model, depends on the volume fraction, A/A_0 , made amorphous by the bombardment. Assuming a layer of average thickness d_0 to be damaged, the number of unit cells made amorphous per incident proton will be

$$N = d_0 \cdot \frac{dA}{dP} / \alpha_0^3 = d_0 \left(1 - \frac{A}{A_0} \right) \sigma(\phi) / \alpha_0^3 \quad [18]$$

where α_0 is the lattice constant for GaAs (5.65Å).

Using Eq. [12] and [15]-[18], we find from the E_0 ER data

$$N = - \frac{ad_0}{\phi \alpha_0^3} = \frac{1.8 \times 10^{17} / \text{cm}^2}{\phi}$$

which corresponds to 28 unit cells amorphized per incident proton for $\phi = 5 \times 10^{15}$ p/cm². Wempe et al. (3) found that in a 300 keV proton bombardment of GaP a similar number of unit cells was made amorphous per incident proton: i.e., 10 for a dose of 10^{15} or 10^{16} protons/cm². The ER signal at E_0 is reduced below the detection limit ($\Delta R/R \sim 10^{-6}$) at $\phi \sim 2.5 \times 10^{16}$ p/cm² while the ER at E_1 is reduced to that level only at $\phi \sim 10^{17}$ p/cm². According to our model this implies that a dose of about 10^{17} p/cm² amorphizes the sample throughout the damaged layer of thickness $\sim 1.5 \mu\text{m}$, whereas 2.5×10^{16} p/cm² amorphizes it only in the region near $1.5 \mu\text{m}$ away from the surface.

The electronic band structure of a tetrahedrally bonded amorphous material is expected to have tails in the density of states which extend from the valence and conduction bands into the bandgap (23, 24). The tail in the EA signal at E_0 is tentatively attributed to transitions between these tails of the density of states.

Acknowledgment

This work was supported in part by the Office of Naval Research under Contract N00014-76-C-0690.

Manuscript submitted June 23, 1977; revised manuscript received Oct. 20, 1977.

Any discussion of this paper will appear in a Discussion Section to be published in the December 1978 JOURNAL. All discussions for the December 1978 Discussion Section should be submitted by Aug. 1, 1978.

REFERENCES

1. (a) T. Pankey, Jr. and J. E. Davey, *J. Appl. Phys.*, **41**, 697 (1970). (b) D. D. Sell and A. V. MacKee, *ibid.*, **41**, 4929 (1970).
2. B. R. Prumax, J. C. North, and G. L. Miller in, "Second International Conference on Ion Implantation in Semiconductors," I. Ruge and J. Graul, Editors, p. 212. Springer-Verlag, New York (1971).
3. S. H. Wemple, J. C. North, and J. M. Dishman, *J. Appl. Phys.*, **45**, 1578 (1974).
4. B. L. Crowder, R. S. Title, H. H. Brodsky, and G. D. Pettit, *Appl. Phys. Lett.*, **16**, 205 (1970).
5. For general reference on modulation spectroscopy see: (a) M. Cardona, "Solid State Physics," Suppl. 11, Academic Press, New York (1969); (b) "Semiconductors and Semimetals," Vol. 9, R. K. Willardson and A. C. Beer, Editors, Academic Press, New York (1972).
6. A. D. Jonath, E. Voronkov, and R. H. Bube, *J. Appl. Phys.*, **46**, 1754 (1975).
7. R. S. Bauer, *J. Electron. Mater.*, **4**, 1067 (1975).
8. V. I. Gavrilenko, A. V. Drazhan, V. A. Zuev, D. V. Korbutyak, and V. G. Litovchenko, *Sov. Phys. Semicond.*, **10**, 185 (1976).
9. V. I. Gavrilenko, A. P. Dubchak, V. A. Zuev, V. G. Litovchenko, and V. S. Lysenko, *ibid.*, **9**, 460 (1975).
10. W. J. Anderson, C. A. Douglass III, and Y. S. Park, *J. Appl. Phys.*, **46**, 3875 (1975).
11. V. Rehn and D. S. Kysen, *Phys. Rev. Lett.*, **18**, 848 (1967).
12. A. H. Kalma, *IEEE Trans. Nucl. Sci.*, **ns-19**, 200 (1972); also see Ref. 1(a).
13. S. M. Spitzer and J. C. North, *J. Appl. Phys.*, **44**, 214 (1973).
14. B. L. Gregory and H. H. Sander, *Proc. IEEE*, **58**, 1328 (1970).
15. A. W. Tinsley, *Radiat. Eff.*, **23**, 165 (1974).
16. J. F. Gibbons, W. S. Johnson, and S. W. Myroia, "Projected Range Statistics," 2nd ed., Halsted Press, New York (1975).
17. A. A. Gutkin, D. N. Nasledov, and F. E. Faradzhev, *Sov. Phys. Semicond.*, **8**, 298 (1974).
18. B. O. Seraphin and H. G. Bennett, in "Semiconductors and Semimetals," Vol. 3, R. K. Willardson and A. C. Beer, Editors, Academic Press, New York (1967).
19. F. F. Morhead and B. L. Crowder, *Radiat. Eff.*, **6**, 27 (1970).
20. J. C. Dymont, J. C. North, and L. A. D'Asaro, *J. Appl. Phys.*, **44**, 207 (1973).
21. L. W. Aukerman, P. W. Davis, R. D. Graft, and T. S. Shilliday, *This Journal*, **34**, 3590 (1963).
22. E. W. Mitchell and C. Norris, *J. Phys. Soc. Jpn.*, **21**, 656 (1967).
23. B. A. Bobylev, A. F. Kravchenko, and A. S. Terekhov, *Sov. Phys. Semicond.*, **7**, 1381 (1974).
24. W. J. Anderson and Y. S. Park, *J. Appl. Phys.*, **47**, 3094 (1976).

LUMINESCENCE IN GaAs:Cr FANO RESONANCES AND LOCAL MODES*

C.M. Penchina**

Dept. of Physics and Astronomy, University of Massachusetts,
Amherst, Mass. 0105 USA

E.C. Lightowers and M.C. Henry

Dept. of Physics, King's College, London WC2R 2LS, England
M. Závřtová and B. Velický

Institute of Physics, Na Slovance 2, 180 40 Praha 8,
Czechoslovakia

1. Introduction

A luminescence band with a triplet of zero-phonon lines around 0.57 eV (2.16 μ m) was reported in [1]. The band was first found in [2], although the authors failed to observe its fine structure. This band is difficult to study with high accuracy mostly because of an oxygen related background luminescence [3, 4]. Careful choice of spectrometer resolution to increase signal-to-noise, led to the discovery of much structure in this band [3]. In this paper, we discuss the rich details of the luminescence between 2.1 and 2.4 μ m associated with the zero-phonon triplet at 2.16 μ m. This spectrum is shown in Fig. 1.

2. Results

We point out five salient features of Fig. 1 as follows:

(A) A triplet of zero-phonon lines, somewhat distorted in this figure by the low resolution, was studied in more detail in [1], see Fig. 2.

(B) The sloping background signal is oxygen related. When

*Supported in part by the ONR under contract N 00014-76-C-0890, by the Science Research Council, and by the University of London Central Research Fund.

**MAS Exchange Scientist, Inst. of Physics, Academy of Sciences, Prague, and Inst. for Technical Physics, Academy of Sciences, Budapest.

Proceedings
of the International Conference

RADIATIVE RECOMBINATION AND

RELATED PHENOMENA

IN III-V COMPOUND SEMICONDUCTORS

R E C O N ' 7 9

Short Contributions

PRAGUE, CZECHOSLOVAKIA
September 4-7 1979

CZECHOSLOVAK ACADEMY OF SCIENCES
INSTITUTE OF RADIO ENGINEERING AND ELECTRONICS
in cooperation with
INSTITUTE OF PHYSICS

P R A G U E
CZECHOSLOVAKIA

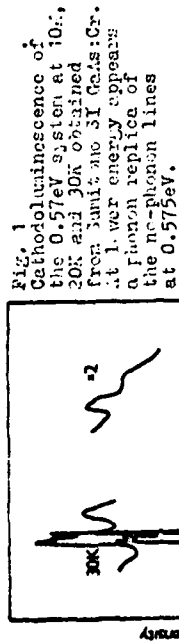
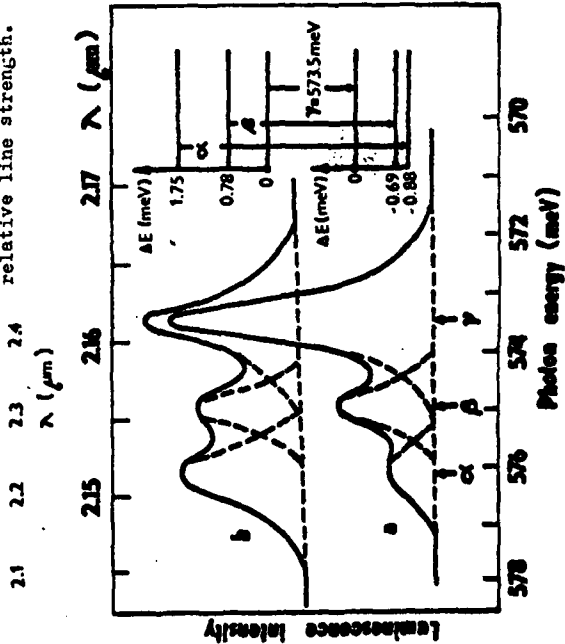


Fig. 1
Cathodoluminescence of the 0.57eV system at 10x; 20K and 30K obtained from 3000 Å Si GaAs:Cr. At 1.1 eV energy appears a phonon replica of the no-phonon lines at 0.575eV.

Fig. 2
The no-phonon structure at 0.575eV at a) 7.7K and b) 21.2K.
Insert:
The energy level scheme inferred from the temperature dependence of the relative line strength.



much larger, makes the chromium band hard to observe.
(C) A system of broad phonon sidebands on the long wavelength side of the zero-phonon lines [1].
(D) A sharp replica of the zero-phonon lines, shifted 40.7 meV to longer wavelength, which was reported in [3] as a local phonon sideband.

(E) A fairly sharp decrease in the background luminescence on the short wavelength side of the zero-phonon lines.

In the remainder of this paper, we concentrate on an explanation for features C, D & E.

3. Features C & D Long wavelength sidebands

The broad long wavelength sidebands (Fig. 3a) look quite similar to the density of lattice phonons of GaAs [5] (Fig. 3b). A major difference is the LO phonon peak in the DOS missing in the sideband spectrum. There is instead a peak shifted by 40.7 meV to longer wavelength which has the same shape as the zero-phonon triplet, and thermalizes with it. If the DOS could be represented by a single Einstein frequency, then the shifted peak would be explained as a local vibration of Cr on a Ga site with no major change in force constants. Since $\omega = (\kappa/m)^{1/2}$, the ratio of the frequencies would be

$$(M_{Ga} / M_{Cr})^{1/2} = (69.72 / 52.00)^{1/2} = 1.16$$

in good agreement with the measured ratio 1.18.

A more accurate treatment extending [6] determines the local mode density from the entire lattice phonon spectrum. A more mass defect does not yield the local DOS resembling the experiment: the Cr mass defect is too weak (Fig. 3c), an $M = 40$ defect is unlikely, and distorts the acoustic mode sidebands (Fig. 3d). A defect with the Cr mass, plus the nearest neighbour interactions increased by ~20%, on the other hand, results in a satisfactory overall agreement (Fig. 3e). The force constant enhancement could come from the d-shell of Cr and/or from the charge state of the Cr impurity substituting for Gallium.

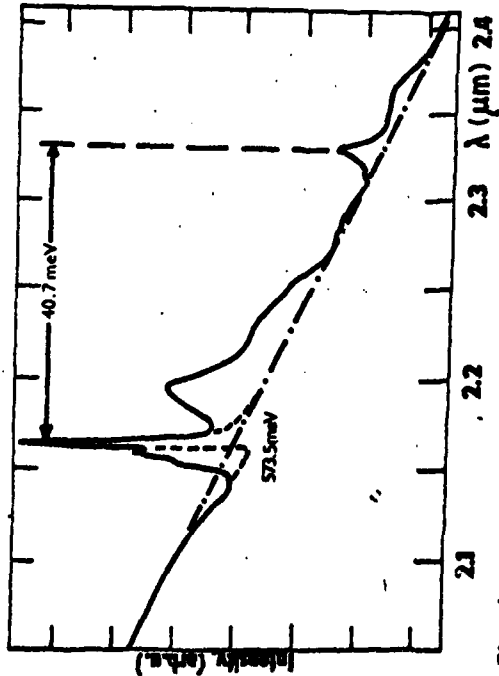


Fig. 4 Fano theory fit of experimental luminescence spectrum

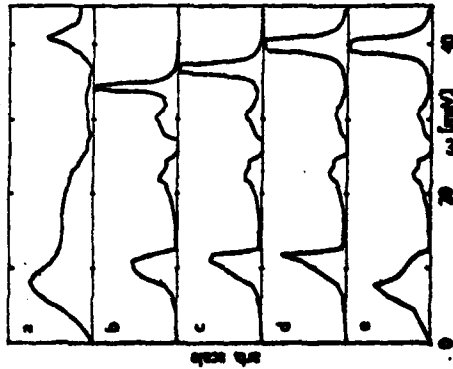


Fig. 3 Local phonon DOS at the defect:
 a) experimental phonon sideband with background and no-phonon lines removed (cf. Fig. 4)
 b) bulk phonon DOS in GaAs [5]
 c) local phonon DOS at the defect:
 Defect mass change
 d) $M_{Cr} = 52$
 e) $M_{Cr} = 20\%$

4. Feature E: anti-resonance

The broad spectral scan (Fig. 1,4) of the luminescence shows a sharp dip in the luminescence intensity, just to the short wavelength side of the zero-phonon lines near 575 meV. It might be due to self absorption of the oxygen related background luminescence by a Stokes shifted phonon replica of the zero-phonon Cr lines. This tentative explanation was ruled out, because the related IR absorption should have been easily detected, but was in fact never observed.

Another feature of the 0.57 eV zero-phonon lines is their considerable width at the LH temperature compared with the width of the 0.84 zero-phonon lines, and with M_{Cr} (FWHM ~ 1 meV vs. ~ 0.2 meV vs. ~ 0.3 meV) [1, 7]. This additional width is in spite of an apparently weaker phonon sideband spectrum. We suggest here that both the broadening and the anti-resonant dip indicate a Fano resonance, known to be formed due to a coupling of a "discrete" state with an overlapping continuum [8, 9]. The theoretical cross-section to be fitted is

$$\sigma(E) = \sigma_{cont}(E) \cdot \left[\frac{\rho^2(q + \epsilon)^2}{1 + \epsilon^2} + (1 - \rho^2) \right]$$

where $\epsilon = (E - E_{cr}) / (\hbar\Gamma)$. A satisfactory fit to the strongest zero-phonon line is obtained for $\Gamma = 0.68$ meV, $q = -4$, and $\rho^2 = 0.37$ (Fig. 4). A fit to all three lines would require additional knowledge of their coherence with each other.

5. Discussion

Our study of the 0.57 eV luminescence band in GaAs:Cr indicates that the main features can be explained in terms of a triplet of zero-phonon lines of chromium which are degenerate with a continuum, and thus exhibit both broadening, and a Fano type anti-resonance. The optical transitions are coupled to local vibrations of the chromium impurity which exhibits a 20% increase in local force constants. By comparison, the 0.84 eV luminescence shows no evidence of Fano resonance or coupling to local phonons.

Since the coupling to phonons is so different for the 0.57 eV and the 0.84 eV luminescence, they are presumed to be due to two different charge states of Cr. The 0.84 eV luminescence is thought to be in some ways related to Cr^{2+} (i.e. singly negatively charged chromium on a gallium site), perhaps paired with some shallow impurity. Thus, we expect that the 0.57 eV luminescence is related to Cr^{3+} (neutral chromium on a gallium site) which should also be present in semi-insulating Gallium arsenide.

Acknowledgements

We wish to thank Dr. Hans Stocker and Dr. A. M. White and Dr. E. Swiggard for providing samples. The aid of Dr. A. Collins and Ms. H. Hajkova is gratefully acknowledged.

References

- [1] E.C. Lightowler and C.M. Penchina: *J. Phys. C* **11** (1978), L405.
- [2] W.H. Koschel, S.G. Bishop and B.D. McCombe: *Solid State Comm.* **19** (1978), 521.
- [3] E.C. Lightowler, M.C. Henry and C.M. Penchina: *Int. Conf. on Recomb. in Semicond.*, Southampton, U.K. (unpublished) (1978).
- [4] C.M. Penchina, E.C. Lightowler, M.C. Henry, M. Závátová and B. Velický: *Proc. Internat. Summer School on New Develop. in Semicond.*, Szeged, Hungary, 1979 (to be published).
- [5] F.A. Johnson: *Progress in Semiconductors* **9** (1966), p. 181.
- [6] P.G. Dewber and R.J. Elliott: *Proc. Roy. Soc.* **273** (1963), 222.
- [7] E.C. Lightowler, M.C. Henry and C.M. Penchina: *Int. Conf. Phys. Semicond.*, Edinburgh, 1978. *Inst. of Physics Conf. Series* **43** (1979), 307.
- [8] U. Fano and J.V. Cooper: *Rev. Mod. Phys.* **40** (1968), 441.
- [9] B. Velický and J. Sak: *phys. stat. sol.* **16** (1966), 147.

reprint for Limited Distribution from "New Developments in Semiconductor Physics"
"Lecture Notes in Physics No. 122", Springer Verlag, May 1980

LUMINESCENCE OF CHROMIUM IN GALLIUM ARSENIDE*

P.97

Claude M. Penchina**
Department of Physics and Astronomy
University of Massachusetts
Amherst Mass. 01003 USA

Research done in collaboration with
Edward C. Lightowers and Martin O. Henry, King's College, London
Milena Zavetova and Bedrich Velicky, Inst. of Physics, Academy of Sciences,
Prague

INTRODUCTION

The luminescence of chromium-doped gallium arsenide was found many years ago (Allen 1968) to exhibit a broad bright band in the near infrared. However, it was not until 1976 that a 0.84 eV zero-phonon line associated with this band was first reported (Stocker & Schmidt 1976, Koschel, Bishop & McCombe 1976). This zero-phonon "line" was soon observed to have fine structure (Lightowers & Penchina 1978) which has since been resolved into a multiplet of at least 13 zero-phonon lines; 4 of these are easily visible even on a broad scan of this luminescence band shown in Fig. 1. Presumably the fine structure was not observed long ago because of either poor signal-to-noise ratio or inappropriate choice of spectrometer resolution.

An investigation of Cr-doped semi-insulating GaAs from various sources has revealed the presence of a number of other luminescence bands, the most common being a broad band around 2 μm which is generally present in materials doped with oxygen (Fig. 2). In crystals where this oxygen related band is weak or absent, a further sharp line system was observed (Lightowers & Penchina 1978) around 0.57 eV (2.16 μm) as shown in Fig. 3. This luminescence band was first reported by Koschel et al. (1976) who failed to observe the fine structure of the zero-phonon multiplet. We have observed it also in the LPE sample used by Stocker & Schmidt (1976) and in a variety of bulk samples. We presume this band accompanies the 0.84 eV band in all samples, but may be hard to observe due to problems of signal-to-noise when the oxygen related band is strong.

* Supported in part by the OMR under contract N 00014-76-C-0890, by the Science Research Council, and by the University of London Central Research Fund.

** IAS Exchange scientist, Inst. of Physics, Academy of Sciences, Prague, and Inst. for Technical Physics, Academy of Sciences, Budapest.

84

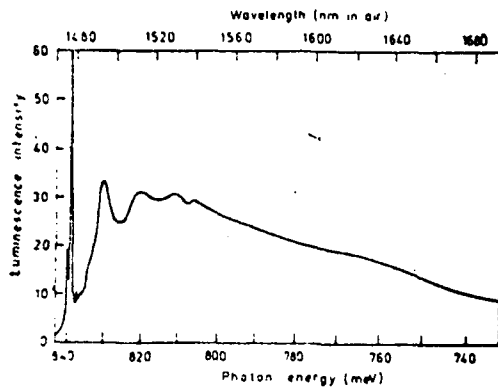


Fig. 1.

Cathodoluminescence spectrum of the 0.80 eV system, uncorrected for the transfer function of the optical system, obtained from Sumitomo SI GaAs:Cr with a cold finger temperature of 4.8 K and a beam current of 2.0 μ A. The temperature of the emitting region was 6.0 ± 0.5 K. The no-phonon structure is distorted by the slitwidth of the monochromator and system response time. The main peak at 839.37 meV has a height of 150 on this scale.

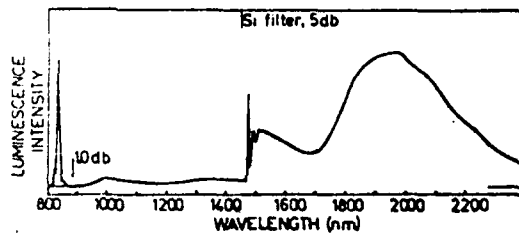
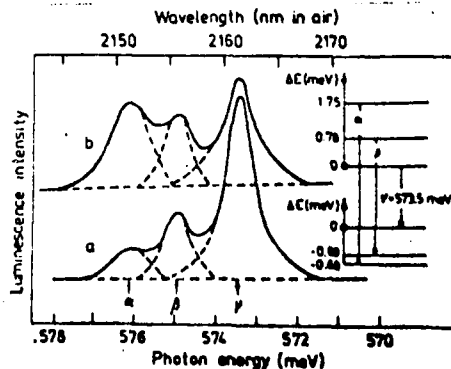


Fig. 2. Cathodoluminescence spectrum of GaAs:Cr produced by Crystal Specialties obtained at ~ 10 K, uncorrected for the transfer function of the optical system. The long wavelength band is thought to be related to the presence of oxygen.

Fig. 3.

Cathodoluminescence spectra of the no-phonon structure at 0.575 eV obtained from Sumitomo SI GaAs:Cr at (a) 7.7 K and (b) 21.2 K. The energy level scheme inferred from the temperature dependence of the relative line strengths is shown as an insert.



In this lecture, we shall concentrate mainly on the rather rich details of the luminescence between 2.1 and 2.4 μm associated with the zero-phonon triplet near 0.57 eV, and shown in Fig. 4.

Fig. 4a.

Cathodoluminescence spectra of the 0.57 eV system at ~ 10 K, 20 K and 30 K obtained from Sumitomo SI GaAs:Cr. The sharp structure at lower energy appears to be a phonon replica of the no-phonon lines at 0.575 eV (2.16 μm).

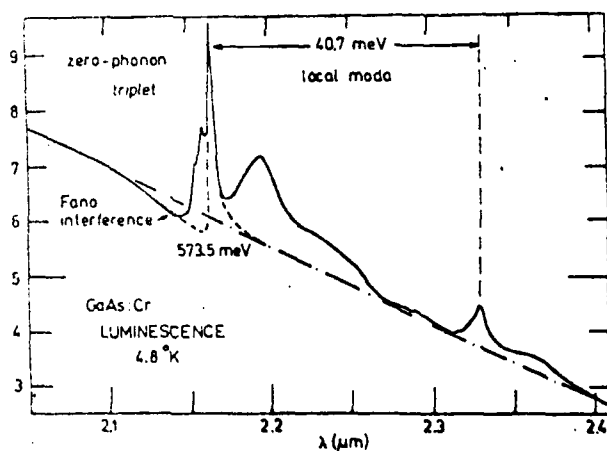
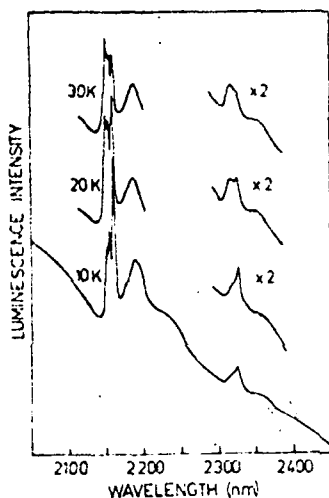
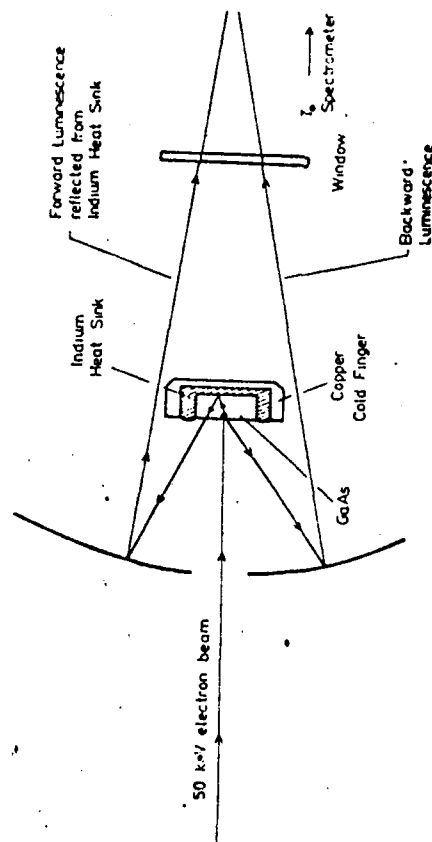


Fig. 4b. Fit of Fano theory (----) to experimental luminescence spectrum (—) where the background is interpolated (-.-.-) between smooth regions of the spectrum. $q = -4$, $\Gamma = 0.68$ eV, $p^2 = 0.37$.

EXPERIMENTAL ARRANGEMENT

Luminescence was excited by an electron beam of 50 keV and a typical beam current of 3 μ A. The beam was deflected on and off the sample electronically to allow lock-in detection, so the average power was about 75 mW. The arrangement of the experiment is shown schematically in Fig. 5. The cathodoluminescence seems to be more effective



than photo-luminescence excited by visible lasers; the visible light is absorbed so close to the surface that it excites a region of lower quality than the deeper bulk, and also causes some local heating. The luminescence is dispersed through a grating spectrometer and detected with a cooled lead-sulphide photoconductor. An important feature in the study of this spectrum is the optimization of signal-to-noise. This requires that the spectrometer slits be made as wide as possible without degrading the resolution required for the experiment. Since the spectral lines in this region are already broad, this allowed us to use 1mm slitwidth, permitting the detection of features which had been previously unobserved.

Fig. 5. Experimental arrangement for cathodoluminescence

RESULTS

Figure 4a shows much interesting structure, of which we shall concentrate on these five features:

- A) A triplet of zero-phonon lines around 575 meV.
- B) A large broad background signal which decreases towards longer wavelength.
- C) A broad system of sidebands to the long wavelength side of the zero-phonon lines.
- D) A sharp sideband shifted 40.7 meV to longer wavelength from the zero-phonon lines.
- E) A dip in the luminescence intensity on the short wavelength side of the zero-phonon lines.

Feature A, the zero-phonon lines, has been studied to higher resolution (Lightowlers & Penchina 1978) as a function of temperature, and the splittings in the ground state and excited state deduced as shown in Fig. 3. It is generally thought to be due to an excitation of Cr^{3+} (ESR notation for Cr in which 3 electrons have contributed to the valence bonding in the crystal, i.e. neutral chromium when substituting for gallium).

Feature B, the broad background, is due largely to the broad 2 μm oxygen related luminescence band reported by Lightowlers et al. in 1978 (Lightowlers, Henry & Penchina 1978).

Feature C, the broad sidebands, looks like a familiar crystal phonon replica of the zero-phonon luminescence. It seems to be missing a contribution from the large peak in the phonon density of states due to longitudinal optical phonons (Johnson 1966).

Feature D, is a sharp replica of the zero-phonon lines, which was first reported to be a local phonon replica in 1978 (Lightowlers, Henry & Penchina 1978).

Feature E, which appears to be some sort of anti-resonance, has not been previously explained.

In the remainder of this lecture, we shall concentrate on an explanation for features E and B, and for features C and D which will be treated together.

Feature E: anti-resonance

The broad spectral scan (Fig. 4a) of the luminescence shows quite clearly a rather sharp dip in the luminescence intensity, just to the short wavelength side of the zero-phonon lines near 575 meV. One possible explanation which first came to mind was that it might be due

to self absorption of the oxygen related background luminescence (Fig.2) by a Stokes shifted phonon replica of the zero-phonon Cr lines. Because of the experimental arrangement used (Fig. 5) in which the luminescence is observed in the backward direction, this absorption would have to occur in only a few microns (the electron penetration depth) for the primary luminescence in the back direction, or in a total of twice the sample thickness (about 0.4 mm thick) if it were absorption of the forward luminescence reflected back by the indium heat sink. In either case, this strong absorption should be easily detected in an infrared absorption measurement. No such sharp absorption band was observed, thus ruling out this tentative explanation.

Another explanation is suggested by the relatively large width of the 0.57 eV zero-phonon lines (FWHM about 1 meV) compared with the width of the 0.84 eV zero-phonon lines (FWHM about 0.2 meV) (Lightowers & Penchina 1978) at liquid helium temperature. This additional width is in spite of an apparently weaker phonon sideband spectrum. We suggest here that the broadening and the anti-resonant dip are both due to a degeneracy in energy of a discrete state of the impurity and a continuum state, a so-called Fano-resonance. Fano has shown (Fano & Cooper 1968, Velicky & Sak 1966) that when a "discrete" state is degenerate with a continuum, the interaction broadens the discrete level into a resonant level, with interference terms causing a nearly anti-resonance and asymmetric lineshape. The theory predicts

$$\sigma(E) = \sigma_{\text{cont.}}(E) \left[\frac{p^2(q + \epsilon)^2}{1 + \epsilon^2} + (1 - p^2) \right]$$

where

$$\epsilon = \frac{E - E_{\text{resonance}}}{\frac{1}{2} \Gamma}$$

Fitting this theoretical expression to our experimental spectra (Fig 4b) yields a linewidth $\Gamma = 0.88$ meV, which is much larger than kT (about 0.3 meV at 4.2°K), a resonance lineshape given by $q = -4$, and a coherence with the background given by $p^2 = 0.37$. We fit the theory only to the strongest zero-phonon line. A fit to all three lines would require some additional knowledge of their coherence with each other. The relatively nice fit, as well as the lack of other plausible explanation for the line broadening and anti-resonance, leads us to conclude that there is indeed a Fano interference between a discrete level and a continuum.

Feature B: oxygen related background

This background luminescence band is illustrated in Fig. 2 for a sample of chromium doped GaAs from Crystal Specialties. The same band is much brighter in their chromium/oxygen doped material, and is the only important feature in their GaAs:O. This band appears also in other samples of GaAs with intentional oxygen doping from RSRE and Sumitomo, and does not appear in an undoped GaAs sample from NRL grown in boron nitride to specifically exclude oxygen contamination (Swiggard et al. 1977). On the other hand, we have studied two samples with intentional oxygen doping which do not show this feature either: one from RSRE shows several other broad bands, while one from Sumitomo shows only luminescence characteristic of Cr, though its photoconductivity shows evidence of oxygen (Tyler, Jaros & Penchina 1977). Thus, we conclude that the broad 2 μ m band is evidence of oxygen impurities. The absence of this band does not, however, necessarily prove the absence of oxygen, which might enter GaAs in some other state, complex, etc.

Features C and D: low wavelength sidebands

The intensity of the broad long-wavelength sidebands of the 0.57 eV zero-phonon lines (Fig. 6a) looks quite similar to the density of lattice phonons of GaAs (Johnson 1966) (Fig. 6b). A major difference is that the peak in the density of states due to longitudinal optical phonons does not appear in the sideband spectrum. There is instead a peak shifted by 40.7 meV to longer wavelength which has the same shape as the zero-phonon triplet, and thermalizes with it. If one assumes the peak in the density of phonon states can be represented by a single frequency (i.e. Einstein spectrum), then the shifted peak is explained quite well as a local vibration of Cr on a Ga site with no major change in force constants. Since $\omega = (k/m)^{1/2}$, the ratio of the frequencies would be

$$\sqrt{\frac{M_{\text{Ga}}}{M_{\text{Cr}}}} = \sqrt{\frac{69.72}{52.00}} = 1.16$$

which is in quite good agreement with the measured ratio

$$\omega_{\text{local}}/\omega_{\text{peak}} = 1.18.$$

A more accurate treatment (Penchina et al. 1979), using the theory of Dawber and Elliott (1963) extended to the case of a compound semiconductor, determines the local mode frequency from the mass defect and an integral over the full lattice phonon spectrum. This, however, gives a local mode frequency which is too low to give a good fit to the experiment (Fig. 6c). A sufficiently high frequency could be obtained

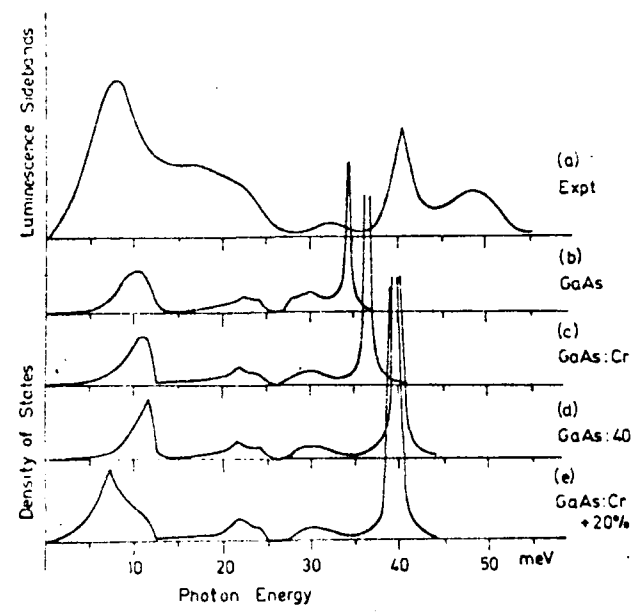


Fig. 6. a) Experimental phonon sidebands of 0.57 eV GaAs:Cr luminescence after removal of zero-phonon lines and background luminescence. The structure beyond the 40.7 meV peak is due to emission of a local phonon and a band phonon.
 b) Lattice phonon density of states of GaAs, from Johnson (1966)
 c) Density of phonons at defect for Cr on Ga site, no change of force constants.
 d) Density of phonons at defect for mass 40 on Ga site, no change of force constants.
 e) Density of phonons at defect for Cr on Ga site, 20 % increase in local force constants.
 The vertical scales of $\delta(a)-(e)$ are arbitrary, and vary from curve to curve.

By using a mass of about 40 atomic units (a rather unlikely impurity mass), at the cost of getting a worse fit to the low energy acoustic phonon sidebands (Fig. 6d). On the other hand, for a Cr impurity, a model using nearest neighbour interactions enhanced by about 20 % (Penchina et al. 1979) gets the correct local mode frequency and simultaneously improved the fit for the low energy acoustic phonon sidebands as well (Fig. 6e).

It might seem at first surprising that an increased force constant would increase the local mode frequency but decrease the acoustic phonon frequencies. This is easily explained when one realizes that in

(9)

the low energy acoustic modes, nearest neighbours move in phase. Increasing the force constant tends to bind the defect more rigidly to its neighbours, thus causing it to "drag" the neighbours along, an effect similar to increasing the local mass, which then lowers the frequency. The increase in force constant could come from the interactions involving the unfilled d shell of Cr, and/or from a difference in charge state between the Cr impurity and the Ga for which it substitutes.

DISCUSSION

Our study of the 0.57 eV luminescence band in GaAs:Cr indicates that the main features can be explained in terms of a triplet of zero-phonon lines of chromium which are degenerate with a continuum, and thus exhibit both broadening, and a Fano type anti-resonance. The optical transitions are coupled to local vibrations of the chromium impurity which exhibits a 20 % increase in local force constants. By comparison, the 0.84 eV luminescence shows no evidence of Fano resonance or coupling to local phonons. Since the coupling to phonons is so different for the 0.57 eV and the 0.84 eV luminescence, they are presumed to be due to two different charge states of Cr: The 0.84 eV luminescence is thought to be in some ways related to Cr^{2+} (i.e. singly negatively charged chromium on a gallium site), perhaps paired with some shallow impurity. Thus, we expect that the 0.57 eV luminescence is related to Cr^{3+} (neutral chromium on a gallium site) which should also be present in semi-insulating gallium arsenide.

The broad luminescence band around 2 μm was found to be characteristic of oxygen in GaAs. There were, however, samples which supposedly contained oxygen which did not show this band. Thus, it is likely that oxygen enters GaAs in more than one state or complex, only one of which produces this luminescence band. Additional study of oxygen-doped and oxygen-free samples will be needed before this luminescence band can be used as a definitive test for oxygen impurities.

REFERENCES

- G.A.Allen, J.Phys.D. 1, 593 (1968)
P.G.Dawber and R.J.Elliott, Proc.Roy Soc. 273, 222-236 (1963)
P.A.Johnson, Progress in Semiconductors 9, 181-235 (1966)
W.H.Koschel, S.G.Bishop and B.D.McCombe, Solid State Commun. 19, 521 (1976)
E.C.Lightowers, M.O.Henry and C.M.Penchina, Int. Conf. on Recombination in Semiconductors, Southampton, U.K. (unpublished) (1978)
E.C.Lightowers, M.O.Henry and C.M.Penchina, Int.Conf. on Physics of Semiconductors, Edinburgh, Scotland 1978. Inst of Physics Conf. Series

AD-A106 695

MASSACHUSETTS UNIV AMHERST DEPT OF PHYSICS AND ASTRONOMY F/6 7/4
DEEP IMPURITY STATES IN GALLIUM ARSENIDE.(U)
OCT 81 C M PENCHINA
CMP811015

N00014-76-C-0890
NL

UNCLASSIFIED

2-2

Pages



END
DATE
FILMED
12-81
DTIC

A study of deep impurity levels in GaAs due to Cr and O by ac photoconductivity^{a)}

H. J. Stocker^{b)}

Department of Physics and Astronomy, University of Massachusetts, Amherst, Massachusetts 01003
(Received 26 January 1977; accepted for publication 18 April 1977)

ac photoconductivity measurements at $T \leq 20$ K allow accurate determination of the energy levels of GaAs:O at E_c 753 meV and of GaAs:Cr at E_c -838 meV. O gives a clearly defined sharp threshold, while Cr shows a peak at 860-870 meV of varying width. These levels have been observed in boat-grown and in n - and p -type LPE material. Oscillatory photoconductivity is observed in conjunction with the O level.

PACS numbers: 71.55.Fr, 72.40.+w

I. INTRODUCTION

A huge amount of literature¹⁻³ exists on the properties of semi-insulating (SI) GaAs, yet the energy levels in these materials have not yet been determined with any great accuracy. There is even disagreement on whether Cr introduces one, two, or three energy levels³ in GaAs. Also, it is often not clear whether or not a given material which is nominally Cr doped also contains other deep impurities in significant numbers. It also has not yet been established whether or not the energy levels seen in boat-grown semi-insulating material exist as well in material grown by liquid-phase epitaxy (LPE).

This paper is intended to help clarify this highly unsatisfactory state of affairs by (a) reporting the most accurate measurements of the optical ionization energies of Cr and O impurity levels in GaAs, (b) extending the measurements of photoconductivity to liquid-He temperature, (c) demonstrating that measurements of the ac photoconductivity at He temperatures provide a simple technique for the detection of Cr and O in GaAs, and (d) applying the same technique to LPE layers on semi-insulating substrates and demonstrating the existence of the same energy levels in LPE material.

This paper does *not* intend to present measurements of the photoionization cross sections of the Cr and O impurities in GaAs. As Grimmeiss and Ledebor⁴ have conclusively shown, measurement of the photoconductive spectral response of deep impurities can be quite drastically dependent on speed of measurement, light intensity, and thermal history. In particular, the spectral response may be strongly influenced by quenching effects. However, the threshold energies measured do *not* depend on these effects and are therefore reliable.

^{a)} Parts of this investigation were carried out while the author was employed by the University of Dayton and supported by U.S. Air Force Contract F33615-72-2114. One sample (K) was measured while the author was at the Max Planck Institut for Solid State Physics, Stuttgart, Germany. The work at the University of Massachusetts was supported by the Office of Naval Research under Contract N00014-76-C-0890.

^{b)} Present address: Bell Laboratories, Murray Hill, N.J. 07974.

II. EXPERIMENTAL

A. Samples

Samples A-G were cut from commercially available SI substrate material from a variety of sources. Table I lists the samples, their sources, and the mass-spectrographic analysis of the Cr and Fe content, as well as other information. The samples were obtained in 1973/74 and therefore may not be indicative of today's material. Samples H and K were Cr-doped LPE layers of room-temperature resistivity $\rho > 10^5 \Omega \text{ cm}$. Samples I and J were nominally undoped LPE layers, n type with carrier concentration in the $5 \times 10^{14} \text{ cm}^{-3}$ range. Samples H-K were grown on Cr-doped SI substrate material. The exact growth conditions are known only for sample K and are to be described elsewhere.⁵

The samples were usually etched briefly in 5:1:1 ($\text{H}_2\text{SO}_4 : \text{H}_2\text{O}_2 : \text{H}_2\text{O}$) before contacts were made with pure In and an ultrasonic soldering iron. While this method does not always give Ohmic contacts (especially at He temperatures), it seems to work as well as any others tried on SI material and is much simpler. For the n -type EPI layers, an In-Sn alloy was used instead of pure In. The contacts were shielded during measurements to minimize photovoltaic effects.

In the case of the LPE layers, contacts were made to the top epitaxial layer only, but the substrate of course

TABLE I. GaAs samples used.

Sample designation	Source	Remarks
A	MIT	SI, 1 ppm Cr, 0.5 ppm Fe
B	Bell and Howell	SI, ~1 ppm Cr, 0.4 ppm Fe
C	Monsanto	SI, 0.03 ppm Cr, 0.7 ppm Fe
D	TI	SI, 0.2 ppm Cr, 0.05 ppm Fe
E	Laser diodes	SI, 1 ppm Cr, 0.1 ppm Fe
F	Laser diodes	SI, 1 ppm Cr, 0.05 ppm Fe
G	Laser diodes	SI
H	RCA	5 μm LPE Cr-doped n -type layer on substrate G
I	RCA	1 μm n -type high-purity LPE on substrate G
J	RCA	1 μm n -type high-purity LPE on H as the substrate
K	MPI	15 μm SI Cr-doped LPE on SI substrate Growth temperature 825°C.

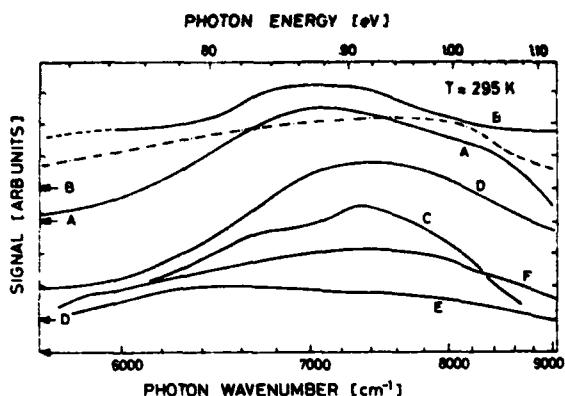


FIG. 1. Photoconductive spectral response of six samples of SI GaAs at room temperature, not corrected for weak variation in source-light intensity (dash-dot line). Note that base line is different for samples A, B, and D.

remained, shunting the LPE layer. This procedure possibly allows signal due to the photoconductivity (PC) in the underlying substrate to be mixed in with the photoconductive signal due to the LPE layer alone. Fortunately, experimentally, the underlying substrate does not appear to influence the PC signal to any great extent. This can be seen, e.g., from Fig. 5. If the Cr-doped substrate were to contribute substantially to the PC response, a peak at Cr level at 0.84–0.86 eV would appear; this is clearly not the case.

B. Measurement of the photoconductivity spectral response

Two methods of measurement were used. For the high-resistivity samples A–H and K, a bias voltage of 50–150 V was applied across the sample and a model 416 Keithley picoammeter in series. The light beam was chopped at 5–15 Hz with a PAR variable-frequency chopper. The output of the Keithley picoammeter was then used as the input of a model 124A PAR lock-in. In this configuration, the Keithley is basically used as a dc amplifier.

The other method of measurement, applied to the *n*-type low-resistance samples I and J, consisted of a lead resistor in series with the sample, with the voltage drop across this load being used as the input of the PAR 124A lock-in.

III. RESULTS AND DISCUSSION

Figure 1 shows the PC spectral response for samples A–F at room temperature. There is an extremely broad peak at 0.84–0.92 eV. Not much difference between the different samples can be discerned. At liquid-nitrogen temperature (Fig. 2), some clearly resolved peaks appear. Note the large differences between these samples, even though they all are supposedly Cr-doped SI GaAs, according to the manufacturers. These peaks shift around considerably with temperature and it is, in fact, rather difficult to make sense out of them. Only by going to still lower temperatures does a well-defined and reproducible structure emerge. Figure 3 shows the same six samples at $T \approx 20$ K. Three features are note-

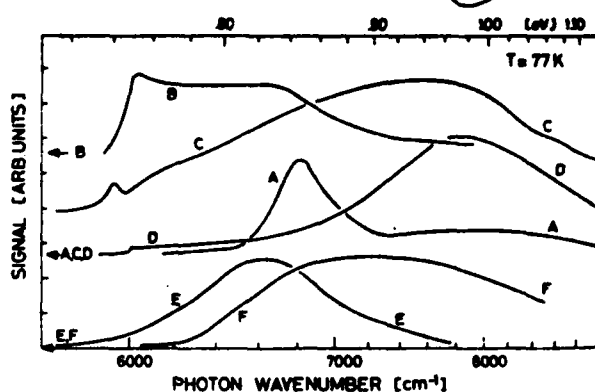


FIG. 2. PC spectral response for the same six samples of Fig. 1 at $T = 77$ K. Note that base line is different for samples A, B, C, and D.

worthy, namely, a sharp threshold at 0.75 eV, a broad peak at ~ 0.86 eV, and an oscillatory structure.

A. Threshold at 0.75 eV

This sharp threshold occurs in samples B, C, D, and F. This threshold we interpret as due to the presence of oxygen in the sample. Its energy agrees well with other measurements such as deep-level transient spectroscopy⁵ (DLTS) and photoluminescence.⁷ It has actually never been proven that this level at 0.75 eV is due to O and, in particular, it is not known whether it is due to interstitial O, substitutional O, or some kind of complex. Be that as it may, we follow the widespread notation and attribute this level to GaAs:O. The threshold energy at He temperature can actually be determined with great precision from the extrapolation of the oscillatory structure (Sec. III C). The exact value is 753 ± 5 meV.

B. Broad peak at 0.86–0.87 eV

This peak is clearly correlated with the presence of Cr in GaAs. This is evident from the present measurements as well as those of many previous authors³

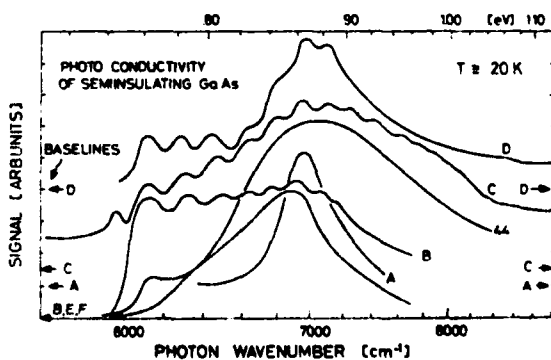


FIG. 3. PC spectral response for the same six samples at $T \approx 20$ K. Note that the base lines of samples A, C, and D are different. Three main features are seen: a threshold at 0.75 eV attributed to GaAs:O, a broader peak at 0.86–0.87 eV due to GaAs:Cr, and an oscillating structure in those samples in which the GaAs:O threshold is strong. See text.

and correlates well with photoluminescent data.^{8,9} The zero phonon line in photoluminescence at $T = 4.2$ K occurs at 838 ± 1 meV. This agrees well with the low-energy onset of the peak. This will be even clearer from data on LPE Cr-doped GaAs (samples H and K).

Only sample B does not show a peak at 0.87 eV, even though the mass-spectrographic analysis shows about 1 ppm Cr present. Possibly this sample was intentionally oxygen doped. The oxygen concentration could completely mask the Cr level. It should be noted that the mass-spectrographic analysis for sample B was less reliable than for the others.

The width of the peak can be seen to vary. In sample A, the half-width is ~ 40 meV; in sample F it is ~ 200 meV. Since the Cr concentration in both samples is around 1 ppm, this does not appear to be a matter of impurity concentration. Homogeneity of doping could be a factor here. Sample F was 1 cm thick, ~ 10 times the thickness of sample A. In any event, as mentioned in Sec. 1, we do not believe one should place too much value on the detailed shape of the ac PC response, but rely on the main features.

C. Oscillatory structure

The oscillations are periodic in photon energy with period 20.9 meV. They disappear at electric field strengths of greater than about 15 V/cm. Their origin is due to the combination of the establishment of a non-equilibrium distribution of photoexcited carriers, the energy dependence of their lifetime and mobility, and the rapid emission of localized phonons of energy 20.9 meV. For a detailed discussion, we refer the reader to Ref. 10. The energy of 20.9 meV was attributed¹⁰ to localized phonons associated with oxygen in GaAs. Dean and Henry¹¹ found energies of 28.4 meV for localized modes of O^{16} and 24.7 meV for O^{18} in the photoluminescence spectrum of the oxygen donor in GaP. Thus, an energy of 20.9 meV for a localized mode of O in the GaAs lattice seems quite reasonable.

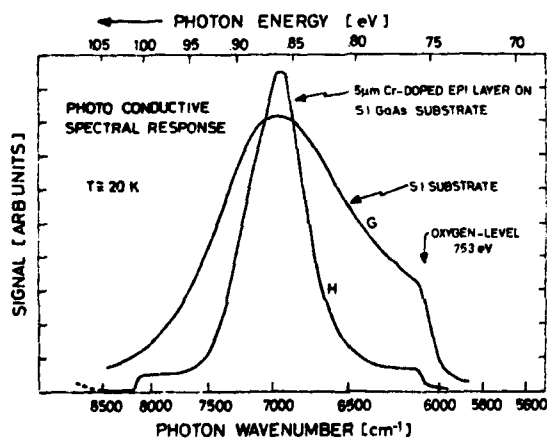


FIG. 4. PC spectral response of a 5 μm Cr-doped LPE layer (sample I) and its substrate (sample G) at $T = 20$ K. Both the threshold due to GaAs : O and the peak due to GaAs : Cr are clearly visible in both samples, although the oxygen content appears much reduced in the LPE layer.

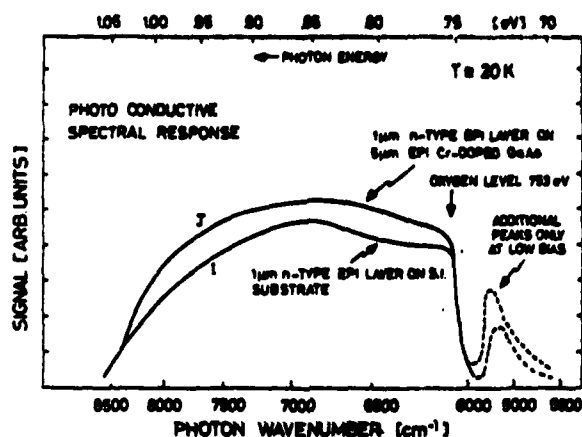


FIG. 5. PC spectral response of two high-purity n -type LPE GaAs layers of 1- μm thickness, sample I directly on Si substrate; sample J with additional 5- μm LPE Cr-doped layer. $T = 20$ K. Both samples show a well-defined threshold due to GaAs : O. Additional peaks at lower photon energy disappear at bias voltages greater than ~ 3 V.

Sample C is the only one in which there is a significant PC response for photon energies lower than 0.75 eV which extended out to at least 0.5 eV. (For experimental reasons, the cut on could not be investigated.) This is almost certainly due to the fact that this sample contains more Fe than Cr (see Table I), even though it was specified to be Cr-doped Si GaAs substrate material. Fe is known¹² to introduce a level at approximately 0.52 eV from the valence band, and the longer wavelength response seen in sample C must be attributed to transitions to these levels. Sample C also exhibits a small peak at 740–742 meV, just before the threshold due to O. This peak persists as the temperature is increased to 77 K (Fig. 2). The origin of this peak is unclear. A similar effect was seen in samples I and J (see below).

Figure 4 shows the PC spectrum of a Cr-doped LPE layer (sample H) and of the substrate alone on which it

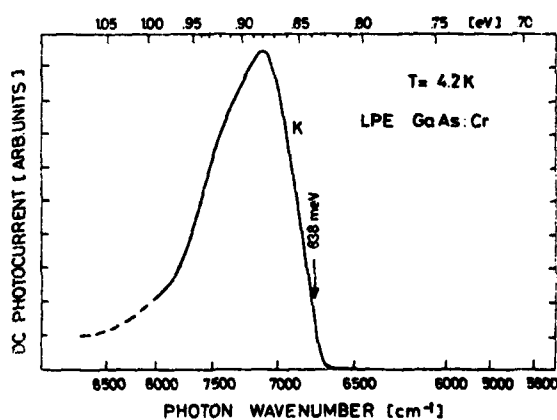


FIG. 6. PC spectral response of 15- μm LPE Cr-doped layer grown at 825°C in H_2 atmosphere. $T = 4.2$ K. No signal due to GaAs : O detectable. Threshold of 838 meV corresponds to zero phonon line of GaAs : Cr observed in luminescence in the same material.

was grown (sample G). The threshold due to GaAs : O is seen in both, although much reduced in the epilayer. A considerable sharpening of the Cr peak at 0.86 eV can also be observed. Whether or not this is due to the much lower Cr concentration in the LPE layer or to the presence of competing quenching effects cannot be determined. That the application of the ac PC technique is suitable for this epilayer is shown in Fig. 5. Contacts were made to the 1- μ m-thick *n*-type LPE layer without removing the SI substrate. For sample J, an additional 5- μ m Cr-doped LPE layer had been grown on top of the SI substrate. The PC spectral response for both samples I and J is practically identical and demonstrates the presence of O in these layers. ~~To our knowledge, this is the first direct observation of the 0.75-eV level in LPE material, which is common in VPE and in boat-grown material.~~

Both samples exhibit an additional peak slightly below the 0.75-eV threshold. These peaks disappeared when the bias across the structure was increased about 3-4 V. The average field strength between the contacts would then be 15-20 V/cm. Although models based on the existence of an excited state, impact ionization, etc., can be constructed, we cannot really offer an explanation for this strange behavior. A similar peak was observed in the bulk sample C.

Figure 6 finally shows the PC spectral response of a Cr-doped LPE layer on a SI substrate in which apparently all O contamination had been eliminated. The low-energy threshold coincides quite clearly with the energy of the zero phonon line of GaAs : Cr measured in photoluminescence.^{8,9}

IV. CONCLUSIONS

ac photoconductivity measurements at $T \leq 20$ K allow an accurate determination of the energy levels and give information about the relative concentrations of Cr and

O in SI GaAs. The technique is also applicable to thin epitaxial layers. O produces a sharp threshold at 753 ± 5 meV at He temperatures, while Cr is recognized by a peak of varying width at 0.86-0.87 eV. These levels are at the identical energetic positions in boat-grown and in LPE material. Commercially available Cr-doped SI substrate material often contains large concentrations of levels due to O and, in one instance, due to Fe. The level at 753 meV, attributed to GaAs : O which is commonly seen in VPE and boat-grown material, ~~has also been observed in LPE material.~~

ACKNOWLEDGMENTS

We wish to thank C. M. Penchina and M. Jaros for many discussions.

¹We do not find it useful to review the extensive literature here but refer the reader to the numerous references in Refs. 2 and 3.
²A. L. Lin, E. Omelianovsky, and R. H. Bube, *J. Appl. Phys.* 47, 1852 (1976).
³A. L. Lin and R. H. Bube, *J. Appl. Phys.* 47, 1859 (1976).
⁴H. G. Grimmeiss and L. A. Ledebor, *J. Appl. Phys.* 46, 2155 (1975).
⁵H. J. Stocker, E. Bauser, and Laurence Schmidt (unpublished).
⁶D. V. Lang and R. A. Logan, *J. Electron. Mater.* 4, 1053 (1975).
⁷W. J. Turner, C. D. Pettit, and N. G. Aninslie, *J. Appl. Phys.* 34, 3274 (1963).
⁸H. J. Stocker and Martin Schmidt, *J. Appl. Phys.* 47, 2450 (1976).
⁹W. H. Koshel, S. G. Bishop, and B. D. McCombe, *Solid State Commun.* 19, 521 (1976).
¹⁰H. J. Stocker, *Solid State Commun.* 16, 525 (1975).
¹¹P. J. Dean and C. H. Henry, *Phys. Rev.* 176, 928 (1968).
¹²A. G. Milnes, *Deep Impurities in Semiconductors* (Wiley, New York, 1973), Chap. 2.

ERRATUM

Samples H, I, J were grown by VPE using the AsH₃/Ga/HCl/H₂ system, not by LPE as assumed in the paper. Sample H was grown using CrO₂Cl₂ as the doping gas.

This fact invalidates the statement made in the paper that the 0-level had been observed in LPE material.

The author wishes to thank S. Y. Narayan, who supplied these samples to the USAF Avionics Laboratory, for pointing out the error.

Dr. H. J. Stocker
 Bell Laboratories
 Room 2D360
 600 Mountain Avenue
 Murray Hill, NJ 07974
 (201) 582-3572

Extrinsic photoconductivity in high-resistivity GaAs doped with oxygen^{a)}

96

E. H. Tyler, M. Jaros,^{b)} and Claude M. Penchina

Department of Physics and Astronomy, Heston Laboratory, University of Massachusetts, Amherst, Massachusetts 01003

(Received 7 April 1977; accepted for publication 23 May 1977)

We report photoconductivity measurements on melt-grown high-resistivity GaAs:O, taken at 80, 190, 275, and 295 K. The data are shown consistent with a model involving an impurity-to-conduction band transition. The impurity binding energy is found at 0.69 eV from the conduction band, at 0 K. This energy decreases with increasing temperature. The data also indicate a Franck-Condon shift of 0.14 eV and a center of axial or lower symmetry. These results enable us to link our observations to earlier reports on GaAs:O and to conclude that they all refer to the "0.75-eV" center associated with the presence of oxygen.

PACS numbers: 72.40 + w, 71.55.Fr

We present experimental results concerning extrinsic photoconductivity in melt-grown GaAs doped with oxygen, taken at 80, 190, 275, and 295 K. Theoretical examination of the data indicates that the observed spectra are consistent with a model of a level at 0.69 eV from the conduction band (at 0 K), with a Franck-Condon shift of 0.14 eV. We predict that the center possesses axial or lower symmetry and might exhibit a large nonradiative capture cross section for electrons. With increasing temperature the binding energy with respect to the conduction band edge decreases. These results suggest that the level is the familiar "oxygen" level, observed for instance by Lang *et al.*¹ in their DLTS experiments and later found to be a commonly occurring center in epitaxial materials.² The large nonradiative capture cross section for electrons and a dipole moment, reported by Lang *et al.*¹ and by Jonath *et al.*,³ respectively, and also the work on Ga_{1-x}In_xAs⁴ which shows that the center is not likely to be a simple substitutional donor oxygen fit nicely into the model proposed here. Although the binding energy reported was 0.75 eV, the temperature dependence of the binding energy deduced from our data implies an additional correction⁵⁻⁷ which brings the estimate to a lower value of ~0.70 eV at 0 K.

Our high-resistivity (~10⁸ Ω cm) GaAs sample was grown by Sumitomo Co., with deliberate oxygen doping. The typical mass-spectrographic data quoted by the manufacturer show 4.539, 0.491, 0.180, and 0.022 atomic ppm of O, Si, Cr, and Cu, respectively. The resistivity is reported to have an activation energy of about 0.72 eV from 300 to 400 K.

The photoconductivity data were taken following the method pioneered by Grimmer *et al.*⁸ By varying the photon flux with wavelength to keep the sample conductivity constant (i.e., keep the current constant with fixed bias voltage), we obtain the optical absorption cross section $\sigma(h\nu) = 1/\Phi$, where Φ is the photon flux. If only one impurity-to-band transition is involved, this result holds good at any photocurrent provided that Φ is small enough for $n \ll N$. (Here N is the number of

impurities in the material, and n is the number of conduction electrons under steady-state conditions.) We found that unless a sufficiently high photocurrent was chosen, the results did depend on the current. (In fact the results of Grimmer and Ledeb⁸ do seem to depend on the current as well; see their Fig. 1.⁹) The data shown in our Fig. 1 indicate, however, that for a sufficiently high photo-to-dark current ratio the results became essentially independent of the current value. (It might be worth remarking that at low currents our results also varied somewhat depending on whether the photon energy was changing from lower values to higher ones or vice versa.)

We can understand this effect if we assume, for example, that there is a second level in the band gap such that $N_1 \ll N_2$ and $\sigma_2 \ll \sigma_1$. In the steady state $dn/dt = 0$, so

$$\sum_i e_i n_i - c_i (N_i - n_i) n = 0, \quad (1)$$

where n_i is the density of impurity levels N_i filled with electrons, c_i is the capture rate, and e_i is the emission rate. In thermal equilibrium, c_i^{th} and e_i (we use superscripts *th* and *o* to represent thermal and optical processes, respectively) are related by detailed balance^{10,11}

$$e_i = c_i^o + c_i^{th} = \Phi \sigma_i + c_i^{th} = \Phi \sigma_i + c_i n_{pi}, \quad (2)$$

where n_{pi} is the value of n in thermal equilibrium if the Fermi level is at E_i . Further, in the steady state $dn/dt = 0$, so

$$\sum_i \sigma_i n_i / c_i = (n^2 - \sum_i n_i n_{pi}) / \Phi. \quad (3)$$

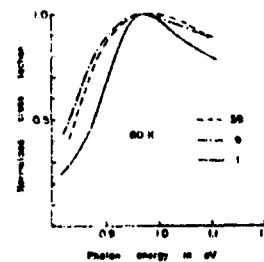


FIG. 1. The normalized cross sections obtained at 80 K, for different photo-to-dark current ratios.

^{a)}Supported in part by ONR under Contract No. N00014-76-C-0880.

^{b)}On leave of absence from Department of Theoretical Physics, The University, Newcastle upon Tyne, U.K.

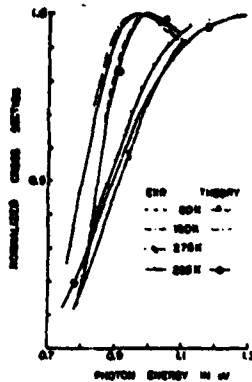


FIG. 2. The normalized cross sections as a function of photon energy. The data taken with the GaAs filter are shown by the dotted lines.

Under the above condition with only two deep levels at E_1 and E_2 , with $N_1 > N_2$ and $\sigma_2/c_2 > \sigma_1/c_1$, for sufficiently high photon flux, $n_2 = 0$ while n_1 is still $\approx N_1$, and the photocurrent is large compared with the dark current so $n > n_{p1}$. Then $q = (c_1 n^2) / (N_1 \Phi) \approx \text{const} / \Phi$ at a constant current and temperature.

In the range of photon energies up to ~ 1.1 eV, we were able to eliminate the intrinsic component of light with a silicon filter and the corresponding results may provide reliable information about σ . Above 1.1 eV (the dotted lines in Fig. 2), we had to use a GaAs filter and some effect due to the intrinsic signal must be expected. At high temperatures the curves $\sigma(h\nu)$ broaden and the maximum of σ falls at energies above 1.1 eV. Since we were not able to determine the latter part of $\sigma(h\nu)$ very accurately and since the shape of the cross section cannot be accurately evaluated without a knowledge of the position of its maximum, we must expect some error in the result presented in Fig. 2. Also the measurements at high temperatures for a weak signal such as ours are generally less reliable. Indeed the large difference between the room- and ice-temperature runs is probably a good indicator of the error.

An interpretation of these results depends on the following observations. The sharp spectra at low temperatures indicate that the transition matrix element involves a p -like impurity wave function and the conduction-band Bloch functions.¹² The broadening clearly visible when we compare the 80- and 190-K curves indicates a Franck-Condon effect. The shift in the position of the maximum towards lower energy at 190 K shows that the binding energy decreases with increasing temperature. Although we have no evidence to prove that the transition involves the conduction band, such a hypothesis is consistent with all we know about this center. On the basis of these observations we computed the photoionization cross section at 80 and 190 K. The electron-phonon interaction is included via the atomic coupling model, in the semiclassical approximation.¹³

The cross section then becomes

$$\sigma = \frac{\text{const}}{h\nu} \int_0^\infty dE \frac{E^{1/2}}{(|E_{10}| + E)^2} \exp\left(-\frac{(h\nu - (|E_{10}| + E))^2}{4\hbar_s^2 \tau_{rc}}\right) \quad (4)$$

The notation is explained in Fig. 3. The values of the binding energy derived in this way are E_1 (80 K) = 0.88 eV and E_1 (190 K) = 0.84 eV, and $d_{rc} = 0.14$ eV. The theoretical curves are shown in Fig. 2. It would seem that the level is "pinned" at 0.83 eV from the valence band in this range of temperature.

Spectra of oxygen-doped GaAs have been studied by a number of researchers. However, the spectra reported there always show many transitions perhaps due to several optically active centers in their material.

Lang *et al.* in their DLTS measurements¹ on melt-grown GaAs reported a deep level at 0.75 eV, with a large electron capture cross section and a barrier energy $E_B = 80$ meV (see Fig. 3), and related it to the earlier data often associated with the presence of oxygen. Mircea *et al.*² found that a trap of precisely the same description appears in undoped epitaxial (VPE) GaAs. This measurement was extended to include $\text{Ga}_{1-x}\text{In}_x\text{As}$ alloys.¹ A comparison of these results with theoretical calculations of the binding energy in the alloy indicates that the level is not likely to be a simple substitutional donor oxygen. Indeed the capture data would be inconsistent with such a notion. The large (nonradiative) capture cross section and a small barrier energy E_B imply a large Franck-Condon shift. Furthermore, no such effects have been reported for the single-donor oxygen in GaP which should exhibit very similar properties to its analog in GaAs.¹⁴ Finally, Jonath *et al.*³ found a deep center in GaAs:O near the middle of the gap which possesses a dipole moment. This and the failure to simply correlate the density of this center with the doping levels of oxygen¹¹ also support the idea of a more complex center.

The binding energy of 0.75 eV¹ was deduced from the detailed balance equation where the capture cross section was corrected for its temperature dependence. If, however, with increasing temperature, the level remains fixed in energy with respect to the valence band,

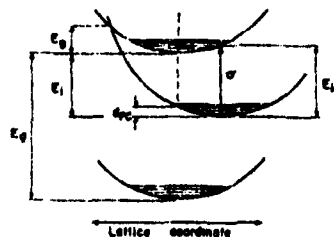


FIG. 3. A configuration-coordinate diagram showing a deep level of binding energy E_1 , exhibiting the Franck-Condon effect (d_{rc}). E_{10} is the optical ionization energy and E_B is the barrier for nonradiative capture. E_0 indicates the band gap. In GaAs (Ref. 8), $E_1 = 1.52 \text{ eV} - \alpha T^2 / (T + \beta)$, where $\alpha = 5.4 \times 10^{-4} \text{ eV K}^{-1}$ and $\beta = 204 \text{ K}$.

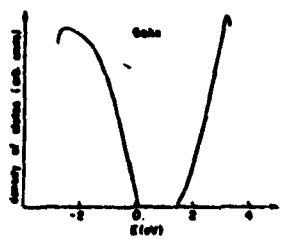


FIG. 4. The "high-temperature" density of states of GaAs near the band edges, smoothed from pseudopotential calculations of Chelikovsky and Cohen (Ref. 18).

then this result overestimates the zero temperature binding energy¹⁰ by about 50 meV. Therefore, the binding energy deduced from our optical experiments, namely, 0.69 eV at 0 K, seems very close to the above estimate of 0.70 eV. Our center does exhibit a significant Franck-Condon effect and most likely possesses axial or lower symmetry, thus making a large nonradiative capture cross section probable. In brief, our assessment of the optical data in terms of the defect binding energy, its temperature dependence, symmetry, and the magnitude of the Franck-Condon effect enables us to connect all the above-mentioned observations and propose that they be related to one particular center associated with the presence of oxygen in GaAs.

The above conclusions were reached without taking into consideration our high-temperature data which also appear in Fig. 2. Although we have cast some doubt on the reliability of these results, their overall character is worth investigating. At low temperature the maximum of the optical cross section appears at energies close to the threshold. Also, the Gaussian in Eq. (4) is fairly narrow. Since the secondary conduction-band minima appear at and above 0.29 eV from the bottom of the conduction band, the calculation of σ at low temperatures could be performed (in the range of energies of interest) employing the simple density of states formula, i.e., $\rho \sim E^{1/2}$. At high temperatures, the cross section would be much more affected by the character of the density of states over a large area of k space. Our approximation, therefore, definitely breaks down there. As has been pointed out earlier,^{14,17} it would manifest itself as a "broadening" of $\sigma(h\nu)$ and a shift of the maximum of

σ towards higher energies. We feel that the flattening of σ observed at high temperatures is due to a combination of both the Franck-Condon and the density of states effects. To appreciate this process quantitatively we would have to go far beyond the simple theory which resulted in Eq. (4). However, some insight might be provided if we substitute for $\rho(E)$ the density of states obtained from pseudopotential calculations,¹⁸ and "smoothed" to account for broadening at higher temperatures (Fig. 4). Taking $I_c(290) = 0.61$ eV and $d_{FC} = 0.14$ (predicted from our low-temperature data) and employing the density of states shown in Fig. 4 instead of the $E^{1/2}$ term, in Eq. (4), we compute a theoretical curve and compare it with the experimental ones in Fig. 2. The comparison seems quite favorable.

We wish to thank Dr. Hans Stocker for donation of samples and for helpful discussions at the early stage of this work, and Bruce Black and Ben Crooker for technical assistance.

¹⁰D. V. Lang and R. A. Logan, *J. Electron. Mater.* **4**, 1053 (1975).
¹¹A. Mircea and A. Mittonneau, *Appl. Phys.* **8**, 15 (1975).
¹²A. D. Jonath, E. Voronkov, and R. H. Bube, *J. Appl. Phys.* **46**, 1754 (1975).
¹³A. Mircea, M. Jaros, A. Mittonneau, and J. Hallats (unpublished).
¹⁴C. M. Penchina and J. S. Moore, *Phys. Rev. B* **9**, 5217 (1974).
¹⁵C. D. Thurmond, *J. Electrochem. Soc.* **122**, 1133 (1975).
¹⁶J. A. Van Vechten and C. D. Thurmond, *Phys. Rev. B* **8**, 3539 (1976).
¹⁷N. G. Grimmeiss and L. A. Ledebor, *J. Appl. Phys.* **46**, 2155 (1975).
¹⁸Note also that they assume $n_{\text{thermal}} \propto n_{\text{photo}}$. This simplification is, however, not necessary and their conclusions would remain valid even if this condition were not fulfilled.
¹⁹W. Shockley, *Electrons and Holes in Semiconductors* (Van Nostrand, New York, 1950), pp. 254 and 299.
²⁰P. W. Bridgman, *Phys. Rev.* **31**, 101 (1928).
²¹M. Jaros, *Phys. Rev. B* (to be published).
²²A. A. Kopylov and A. N. Pikhin, *Fiz. Tverd. Tela* **16**, 1861 (1974) [*Sov. Phys.-Solid State* **16**, 1200 (1975)].
²³M. Jaros, *J. Phys. C* **8**, 2455 (1975).
²⁴A. L. Lin, E. Omelianovsk, and R. H. Bube, *J. Appl. Phys.* **47**, 1852 (1976).
²⁵M. Jaros, *J. Phys. C* **8**, L264 (1975).
²⁶A. M. White, P. J. Dean, and P. Porteous, *J. Appl. Phys.* **47**, 3210 (1976).
²⁷J. H. Chelikovsky and M. L. Cohen, *Phys. Rev. B* **14**, 556 (1976).

